Electrochemical conversion of biomass-derived furanics for production of renewable chemicals and fuels

by

Xiaotong Han Chadderdon

A dissertation submitted to the graduate faculty

in partial fulfillment of the requirements for the degree of

DOCTOR OF PHILOSOPHY

Major: Chemical Engineering

Program of Study Committee:
Wenzhen Li, Major Professor
Jean-Philippe Tessonnier
Kurt R. Hebert
Wenyu Huang
Robbyn K. Anand

The student author, whose presentation of the scholarship herein was approved by the program of study committee, is solely responsible for the content of this dissertation. The Graduate College will ensure this dissertation is globally accessible and will not permit alterations after a degree is conferred.

Iowa State University

Ames, Iowa

2018

TABLE OF CONTENTS

ACKNOWLEDGMENTS

ABSTRACT

Replacing fossil-based fuels and chemicals with biobased alternatives can help alleviate our heavy dependence on petroleum sources, reduce the global carbon footprint, and strengthen our energy security. Electrocatalytic conversion of biomass-derived platform molecules is an emerging route for sustainable fuel and chemical production, with the advantages of eliminating harmful reagents, being tunable, and potentially being driven by renewable electricity. However, the widespread application of organic electrocatalysis is hindered by limitations such as low catalytic activity, product selectivity and energy efficiency.

The goals of this work were to explore the electrochemical conversion of biobased furanics and develop more efficient electrocatalysts and processes for fuel and chemical production. The electrochemical reduction of furfural was investigated on metal electrodes in acidic aqueous electrolytes. Two mechanisms, namely electrocatalytic hydrogenation and direct electroreduction, were distinguished through a combination of voltammetry, bulk electrolysis, thiol-electrode modifications, and kinetic isotope effect studies. Better understanding of the underlying mechanisms and pathways enabled the manipulation of product selectivity. By rationally tuning applied potential, electrolyte pH, and bulk furfural concentration, the selective and efficient formation of a biofuel additive (i.e. 2-methylfuran) or a precursor for polymer and resin synthesis (i.e. furfuryl alcohol) was achieved.

Pairing 5-(hydroxymethyl)furfural (HMF) reduction and oxidation half-reactions in a single electrochemical cell enabled efficient HMF conversion to biobased monomers. Electrocatalytic hydrogenation of HMF to 2,5-bis(hydroxymethyl)furan (BHMF) was

achieved under mild conditions using Ag/C as the cathode catalyst. The competition between Ag-catalyzed HMF hydrogenation to BHMF and undesired HMF hydrodimerization and hydrogen evolution reactions was sensitive to cathode potential. Accordingly, precise control of the cathode potential was critical for achieving high BHMF selectivity and efficiency. In contrast, the selectivity of HMF oxidation facilitated by a homogeneous electrocatalyst, 4-acetamido-TEMPO (ACT, TEMPO = 2,2,6,6-tetramethylpiperidine-1-oxyl), together with an inexpensive carbon felt electrode was not dependent on anode potential. Thus, it was feasible to conduct HMF hydrogenation to BHMF and oxidation to 2,5-furandicarboxylic acid (FDCA) in a single cathode-potential-controlled cell, achieving remarkable overall electron efficiency.

CHAPTER 1

INTRODUCTION

1.1   The Awakening of Biomass

With an ever increasing demand for energy, it is challenging for humankind to continually develop more sustainable energy cycles and maintain a clean environment.[1-2] According to the US Energy Information Administration (EIA), the global energy demand is projected to increase 48% from 549 quadrillion British thermal units (BTU) in 2012 to 815 quadrillion BTU by 2040.[3] In 2016, over 80% of the total US energy consumption was met by the combustion of fossil fuels including petroleum, coal and natural gas. However, such sources are unsustainable and lead to CO_2 emission – which is the main contribution to global climate change. Therefore, replacing fossil-based energy sources with more accessible, sustainable and affordable alternatives will be inevitable to alleviate our heavy dependence on petroleum sources, reduce the global carbon footprint, and strengthen our energy security.[4] As a result, renewable energy in US, including hydroelectric, geothermal, solar, wind, and biofuels, increased by 87.5% from 1980 to 2016, and is projected to increase 37.8% by 2040, shown in **Figure 1.1**.

As an abundant, cheap, and renewable carbon resource, biomass has attracted great attention to replace petroleum-derived chemicals and fuels in both academics and industry. About 200 billion metric tons of biomass is produced by nature annually through photosynthesis, at a cost about ten times lower than producing crude oil.[5-6] Carbohydrates derived from biomass contain many functional groups and are ideal building blocks for producing value-added compounds.[7] The sustainable processing of biomass (i.e.

biorefinery) becomes one of the most promising strategies. In a biorefinery, biomass is converted into a wide range of useful chemicals, materials, and fuels. In traditional petroleum refineries, the feedstocks have very low oxygen content, and require that functional groups are selectively added to produce chemical intermediates, while avoiding complete oxidation to CO_2. In contrast, biomass-derived compounds provide rich functionalities for fuels and chemicals production.[8] The CO_2 released during combustion of biofuels replaces the CO_2 absorbed during the original plant growth; therefore, this energy utilization can generate much less CO_2 than fossil fuels, or even be CO_2 neutral.[5, 9] Therefore, it is very attractive to shift from the carbon source from petroleum to biomass.
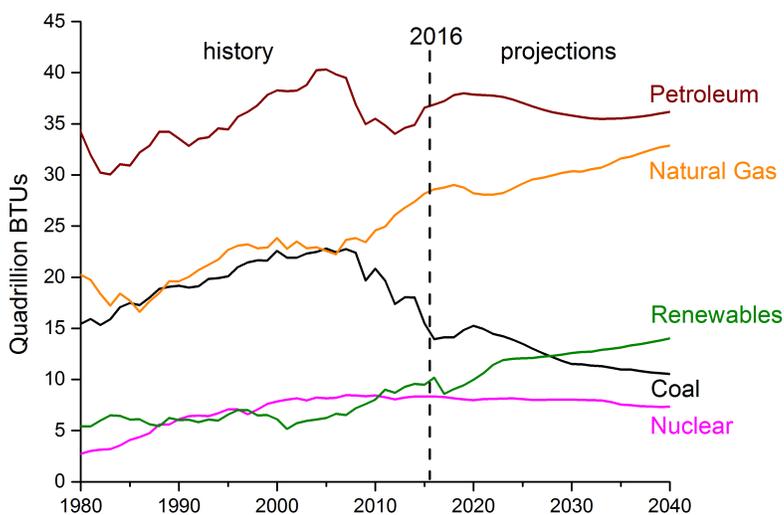
Figure 1.1. US annual energy consumption from US Energy Information Administration.

1.2   Production of Furanics

As the most abundant biomass resource on earth, lignocellulose, which contains cellulose (40–50%), hemicellulose (25–35%), and lignin (15–20%), has achieved great attention to be upgraded to platform compounds.[10] Hemicellulose is a polymer composed of carbon five (e.g. xylose, arabinose) or six (e.g. galactose, glucose, mannose) sugars,

which has been used to produce many byproducts after pretreatment.[11-12] Among the various desired compounds, furanics including furfural and 5-(hydroxymethyl)furfural (HMF) are on the list of the top ten most promising biobased platform molecules released by US Department of Energy (DOE) in 2010, owing to their availability for commercial production and the potential for co-transformation to chemicals and fuels.[13]

Furfural and HMF are acid-catalyzed dehydration products of pentose (e.g. xylose) and hexose (e.g. glucose), respectively. Specifically, furfural is derived from agricultural raw feedstock in which pentosan (polypentose) is abundant. Pentosane undergoes acid-catalyzed hydrolysis reactions to form pentose, and is subsequently dehydrated to furfural.[14] The industrial production of furfural was initiated by Quaker Oats Company in Cedar Rapids, Iowa in 1921, and now has been put into large production by China (~70% total production), Dominican Republic, and South Africa, which account for a total of 90% global furfural production capacity (280 kTon).[15] HMF can be produced from dehydration of furanose form of hexose sugars under acidic and high temperature conditions.[16] Even though HMF has been considered as one of the most versatile platform molecules, its universal industrial-scale production is still under development, resulting in the high cost of HMF.[17] The Dutch company Avantium has announced the scale up of HMF production in Synvina, its joint venture with BASF.[17] Hence the production cost of HMF is projected to decrease in the near future.

1.3   Opportunities for Furanic Derivatives

Furfural and HMF contains multiple functionalities including aldehyde, furan ring, and alcohol (for HMF). Therefore, significant interest has been devoted in furfural and HMF conversion for deriving industrial solvents, fine chemicals, fuel additives and polymers,

owing to their versatility in undergoing many different types of reactions, such as hydrogenation/hydrogenolysis, oxidation and dimerization, shown in **Scheme 1.1**.

Scheme 1.1. Conversion of furfural and HMF to various value added chemicals and biofuels.[18]
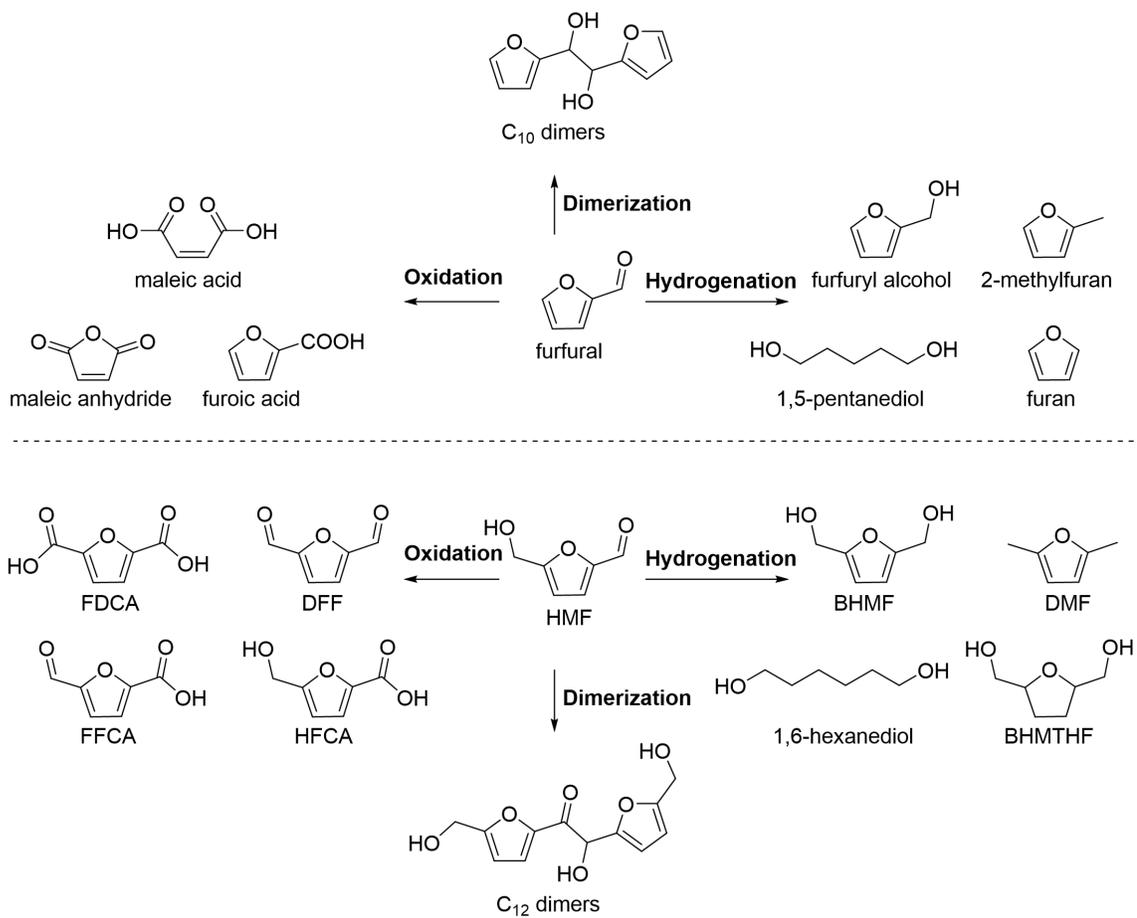
The oxidation products, furoic acid from furfural, and 2,5-furandicarboxylic acid (FDCA) from HMF are both suited as important monomers for biobased polymer materials.[19] Furoic acid can also be used as pharmaceutical intermediate, fungicide, hypolipidemic and anti-inflammatory agents.[20] FDCA is a precursor for the renewable polymer polyethylene 2,5-furandicarboxylate (PEF). PEF has superior barrier properties compared to the conventional PET (polyethylene terephthalate), which is produced from

petrochemical terephthalic acid.[21-22] The selective hydrogenation of C=O in furfural or HMF generates furfuryl alcohol (FA) or 2,5-bis(hydroxymethyl)furan (BHMF), respectively, which are industrially important solvents and precursors for production of polymers, resins, and chemicals.[23-24] FA is mainly used for production of resins, such as dark thermostatic resins that are resistant to acids, bases and various solvent. FA is also widely used as solvent for phenolic resins or pigments with low solubility.[25] BHMF has applications as a co-monomer for preparation of polyisocyanurates, polyurethanes, polyacrylonitriles and polyesters, as an alternative to terephthalyl alcohol.[26] Hydrogenolysis of C–O forms 2-methylfuran (MF) or 2,5-dimethylfuran (DMF), which are potential liquid transportation fuels.[16, 27-28] Both MF and DMF are gaining attention owing to their insolubility in water, and good research octane number (RON, 131 for MF, 119 for DMF). The low boiling and flash points of MF make it suitable to be used for engine ignition. DMF has been shown to have comparable combustion and emission properties to that of gasoline.[27] The general properties of MF and DMF compared to ethanol and gasoline are listed in **Table 1.1**.

Table 1.1. Physical properties of MF, DMF, ethanol and gasoline.[29-30]

Property	2-methylfuran	2,5-dimethylfuran	ethanol	gasoline
Molecular formula	C_5H_6O	C_6H_8O	C_2H_6O	C_6–C_{12}
O/C content	0.2	0.16	0.5	0
Density at 20 °C (g/L)	0.91	0.89	0.79	0.74
Water miscibility at 25 °C (g/L)	3	2.3	miscible	immiscible
Boiling point	63	93	78	32–200
Lower heating value (MJ/L)	28.5	30	23.4	31
Research octane number (RON)	103	119	110	95.8

1.4   Selective Hydrogenation of Furfural and HMF

Among the technologies involved in the hydrogenation of furanic oxygenates, efficient catalytic processes are of great significance and have brought broad and extensive scientific research.[18, 31-32] Furfural and HMF contain C=C and C=O bonds, both of which can be hydrogenated to alkyl or alcohol groups, respectively, over suitable catalysts. Therefore, selective hydrogenation of either C=C or C=O has become a main goal for catalyst design.[33-35] Hydrogenating C=C bonds are thermodynamically and kinetically easier than hydrogenating C=O, and can be facilitated using Pt, Pd, Rh and Ni catalysts.[36] Hydrogenating only the C=O group is traditionally conducted in a homogenous reaction with stoichiometric reducing reagents, such as sodium borohydride ($NaBH_4$) or lithium aluminum hydride ($LiAlH_4$).[37-38] However, such routes can lead to toxic waste and higher costs associated with treatment and separation of the reducing agents and salt byproducts.[24, 39] Homogeneous catalytic hydrogenation using transition metal complexes (e.g. Ru or Ir phosphine ligands) has attracted research attention because of their high activity and selectivity.[36, 40] However, difficult with separation of the catalyst and products makes this process infeasible for large-scale production.[41]

Hydrogenation and hydrogenolysis of furfural is mainly obtained through heterogeneous vapor-phase catalytic reactions, which have been reported with over 90% yields to either FA and MF.[15, 18, 42] Cu-based catalysts have been extensively studied because of their high selectivity to FA. Copper chromite catalysts supported on silica are promising, [43-44] but are toxic and known to suffer from deactivation – possibly from adsorption of species derived from furfural, coke formation, or changes in the oxidation

state of Cu.[15, 23, 45-46] Alcohol solvents are often used in liquid phase hydrogenation instead of water in order to suppress the rearrangement side reactions.[47]

HMF hydrogenation has been mostly conducted in liquid phase processes because of HMF's high boiling point, and has achieved very high yields (>95%) to BHMF over many heterogeneous catalyst systems.[41, 48-55] Deeper hydrogenation of HMF to DMF can be obtained by tuning the hydrogen pressure and reaction temperature. However, high yield to DMF has been more challenging to reach with reasonable amounts of catalyst loading, most reported yields are less than 90%.[30] For example, Dumesic and co-workers introduced a direct conversion from fructose into DMF with 79% yield over a CuRu catalyst in a biphasic process.[56] Recently, Schüth and co-workers reported 98% yield to DMF after a 2 hour reaction over a PtCo bimetallic nanoparticle catalyst.[57]

Conventional heterogeneous catalytic hydrogenation of furfural and HMF generally requires relatively high temperatures (190–300 °C),[15] and often expensive noble metal catalysts, such as supported Pt,[25, 58] or Pd,[59-60]. The use of these materials brings additional operational costs.[23, 32] In addition, H_2 is often used as the hydrogen donor operated under high pressures (5–70 bar).[15, 24] However, H_2 is mainly produced from steam reforming of natural gas, which is a nonrenewable fossil resource and brings high cost for production and transportation.[61] Another effective approach is the catalytic transfer hydrogenation (CTH) process, in which alcohols or formic acid can donate hydrogen with the assistance of a catalyst to conduct hydrogenation instead of H_2 gas.[62] For example, the CTH of furfural and HMF has been reported with 74% yield to MF using butanol as hydrogen donor, and 80% yield to DMF using 2-propanol as hydrogen donor, respectively, using a Ru/RuO$_x$/C

catalyst.[62] However, the reaction mechanisms regarding the active hydrogen species involved in hydrogen transfer step is unclear.

1.5 Electrochemical Hydrogenation of Biobased Molecules

Electrochemical hydrogenation of biobased platform compounds such as furfural,[20, 63-68] HMF,[66, 69-72] levulinic acid,[73-76] glucose,[77-78] itaconic acid,[79] muconic acid,[80-82] and guaiacol[83-84] has been demonstrated as a promising alternative route to conventional heterogeneous hydrogenation. Studies on furfural electrochemical reduction have largely targeted FA production, with MF typically produced as a byproduct with low selectivity. Li et al. studied this system on Ni, Al, Fe, Cu and stainless steel electrodes, and achieved high selectivity to FA on all metals in mild acidic solutions (i.e. pH 5.0).[67] However, their reported carbon balances were low, mainly due to the easy evaporation of the hydrophobic and volatile MF product. Therefore, the true product distributions were difficult to determine. Zhao *et al.* reported over 85% yield for FA production using carbon fiber supported Pt.[68] The metal loading was optimized to improve the faradaic efficiency to 78% compared to a Pt sheet, which had achieved 3% faradaic efficiency to FA product. Green *et al.* demonstrated the reaction in a continuous flow reactor, and achieved FA formation with 100% selectivity at lower conversion and lower applied potential using Pt/C and Pd/C cathode catalysts.[64] However, the selectivity was lost to deeper reduction products MF and 2-methyltetrahydrofuran at higher conversion and higher applied potential. In 2013, Nilges *et al.* compared product distributions on Cu, Pb, Ni, Fe, Al, Pt, and graphite electrodes, and reported high selectivity of about 80% to MF on Cu cathode in acidic electrolyte, while FA was favored (81% selectivity, Pb electrode) in neutral pH.[66] Jung et al. conducted experiments on Cu electrodes in acid media and reported the relationship between product

selectivity and reaction conditions such as current density, electrolyte, and co-solvent ratio.[85] Even though they attributed the low mole balance (<70%) to homogeneous side reaction of products (i.e. FA and MF), the real selectivity remains uncertain, especially for extended reactions.

Electrochemical reduction of HMF was investigated by Kwon *et al.* in both neutral and acidic electrolyte media by combining cyclic voltammetry and online HPLC product analysis techniques for many metal foil electrodes.[69-70] They grouped the electrodes based on their dominant products. However, faradaic efficiency or selectivity cannot be accurately determined by these methods. Reduction of HMF to 2,5-hexanedione (HD), which has application in alternative fuels, was demonstrated by Roylance *et. al.* in acidic media. They found Zn electrode has the unique capability to conduct a one-step hydrogenolysis, Clemson reduction and ring opening reaction with over 80% selectivity to HD product.[72] The same group also studied the reduction of HMF to BHMF in mild aqueous alkaline media (pH 9.2) using a Ag cathode prepared by galvanic displacement of a Cu foil substrate. Close to 100% faradaic efficiency and selectivity to BHMF was achieved at the optimal applied potential (–1.3 V versus Ag/AgCl). Hydrogenolysis product DMF was reported by Nilges *et al.* with 35.8% selectivity on a Cu foil electrode in 0.5 M H_2SO_4 solution,[66] and by Yu *et. al.* with a 30.7% yield on a ZrO_2-doped graphite electrode in KNO_3 solution.[86] Due to the complexity of the HMF molecule, many byproducts and intermediates were also present, with possible reaction pathway shown in **Scheme 1.2**. However, it has not been confirmed whether these intermediates can be further converted to DMF under electrochemical conditions. Therefore, extending the reaction time may or may not increase the yield of DMF.

Scheme 1.2. Possible reaction pathways for electrochemical hydrogenation of the side groups of HMF.
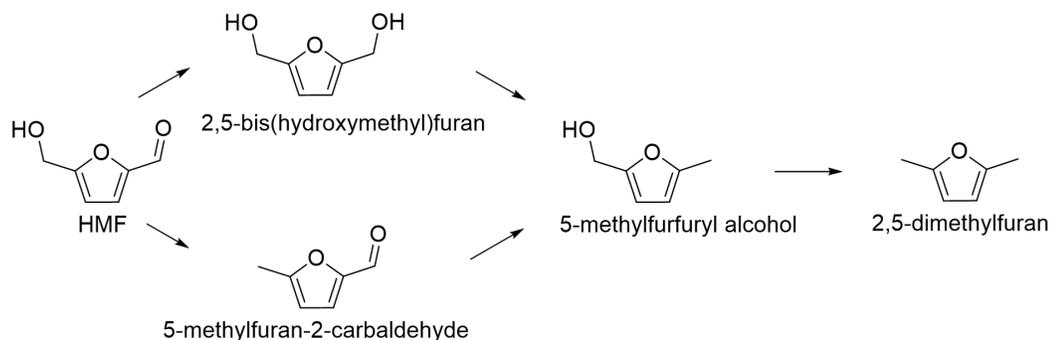
1.6 Mechanism of Electrochemical Hydrogenation

Electrocatalytic hydrogenation (ECH) is an emerging alternative to conventional heterogeneous catalysis routes, with the advantage of being driven by electricity from renewable energy sources, such as hydroelectric, solar, wind or geothermal, during off-peak hours which are often wasted.[87] The reaction mechanism of ECH is analogous to conventional heterogeneous catalytic hydrogenation, with the key difference being that adsorbed hydrogen (H_{ads}) is electrochemically generated *in situ* on the electrode surface (**Scheme 1.3**, Equation 1) from protons or water. In this way, H_2 activation is not needed, thus eliminating the need for external H_2 supply, avoiding the kinetic barriers for H_2 activation, and facilitating hydrogenation reactions at very mild conditions (i.e. low temperature and pressure).[88] The selectivity and production rate of ECH can be controlled by adjusting the applied potential or current through the external circuit. Development of efficient and selective electrochemical processes will certainly broaden our ability to utilize renewable carbon and renewable electricity sources.

ECH of aldehyde and ketone groups may yield alcohols by the hydrogenation of C=O with two H_{ads} (**Scheme 1.3**, Equation 2), or alkyls through hydrogenation/hydrogenolysis reactions with four H_{ads} (**Scheme 1.3**, Equation 3). A fundamental challenge of performing ECH in aqueous solvents is its competition with the hydrogen evolution reaction (HER). When cathodic potentials are applied to metal electrodes, chemisorbed hydrogen (H_{ads}) forms on the electrode surface according to the Volmer reaction through electrochemical reduction of protons (in acidic electrolytes) or water (in neutral or alkaline electrolytes) (**Scheme 1.3**, Equation 1).[88] Then, H_{ads} may either react with another proton (in acid) or water (in neutral and alkaline) and an electron, or a second H_{ads} to form molecular hydrogen (H_2), via Heyrovsky or Tafel steps (**Scheme 1.3**, Equation 4–5), respectively.[89] Because both ECH and HER consume H_{ads} and electricity, faradaic efficiency is usually calculated in order to evaluate their competition.

Scheme 1.3. Reaction steps for ECH and HER.

$$H^+ + e^- \longrightarrow H_{ads} \qquad \text{acidic}$$

Volmer step: \hspace{8cm} (1)

$$H_2O + e^- \longrightarrow H_{ads} + OH^- \qquad \text{neutral or alkaline}$$

$$\underset{R' \quad R''}{O} + 2H_{ads} \longrightarrow \underset{R' \quad R''}{OH} \qquad (2)$$

$$\underset{R' \quad R''}{O} + 4H_{ads} \longrightarrow R' \frown R'' + H_2O \qquad (3)$$

$$H_{ads} + H^+ + e^- \longrightarrow H_2 \qquad \text{acidic}$$

Heyrovsky step: \hspace{8cm} (4)

$$H_{ads} + H_2O + e^- \longrightarrow H_2 + OH^- \qquad \text{neutral or alkaline}$$

Tafel step: \hspace{4cm} $2H_{ads} \longrightarrow H_2$ \hspace{4cm} (5)
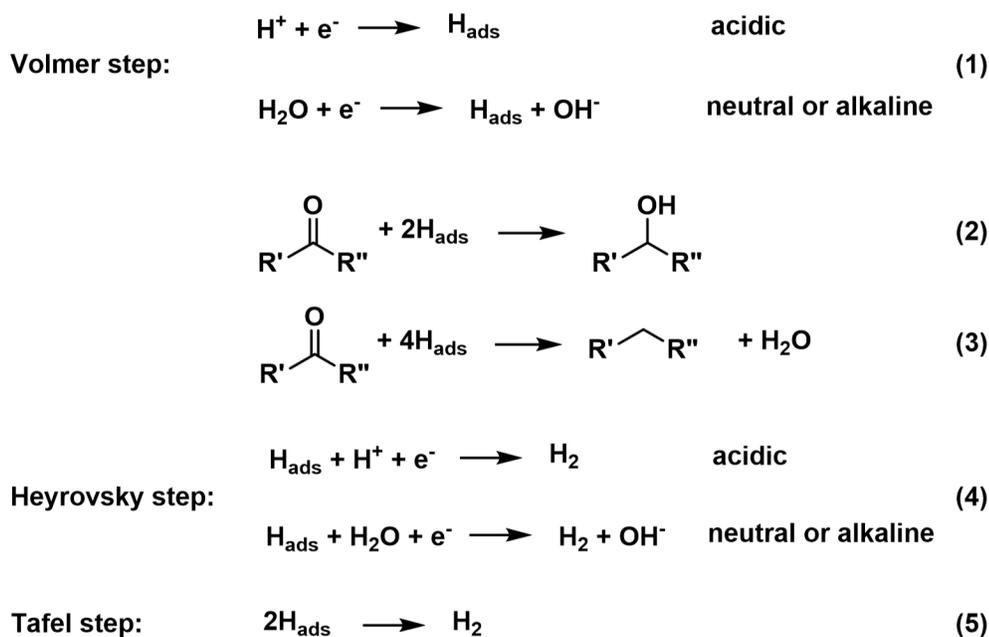
Hydrogen binding strength is often used as a descriptor of HER. Activity has been

shown to exhibit a volcano-type relationship with respect to hydrogen binding strength, as

shown in **Figure 1.2**.[90] It is expected that for the metals with $\Delta G_H < 0$, the hydrogen would

bind to the surface strongly and may poison the electrode by blocking active sites, whereas

for metals with $\Delta G_H > 0$, hydrogen adsorption rate may be limited.
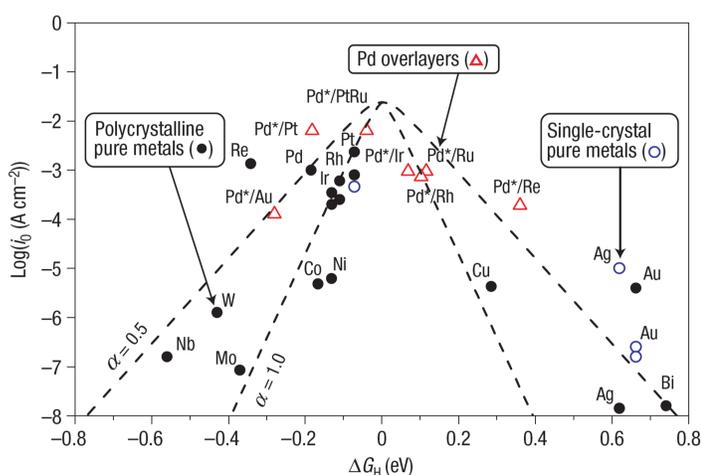
Figure 1.2. Volcano plot of exchange current densities for the HER on various metals as a

function of hydrogen binding strength.[90] Reprinted by permission from Springer Nature:

Nature Materials, Reference 90, Copyright 2006.

Performing ECH in aqueous solvents not only faces challenges due to competition with

HER, but also from competition with direct electroreduction (ER) routes, which do not

involve H_{ads}. Direct ER of aldehyde or ketone groups (C=O) is a well-studied

electrochemical mechanism.[91-92] In acidic electrolytes, C=O undergoes protonation in

solution to $C=OH^+$, which is then directly reduced by a one-electron transfer at potential

E_1 (**Scheme 1.4**) to form a neutral radical intermediate (C·–OH). The radical intermediate

can form hydrodimerization products through C–C coupling with a second radical, or be

further reduced by one-electron transfer at potential E_2 to yield the alcohol product, after protonation.[93] In neutral to basic electrolytes, C=O is reduced at E_3 to a negatively charged radical $C^{\bullet}=O^-$, which is then protonated to $C^{\bullet}-OH$. This radical intermediate can be easily further reduced at E_2 which is less negative than E_3. In stronger alkaline conditions, the reduction starts at E_3 and at more negative potentials E_4, followed by two protonation steps to form the alcohol.[93]

Scheme 1.4. Possible electroreduction pathways for carbonyl groups.[93]
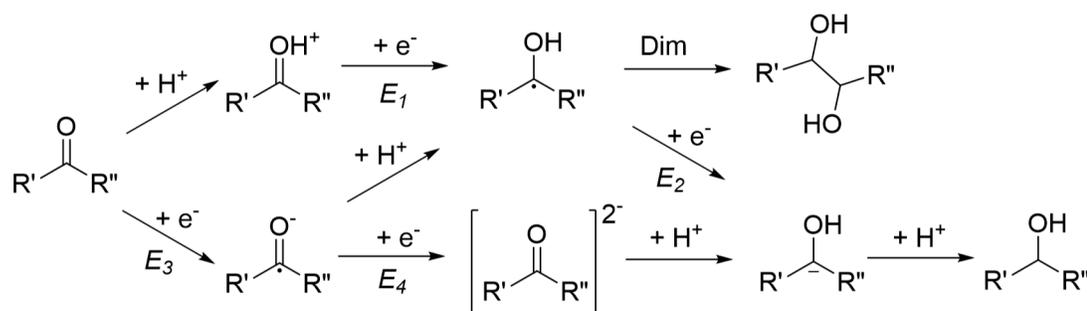
Currently, significant interest has been put into the electrochemical hydrogenation of furanics, especially furfural and HMF, because of their versatility as platform chemicals for production of polymers, fine chemicals, and biofuels, and their availability from biomass by the acid-catalyzed dehydration of pentose and hexose sugars, respectively.[17, 94] It has been demonstrated that the selectivity to hydrogenation or hydrogenolysis products is influenced by the nature of the catalysts, applied potential or current density, electrolyte pH, and initial reactant concentration.[65-67, 69-71, 85] However, much of the recent literature has focused on proof-of-concepts, and it remains unclear whether hydrogenations occur by H_{ads} at the electrode surface from ECH or by electroreduction (ER).[17, 70]

Electrode and catalyst design, together with the choice of reaction conditions, are crucial for avoiding undesirable reactions and achieving selective and efficient electrochemical conversion of C=O to targeted products. The favorability of ECH and ER routes is determined by the relative potentials of C=OH$^+$ reduction (E_1) and H$_{ads}$ formation, respectively. As a result, ECH is strongly preferred on low hydrogen overpotential electrodes (e.g. platinum-group metals), whereas ER is preferred on high hydrogen overpotential electrodes, such as Pb, Hg, Cd, and graphite.[88] However, the two routes may be in competition if the potentials are of similar values. This is a complicating factor when studying mechanisms on electrodes with intermediate hydrogen overpotentials (e.g. Ni, Co, Fe, Cu, Ag and Au), where both ECH and ER mechanisms may occur, especially considering that alcohol formation is possible from either mechanism (cf. **Scheme 1.3** and **1.4**). For example, in the case of electrochemical conversion of furfural and HMF in acidic electrolytes, it is unclear whether hydrogenation/hydrogenolysis occurs by H$_{ads}$ at the electrode surface or directly by H$^+$ in solution.[17, 70] Roylance et. al. proposed that BHMF product from HMF hydrogenation in mild alkaline conditions may be formed without surface adsorbed hydrogen in the potential region before HER initiates. The possible pathways are shown by the blue routes in **Figure 1.3**. They proposed that in the potential region more negative than the onset of HER, BHMF formation would likely be through the mechanism that involves H$_{ads}$, as shown in the red routes.
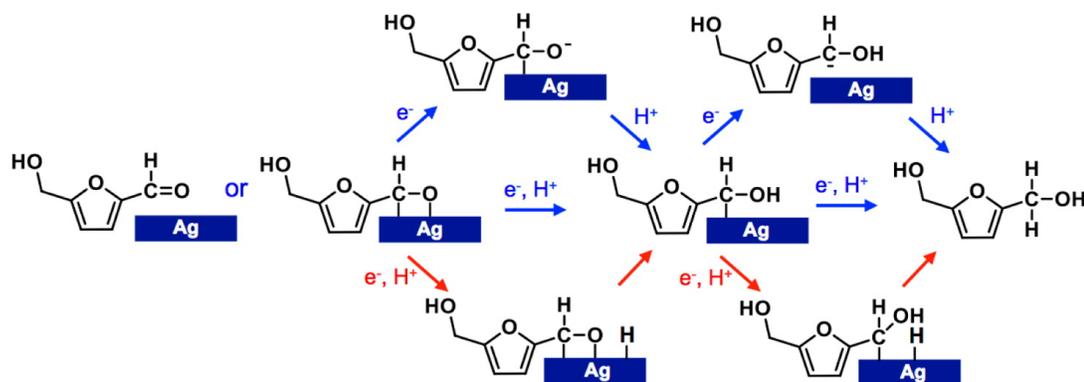
Figure 1.3. Possible HMF hydrogenation pathways.[71] Reprinted with permission from Reference 71, Copyright (2016) American Chemical Society. Further permissions related to the material excerpted should be directed to the ACS. Original article is available at the following link: https://pubs.acs.org/doi/abs/10.1021/acscatal.5b02586

1.7 Electrocatalytic Oxidation

Electrocatalytic oxidation of alcohols at the anode of an electrochemical cell can be used to derive valuable aldehyde or acid-containing chemicals at ambient temperatures and pressures. Oxidation of C1–C3 alcohols including methanol, ethanol, ethylene glycol, and glycerol has been extensively studied, for which the oxidation kinetics are enhanced in alkaline media compare to acid.[95] Alkaline environments are also desired due to fast removal of surface poisoning species such as CO.[96] Such electrochemical processes have been used in anion exchange membrane fuel cells to cogenerate electricity and value-added chemicals (e.g. formic acid and tartronic acid) by coupling with the thermodynamically-favorable oxygen reduction reaction at the cathode.[97] Supported precious metal catalysts such as Pt, Pd, Au and their bimetallic alloys have been shown to be active, selective and stable for alcohol oxidation reactions. For example, Li group reported that the electrocatalytic HMF oxidation to FDCA can be achieved with good yield using a

bimetallic PdAu catalyst.[19] However, the product distribution was highly dependent on the electrode potential and Pd/Au surface ratio, and thus high selectivity to FDCA was limited by other intermediate oxidation products shown in **Scheme 1.5**.

Choi group demonstrated the electrochemical oxidation of HMF to FDCA using a homogeneous electrocatalyst, 2,2,6,6-tetramethylpoperidine 1-oxyl (TEMPO), with nearly 100% yield and faradaic efficiency in pH 9.2 aqueous buffer solution.[98] TEMPO can be oxidized at the electrode to TEMPO$^+$, which is a strong and selective oxidant. TEMPO$^+$ reacts with HMF to generate HMF oxidation products and a TEMPO-hydroxylamine, TEMPOH. TEMPOH and TEMPO$^+$ undergo comproportionation in basic solutions to regenerate TEMPO, thereby closing the catalytic cycle.[99] By this mechanism, the high overpotentials required for direct oxidation of HMF are avoided. The final product FDCA can be precipitated from solution by adjusting the solution pH to be acidic (i.e. pH<3). By using TEMPO as a mediator, the selectivity can be tuned by the total transferred charge, and the reaction rate can be determined by the applied potential, which eliminates the requirement for precious metal catalysts.

Scheme 1.5. Reaction pathways of HMF oxidation to FDCA.
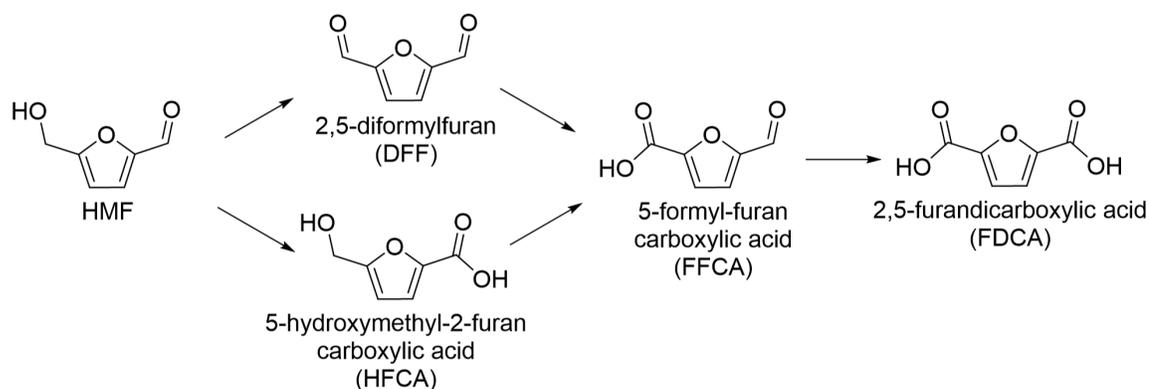
1.8   Paired Electrolysis

For most electrochemical investigations, only the working electrode is of interest, while the counter electrode serves to complete the circuit by water splitting, either generating H_2 or O_2, both of which have limited commercial value. An integrated paired electrolysis can combine two desirable half-reactions in one electrolysis cell that generates chemicals on both the anode and cathode, thereby significantly increasing or even doubling the energy efficiency.[100] Divergent paired electrochemical reactions refer to the production of two different products by oxidizing and reducing the same feedstock at the anode and cathode. Such processes have been demonstrated through glucose oxidation to gluconic acid with 100% efficiency paired with reduction to sorbitol with 80–100% efficiency.[77, 101] Paired electrolysis of furfural has been studied through cyclic voltammetry and preparative electrolysis, where furfural is the reactant at both the anode and cathode to produce furoic acid and furfuryl alcohol, respectively.[20, 65] Electrodeposited Cu and Ni onto graphite felt electrodes were used as cathode and anode, respectively, with different electrolytes (catholyte: H_3PO_4 + NaOH, pH 6.6; anolyte: NaCl + NaOH + LiOH, pH 12) separated by a cationic exchange membrane.[20] However, much lower yields were obtained when the reactions were coupled in a single reactor compare to when operated separately, possibly resulting from a mismatch in optimum current densities for the two half-reactions.

Even though early studies showed promising outcomes, the paired electrolysis research still faces difficulties. Successful design of divergent paired electrolysis requires fundamental understanding of the reaction mechanism, well-designed catalysts, compatible electrolytes (composition and pH), well-controlled electrode potentials, and low material crossover. Recently, a paired electrochemical method for synthesis of sulfonamides,

diarylsulfones, and bis(arylsulfonyl)aminophenols using nitrobenzene derivatives and arylsulfinic acids as feedstocks was demonstrated in an undivided cell over carbon electrodes in aqueous solutions under current controlled electrolysis conditions with good yields (~70%).[102] Llorente et. al. investigated paring CO_2 reduction with oxidative condensation reaction of syringaldehyde, mediated by molecular electrocatalysts.[103]

1.9   Current State of the Research

It has been demonstrated that selectivity to hydrogenation or hydrogenolysis products can be influenced by nature of the electrocatalysts, applied potential or current density, and electrolyte composition (pH and bulk concentration).[65-67, 69-71, 85] However, much of the previous literature has focused on proof-of-concepts, and there remain understanding gaps between reaction conditions, underlying mechanisms, and observed product selectivity. With deep insight provided from studying the reaction mechanism, electrochemical reduction can be manipulated by rationally tuning the reaction conditions instead of trial and error, and better electrocatalysts and electrochemical conditions can be designed toward the optimal selective formation of important biobased polymer precursors and fuels.[2]

In addition, metal foils have been directly used as electrocatalysts for electrochemical hydrogenation in the past, but are not very applicable for industrial large-scale production owing to their low surface area, limited number of active sites and high cost. Switching from bulk metals to supported metal nanoparticles brings great benefits to potentially enhance reaction rates, improve selectivity and reduce catalysts cost.[104]

For many electrochemical hydrogenation studies, only the cathode is considered to be of interest. However, much of the energy demand results from driving the counter electrode

reaction, typically oxygen evolution reaction (OER) in aqueous electrolytes. The produced O_2 is not valuable; thus, much of the total energy input is wasted. Paired electrolysis is a promising approach to increase the overall electron efficiency to desired products by coupling productive oxidation and hydrogenation half-reactions in a single cell reactor. However, very few successes have been reported in this area due to complications of electrolyte incompatibility (composition and pH), limitations in potential control, and material crossover issues.

1.10   Research Goals and Significance

To address the current issues in this research area, combined science and engineering approaches are devoted to study electrochemical conversion of biobased furanic oxygenates – furfural and HMF for tunable production of value-added chemicals and fuels. My overall research goals are: (1) to gain mechanistic insight into electrochemical hydrogenation on metal electrodes, (2) to explore the competition of ECH in both acidic and alkaline aqueous solutions with HER and hydrodimerization reactions, (3) to synthesize and evaluate carbon-supported nanoparticle catalysts for hydrogenation reactions, and (4) to develop a new approach to pair HMF hydrogenation and oxidation for the coproduction of sustainable biobased polymer precursors with high selectivity, yield and efficiency.

Specifically, the main objective of **Chapter 2** is to distinguish the two hydrogenation/reduction mechanisms on metal foil electrodes in acidic electrolytes, and relate those mechanisms to the observed trends in product selectivity for electrochemical hydrogenation of furfural. Furfural is an important biobased platform molecule and serves as a model for aldehyde reduction. Electrochemical approaches including the use of

electrodes modified with organothiol SAMs, H/D kinetic isotope effects, cyclic voltammetry and preparative electrolysis are used for the mechanistic study. The contributions of catalytic and non-catalytic routes to the observed product distributions are clarified by evaluating the requirement for direct chemical interactions with the electrode surface and the role of adsorbed hydrogen.

Chapter 3 builds on the previous chapter to study the more complex molecule, HMF, with the goal of providing mechanistic insights into the selective electrochemical hydrogenation to BHMF on Ag electrodes, developing supported Ag nanoparticle catalysts and pairing HMF hydrogenation and oxidation to generate two valuable products in a single electrolysis cell. Carbon supported Ag nanoparticles cathode catalysts are compared to Ag foil over a wide potential region for HMF hydrogenation. A homogeneous redox electrocatalyst is used at the anode, for which the potential determines the rate but not the selectivity to final product FDCA. The HMF hydrogenation and oxidation in a paired electrolytic process is optimized to maximize the overall energy efficiency, enhance the atom economy, and minimize the energy demand.

1.11   REFERENCES

[1] Chu, S.; Majumdar, A., Opportunities and challenges for a sustainable energy future. *Nature* **2012,** *488*, 294-303.

[2] Seh, Z. W.; Kibsgaard, J.; Dickens, C. F.; Chorkendorff, I.; Norskov, J. K.; Jaramillo, T. F., Combining theory and experiment in electrocatalysis: Insights into materials design. *Science* **2017,** *355*.

[3]   International Energy Outlook 2016. U.S. Energy Information Administration: Washington, DC, 2016.

[4] Technology Roadmap, Biofuels for Transport. IEA Renewable Energy Division, 2011.

[5] Demirbaş, A., Biomass resource facilities and biomass conversion processing for fuels and chemicals. *Energy Convers. Manage.* **2001,** *42*, 1357–1378.

[6] Huber, G. H., *Breaking the chemical and engineering barriers to lignocellulosic biofuels: Next generation hydrocarbon biorefineries*. U. Massachusetts Amherst, 2007.

[7] Chheda, J. N.; Huber, G. W.; Dumesic, J. A., Liquid-Phase Catalytic Processing of Biomass-Derived Oxygenated Hydrocarbons to Fuels and Chemicals. *Angew. Chem. Intl. Ed.* **2007,** *46*, 7164-7183.

[8] de Jong, E.; Jungmeier, G., Biorefinery Concepts in Comparison to Petrochemical Refineries. In *Industrial Biorefineries & White Biotechnology*, Pandey, A.; Hofer, R.; Larroche, C.; Taherzadeh, M.; Nampoothiri, M., Eds. Elsevier: 2015; pp 3-33.

[9] Huber, G. W.; Iborra, S.; Corma, A., Synthesis of transportation fuels from biomass chemistry catalysts and engineering Chemical Reviews. *Chem. Rev.* **2006,** *106*, 4044−4098.

[10] Alonso, D. M.; Bond, J. Q.; Dumesic, J. A., Catalytic conversion of biomass to biofuels. *Green Chem.* **2010,** *12*, 1493–1513.

[11] Kumar, P.; Barrett, D. M.; Delwiche, M. J.; Stroeve, P., Methods for pretreatment of lignocellulosic biomass for efficient hydrolysis and biofuel production. *Ind. Eng. Chem. Res.* **2009,** *48*, 3713–3729.

[12] Jiang, Y.; Wang, X.; Cao, Q.; Dong, L.; Guan, J.; Mu, X., Chemical Conversion of Biomass to Green Chemicals. In *Sustainable Production of Bulk Chemicals*, Xian, M., Ed. Springer: 2016.

[13] Bozell, J. J.; Petersen, G. R., Technology development for the production of biobased products from biorefinery carbohydrates—the US Department of Energy's "Top 10" revisited. *Green Chem.* **2010,** *12*, 539-554.

[14] Zeitsch, K. J., *The Chemistry and Technology of Furfural And Its Many By-products*. First Edition ed.; Elsevier Science B.V.: 2000.

[15] Mariscal López, R.; Maireles-Torres, P.; Ojeda, M.; Sadaba, I.; López Granados, M., Furfural: a renewable and versatile platform molecule for the synthesis of chemicals and fuels. *Energy Environ. Sci.* **2016,** *9*, 1144-1189.

[16] Caes, B. R.; Teixeira, R. E.; Knapp, K. G.; Raines, R. T., Biomass to Furanics: Renewable Routes to Chemicals and Fuels. *ACS Sustainable Chem. Eng.* **2015,** *3*, 2591-2605.

[17] Kwon, Y.; Schouten, K. J. P.; van der Waal, J. C.; de Jong, E.; Koper, M. T. M., Electrocatalytic Conversion of Furanic Compounds. *ACS Catal.* **2016,** *6*, 6704–6717.

[18] Nakagawa, Y.; Tamura, M.; Tomishige, K., Catalytic Reduction of Biomass-Derived Furanic Compounds with Hydrogen. *ACS Catal.* **2013,** *3*, 2655-2668.

[19] Chadderdon, D. J.; Xin, L.; Qi, J.; Qiu, Y.; Krishna, P.; More, K. L.; Li, W., Electrocatalytic oxidation of 5-hydroxymethylfurfural to 2,5-furandicarboxylic acid on supported Au and Pd bimetallic nanoparticles. *Green Chem.* **2014,** *16*, 3778-3786.

[20] Chamoulauda, G.; Flonerb, D.; Moinetb, C.; Lamya, C.; Belgsir, E. M., Biomass conversion II: simultaneous electrosyntheses of furoic acid and durduryl alcohol on modified graphite felt electrodes. *Electrochim. Acta* **2001,** *46*, 2757-2760.

[21] Nakajima, H.; Dijkstra, P.; Loos, K., The Recent Developments in Biobased Polymers toward General and Engineering Applications: Polymers that are Upgraded from Biodegradable Polymers, Analogous to Petroleum-Derived Polymers, and Newly Developed. *Polymers* **2017,** *9*, 523.

[22] de Jong, E.; Dam, M. A.; Sipos, L.; Gruter, G. J. M., Furandicarboxylic Acid (FDCA), A Versatile Building Block for a Very Interesting Class of Polyesters. In *Biobased Monomers, Polymers, and Materials*, Smith, P. B.; Gross, R. A., Eds. American Chemical Society: Washington, DC, 2012; Vol. 1105, pp 1-13.

[23] Yan, K.; Wu, G.; Lafleur, T.; Jarvis, C., Production, properties and catalytic hydrogenation of furfural to fuel additives and value-added chemicals. *Renew. Sustainable Energy Rev.* **2014,** *38*, 663-676.

[24] Hu, L.; Lin, L.; Wu, Z.; Zhou, S.; Liu, S., Recent advances in catalytic transformation of biomass-derived 5-hydroxymethylfurfural into the innovative fuels and chemicals. *Renew. Sustainable Energy Rev.* **2017,** *74*, 230-257.

[25] Kijenski, J.; Winiarek, P.; Paryjczak, T.; Lewickib, A.; Mikołajska, A., Platinum deposited on monolayer supports in selective hydrogenation of furfural to furfuryl alcohol. *Appl. Catal., A* **2002,** *233*, 171–182.

[26] Hu, L.; Xu, J.; Zhou, S.; He, A.; Tang, X.; Lin, L.; Xu, J.; Zhao, Y., Catalytic Advances in the Production and Application of Biomass-Derived 2,5-Dihydroxymethylfuran. *ACS Catal.* **2018**, 2959-2980.

[27] Bohre, A.; Dutta, S.; Saha, B.; Abu-Omar, M. M., Upgrading Furfurals to Drop-in Biofuels: An Overview. *ACS Sustainable Chem. Eng.* **2015,** *3*, 1263-1277.

[28] Hu, L.; Lin, L.; Liu, S., Chemoselective hydrogenation of biomass-derived 5-hydroxymethylfurfural into the liquid biofuel 2,5-dimethylfuran. *Ind. Eng. Chem. Res.* **2014,** *53*, 9969-9978.

[29] Ma, X.; Jiang, C.; Xu, H.; Ding, H.; Shuai, S., Laminar burning characteristics of 2-methylfuran and isooctane blend fuels. *Fuel* **2014,** *116*, 281-291.

[30] Saha, B.; Abu-Omar, M. M., Current Technologies, Economics, and Perspectives for 2,5-Dimethylfuran Production from Biomass-Derived Intermediates. *ChemSusChem* **2015,** *8*, 1133-1142.

[31] Hu, X.; Westerhof, R. J. M.; Wu, L.; Dong, D.; Li, C.-Z., Upgrading biomass-derived furans via acid-catalysis/hydrogenation: the remarkable difference between water and methanol as the solvent. *Green Chem.* **2015,** *17*, 219-224.

[32] Climent, M. J.; Corma, A.; Iborra, S., Conversion of biomass platform molecules into fuel additives and liquid hydrocarbon fuels. *Green Chem.* **2014,** *16*, 516-547.

[33] Ponec, V., On the role of promoters in hydrogenations on metals; α, β-unsaturated aldehydes and ketones. *Appl. Catal., A* **1996,** *149*, 27-48.

[34] Mäki-Arvela, P.; Hájek, J.; Salmi, T.; Murzin, D. Y., Chemoselective hydrogenation of carbonyl compounds over heterogeneous catalysts. *Appl. Catal., A* **2005,** *292*, 1-49.

[35] Medlin, J. W., Understanding and Controlling Reactivity of Unsaturated Oxygenates and Polyols on Metal Catalysts. *ACS Catal.* **2011,** *1*, 1284-1297.

[36] Ghosh, A.; Kumar, R., Synthesis, characterization and catalytic application of Ru^{II}–ethylenediamine complex—mesoporous silica as heterogeneous catalyst system in chemo-selective hydrogenation of α,β-unsaturated carbonyl compounds. *Microporous Mesoporous Mater.* **2005,** *87*, 33–44.

[37] Pavlov, V. A.; Klabunovskii, E. I.; Struchkov, Y. T.; Voloboev, A. A.; Yanovsky, A. I., Asymmetric reduction of C=C and C=O bonds: stereochemical approach. *J. Mol. Catal.* **1988,** *44*, 217-243.

[38] Goswami, S.; Dey, S.; Jana, S., Design and synthesis of a unique ditopic macrocyclic fluorescent receptor containing furan ring as a spacer for the recognition of dicarboxylic acids. *Tetrahedron* **2008,** *64*, 6358-6363.

[39] Delidovich, I.; Palkovits, R., Catalytic versus stoichiometric reagents as a key concept for Green Chemistry. *Green Chem.* **2016,** *18*, 590-593.

[40] Thananatthanachon, T.; Rauchfuss, T. B., Efficient route to hydroxymethylfurans from sugars via transfer hydrogenation. *ChemSusChem* **2010,** *3*, 1139-1141.

[41] Tamura, M.; Tokonami, K.; Nakagawa, Y.; Tomishige, K., Rapid synthesis of unsaturated alcohols under mild conditions by highly selective hydrogenation. *Chem. Commun.* **2013,** *49*, 7034-7036.

[42] Lessard, J.; Morin, J.-F.; Wehrung, J.-F.; Magnin, D.; Chornet, E., High Yield Conversion of Residual Pentoses into Furfural via Zeolite Catalysis and Catalytic Hydrogenation of Furfural to 2-Methylfuran. *Top. Catal.* **2010,** *53*, 1231-1234.

[43] Rao, R. S.; Baker, R. T. K.; Vannice, M. A., Furfural hydrogenation over carbon-supported copper. *Catal. Lett.* **1999,** *60*, 51-57.

[44] Jiménez-Gómez, C. P.; Cecilia, J. A.; Durán-Martín, D.; Moreno-Tost, R.; Santamaría-González, J.; Mérida-Robles, J.; Mariscal, R.; Maireles-Torres, P., Gas-phase hydrogenation of furfural to furfuryl alcohol over Cu/ZnO catalysts. *J. Catal.* **2016,** *336*, 107-115.

[45] Rao, R.; Dandekar, A.; Baker, R. T. K.; Vannice, M. A., Properties of copper chromite catalysts in hydrogenation reactions. *J. Catal.* **1997,** *171*, 406–419.

[46] Liu, D.; Zemlyanov, D.; Wu, T.; Lobo-Lapidus, R. J.; Dumesic, J. A.; Miller, J. T.; Marshall, C. L., Deactivation mechanistic studies of copper chromite catalyst for selective hydrogenation of 2-furfuraldehyde. *J. Catal.* **2013,** *299*, 336-345.

[47] Alamillo, R.; Tucker, M.; Chia, M.; Pagán-Torres, Y.; Dumesic, J., The selective hydrogenation of biomass-derived 5-hydroxymethylfurfural using heterogeneous catalysts. *Green Chem.* **2012,** *14*, 1413-1419.

[48] Ohyama, J.; Esaki, A.; Yamamoto, Y.; Arai, S.; Satsuma, A., Selective hydrogenation of 2-hydroxymethyl-5-furfural to 2,5-bis(hydroxymethyl)furan over gold sub-nano clusters. *RSC Adv.* **2013,** *3*, 1033-1036.

[49] Cai, H.; Li, C.; Wang, A.; Zhang, T., Biomass into chemicals: One-pot production of furan-based diols from carbohydrates via tandem reactions. *Catal. Today* **2014,** *234*, 59-65.

[50] Chatterjee, M.; Ishizaka, T.; Kawanami, H., Selective hydrogenation of 5-hydroxymethylfurfural to 2,5-bis-(hydroxymethyl)furan using Pt/MCM-41 in an aqueous medium: a simple approach. *Green Chem.* **2014,** *16*, 4734-4739.

[51] Ohyama, J.; Hayashi, Y.; Ueda, K.; Yamamoto, Y.; Arai, S.; Satsuma, A., Effect of FeO_x modification of Al_2O_3 on its supported Au catalyst for hydrogenation of 5-hydroxymethylfurfural. *J. Phys. Chem. C* **2016,** *120*, 15129-15136.

[52] Kumalaputri, A. J.; Bottari, G.; Erne, P. M.; Heeres, H. J.; Barta, K., Tunable and selective conversion of 5-HMF to 2,5-furandimethanol and 2,5-dimethylfuran over copper-doped porous metal oxides. *ChemSusChem* **2014,** *7*, 2266-2275.

[53] Pasini, T.; Solinas, G.; Zanotti, V.; Albonetti, S.; Cavani, F.; Vaccari, A.; Mazzanti, A.; Ranieri, S.; Mazzoni, R., Substrate and product role in the Shvo's catalyzed selective hydrogenation of the platform bio-based chemical 5-hydroxymethylfurfural. *Dalton Trans.* **2014,** *43*, 10224-10234.

[54] Bottari, G.; Kumalaputri, A. J.; Krawczyk, K. K.; Feringa, B. L.; Heeres, H. J.; Barta, K., Copper-zinc alloy nanopowder: a robust precious-metal-free catalyst for the conversion of 5-hydroxymethylfurfural. *ChemSusChem* **2015,** *8*, 1323-1327.

[55] Yu, L.; He, L.; Chen, J.; Zheng, J.; Ye, L.; Lin, H.; Yuan, Y., Robust and recyclable nonprecious bimetallic nanoparticles on carbon nanotubes for the hydrogenation and hydrogenolysis of 5-hydroxymethylfurfural. *ChemCatChem* **2015,** *7*, 1701-1707.

[56] Roman-Leshkov, Y.; Barrett, C. J.; Liu, Z. Y.; Dumesic, J. A., Production of dimethylfuran for liquid fuels from biomass-derived carbohydrates. *Nature* **2007,** *447*, 982-985.

[57] Wang, G. H.; Hilgert, J.; Richter, F. H.; Wang, F.; Bongard, H. J.; Spliethoff, B.; Weidenthaler, C.; Schuth, F., Platinum-cobalt bimetallic nanoparticles in hollow carbon nanospheres for hydrogenolysis of 5-hydroxymethylfurfural. *Nat. Mater.* **2014,** *13*, 293-300.

[58] Pushkarev, V. V.; Musselwhite, N.; An, K.; Alayoglu, S.; Somorjai, G. A., High structure sensitivity of vapor-phase furfural decarbonylation/hydrogenation reaction network as a function of size and shape of Pt nanoparticles. *Nano Lett.* **2012,** *12*, 5196-5201.

[59] Sitthisa, S.; Pham, T.; Prasomsri, T.; Sooknoi, T.; Mallinson, R. G.; Resasco, D. E., Conversion of furfural and 2-methylpentanal on Pd/SiO_2 and $Pd–Cu/SiO_2$ catalysts. *J. Catal.* **2011,** *280*, 17-27.

[60] Sitthisa, S.; Resasco, D. E., Hydrodeoxygenation of furfural over supported metal catalysts: a comparative study of Cu, Pd and Ni. *Catal. Lett.* **2011,** *141*, 784-791.

[61] Ogden, J. M., Prospects for building a hydrogen energy infrastructure. *Annu. Rev. Energy Environ.* **1999,** *24*, 227-279.

[62] Gilkey, M. J.; Xu, B., Heterogeneous Catalytic Transfer Hydrogenation as an Effective Pathway in Biomass Upgrading. *ACS Catal.* **2016**, 1420-1436.

[63] Antunes, M. M.; Lima, S.; Fernandes, A.; Pillinger, M.; Ribeiro, M. F.; Valente, A. A., Aqueous-phase dehydration of xylose to furfural in the presence of MCM-22 and ITQ-2 solid acid catalysts. *Appl. Catal., A* **2012,** *417-418*, 243-252.

[64] Green, S. K.; Lee, J.; Kim, H. J.; Tompsett, G. A.; Kim, W. B.; Huber, G. W., The electrocatalytic hydrogenation of furanic compounds in a continuous electrocatalytic membrane reactor. *Green Chem.* **2013,** *15*, 1869-1879.

[65] Parpot, P.; Bettencourt, A. P.; Chamoulaud, G.; Kokoh, K. B.; Belgsir, E. M., Electrochemical investigations of the oxidation–reduction of furfural in aqueous medium. *Electrochim. Acta* **2004,** *49*, 397-403.

[66] Nilges, P.; Schroder, U., Electrochemistry for biofuel generation: production of furans by electrocatalytic hydrogenation of furfurals. *Energy Environ. Sci.* **2013,** *6*, 2925-2931.

[67] Li, Z.; Kelkar, S.; Lam, C. H.; Luczek, K.; Jackson, J. E.; Miller, D. J.; Saffron, C. M., Aqueous electrocatalytic hydrogenation of furfural using a sacrificial anode. *Electrochim. Acta* **2012,** *64*, 87-93.

[68] Zhao, B.; Chen, M.; Guo, Q.; Fu, Y., Electrocatalytic hydrogenation of furfural to furfuryl alcohol using platinum supported on activated carbon fibers. *Electrochim. Acta* **2014,** *135*, 139-146.

[69] Kwon, Y.; de Jong, E.; Raoufmoghaddam, S.; Koper, M. T., Electrocatalytic hydrogenation of 5-hydroxymethylfurfural in the absence and presence of glucose. *ChemSusChem* **2013,** *6*, 1659-1667.

[70] Kwon, Y.; Birdja, Y. Y.; Raoufmoghaddam, S.; Koper, M. T., Electrocatalytic hydrogenation of 5-hydroxymethylfurfural in acidic solution. *ChemSusChem* **2015,** *8*, 1745-1751.

[71] Roylance, J. J.; Kim, T. W.; Choi, K.-S., Efficient and Selective Electrochemical and Photoelectrochemical Reduction of 5-Hydroxymethylfurfural to 2,5-Bis(hydroxymethyl)furan using Water as the Hydrogen Source. *ACS Catal.* **2016,** *6*, 1840-1847.

[72] Roylance, J. J.; Choi, K.-S., Electrochemical reductive biomass conversion: direct conversion of 5-hydroxymethylfurfural (HMF) to 2,5-hexanedione (HD) via reductive ring-opening. *Green Chem.* **2016,** *18*, 2956-2960.

[73] Nilges, P.; Santos, T. R. d.; Harnisch, F.; Schroder, U., Electrochemistry for biofuel generation: Electrochemical conversion of levulinic acid to octane. *Energy Environ. Sci.* **2012,** *5*, 5231-5235.

[74] Xin, L.; Zhang, Z.; Qi, J.; Chadderdon, D. J.; Qiu, Y.; Warsko, K. M.; Li, W., Electricity storage in biofuels: selective electrocatalytic reduction of levulinic acid to valeric acid or gamma-valerolactone. *ChemSusChem* **2013,** *6*, 674-686.

[75] Qiu, Y.; Xin, L.; Chadderdon, D. J.; Qi, J.; Liang, C.; Li, W., Integrated electrocatalytic processing of levulinic acid and formic acid to produce biofuel intermediate valeric acid. *Green Chem.* **2014,** *16*, 1305-1315.

[76] dos Santos, T. R.; Nilges, P.; Sauter, W.; Harnisch, F.; Schröder, U., Electrochemistry for generation of renewable chemicals: Electrochemical conversion of levulinic acid. *RSC Adv.* **2015,** *5*, 26634-26643.

[77] Pintauro, P. N.; Johnson, D. K.; Park, K.; Baizer, M. M.; Nobe, K., The paired electrochemical synthesis of sorbitol and gluconic acid in undivided flow cells. I. *J. Appl. Electrochem.* **1984,** *14*, 209-220.

[78] Kwon, Y.; Koper, M. T., Electrocatalytic hydrogenation and deoxygenation of glucose on solid metal electrodes. *ChemSusChem* **2013,** *6*, 455-462.

[79] Holzhäuser, F. J.; Artz, J.; Palkovits, S.; Kreyenschulte, D.; Büchs, J.; Palkovits, R., Electrocatalytic upgrading of itaconic acid to methylsuccinic acid using fermentation broth as a substrate solution. *Green Chem.* **2017**, 2390-2397.

[80] Suastegui, M.; Matthiesen, J. E.; Carraher, J. M.; Hernandez, N.; Quiroz, N. R.; Okerlund, A.; Cochran, E. W.; Shao, Z.; Tessonnier, J.-P., Combining MetabolicEngineering and Electrocatalysis:Application to the Production of Polyamides from Sugar. *Angew. Chem. Intl. Ed.* **2016,** *55*, 2368 –2373.

[81] Matthiesen, J. E.; Carraher, J. M.; Vasiliu, M.; Dixon, D. A.; Tessonnier, J.-P., Electrochemical Conversion of Muconic Acid to Biobased Diacid Monomers. *ACS Sustainable Chem. Eng.* **2016,** *4*, 3575–3585.

[82] Matthiesen, J. E.; Suástegui, M.; Wu, Y.; Viswanathan, M.; Qu, Y.; Cao, M.; Rodriguez-Quiroz, N.; Okerlund, A.; Kraus, G.; Raman, D. R.; Shao, Z.; Tessonnier, J.-P., Electrochemical Conversion of Biologically Produced Muconic Acid: Key Considerations for Scale-Up and Corresponding Technoeconomic Analysis. *ACS Sustainable Chem. Eng.* **2016,** *4*, 7098-7109.

[83] Li, Z.; Garedew, M.; Lam, C. H.; Jackson, J. E.; Miller, D. J.; Saffron, C. M., Mild electrocatalytic hydrogenation and hydrodeoxygenation of bio-oil derived phenolic compounds using ruthenium supported on activated carbon cloth. *Green Chem.* **2012,** *14*, 2540-2549.

[84] Lam, C. H.; Lowe, C. B.; Li, Z.; Longe, K. N.; Rayburn, J. T.; Caldwell, M. A.; Houdek, C. E.; Maguire, J. B.; Miller, D. J.; Saffron, C. M.; Jackson, J. E., Electrocatalytic Upgrading of Model Lignin Monomers with Earth Abundant Metal Electrodes. *Green Chem.* **2015,** *17*, 601-609.

[85] Jung, S.; Biddinger, E. J., Electrocatalytic Hydrogenation and Hydrogenolysis of Furfural and the Impact of Homogeneous Side Reactions of Furanic Compounds in Acidic Electrolytes. *ACS Sustainable Chem. Eng.* **2016,** *4*, 6500–6508.

[86] Yu, X.; Wen, Y.; Yuan, T.; Li, G., Effective production of 2,5-dimethylfuran from biomass-derived 5-hydroxymethylfurfural on ZrO_2-doped graphite electrode. *ChemistrySelect* **2017,** *2*, 1237-1240.

[87] Hirth, L., The market value of variable renewables. *Energy Econ.* **2013,** *38*, 218-236.

[88] Lessard, J., Electrocatalytic Hydrogenation. In *Organic Electrochemistry*, 5th ed.; Hammerich, O.; Speiser, B., Eds. CRC Press: Boca Raton, FL, 2015; pp 1658-1664.

[89] Saraby-Reintjes, A., Kinetic criteria for the mechanism of the hydrogen evolution reaction. *Electrochim. Acta* **1986,** *31*, 251-254.

[90] Greeley, J.; Jaramillo, T. F.; Bonde, J.; Chorkendorff, I. B.; Norskov, J. K., Computational high-throughput screening of electrocatalytic materials for hydrogen evolution. *Nat. Mater.* **2006,** *5*, 909-913.

[91] Elving, P. J.; Leone, J. T., Mechanism of electrochemical reduction of phenyl ketones. *J. Am. Chem. Soc.* **1958,** *80*, 1021-1029.

[92] Stradins, J. P., Studies on the electrochemical mechanism of reduction of carbonyl compounds. *Electrochim. Acta* **1964,** *9*, 711-720.

[93] Ludvík, J., Reduction of Aldehydes Ketones and Azomethines. In *Organic Electrochemistry*, Hammerich, O.; Speiser, B., Eds. CRC Press: 2015.

[94] Binder, J. B.; Raines, R. T., Simple chemical transformation of lignocellulosic biomass into furans for fuels and chemicals. *J. Am. Chem. Soc.* **2009,** *131*, 1979–1985.

[95] Kabir, S.; Serov, A., Anodic materials for electrooxidation of alcohols in alkaline media. *Electrochemistry* **2017,** *14*, 61-101.

[96] Badwal, S. P. S.; Giddey, S.; Kulkarni, A.; Goel, J.; Basu, S., Direct ethanol fuel cells for transport and stationary applications – A comprehensive review. *Appl. Energy* **2015,** *145*, 80-103.

[97] Qi, J.; Xin, L.; Chadderdon, D. J.; Qiu, Y.; Jiang, Y.; Benipal, N.; Liang, C.; Li, W., Electrocatalytic selective oxidation of glycerol to tartronate on Au/C anode catalysts in anion exchange membrane fuel cells with electricity cogeneration. *Appl. Catal., B* **2014,** *154-155*, 360-368.

[98] Cha, H. G.; Choi, K. S., Combined biomass valorization and hydrogen production in a photoelectrochemical cell. *Nat. Chem.* **2015,** *7*, 328-333.

[99] Ciriminna, R.; Ghahremani, M.; Karimi, B.; Pagliaro, M., Electrochemical alcohol oxidation mediated by TEMPO-like nitroxyl radicals. *ChemistryOpen* **2017,** *6*, 5-10.

[100] Ibanez, J. G.; Frontana-Uribe, B. A.; Vasquez-Medrano, R., Paired electrochemical processes: overview, systematization, selection criteria, design strategies, and projection. *J. Mex. Chem. Soc.* **2016,** *60*, 247-260.

[101] Park, K.; Pintauro, P. N.; Baizer, M. M.; Nobe, K., Flow reactor studies of the paired electro-oxidation and electroreduction of glucose. *J. Electrochem. Soc.* **1985,** *132*, 1850-1855.

[102] Mokhtari, B.; Nematollahi, D.; Salehzadeh, H., Paired electrochemical conversion of nitroarenes to sulfonamides, diarylsulfones and bis(arylsulfonyl)aminophenols. *Green Chem.* **2018,** *20*, 1499-1505

[103] Llorente, M. J.; Nguyen, B. H.; Kubiak, C. P.; Moeller, K. D., Paired electrolysis in the simultaneous production of synthetic intermediates and substrates. *J. Am. Chem. Soc.* **2016,** *138*, 15110-15113.

[104] Costentin, C.; Savéant, J.-M., Catalysis at the nanoscale may change selectivity. *Proc. Natl. Acad. Sci.* **2016,** *113*, 11756–11758.

CHAPTER 2

MECHANISMS OF FURFURAL REDUCTION ON METAL ELECTRODES: DISTINGUISHING PATHWAYS FOR SELECTIVE HYDROGENATION OF BIODERIVED OXYGENATES

Xiaotong H. Chadderdon,[a,b,‡] David J. Chadderdon,[a,b,‡] John E. Matthiesen,[a,b,c] Yang Qiu,[a,b] Jack M. Carraher,[a,c] Jean-Philippe Tessonnier,[a,b,c] Wenzhen Li[a,b,*]

[a]Department of Chemical and Biological Engineering, Iowa State University, 618 Bissell Road, Ames, Iowa 50011, United States

[b]US Department of Energy Ames Laboratory, 2408 Pammel Drive, Ames, Iowa 50011, United States

[c]NSF Engineering Research Center for Biorenewable Chemicals (CBiRC), 617 Bissell Road, Ames, Iowa 50011, United States

[‡]These authors contributed equally to this work and should be considered as co-first authors

[*]Corresponding Author

ABSTRACT

Electrochemical reduction of biomass-derived platform chemicals is an emerging route for the sustainable production of fuels and chemicals. However, understanding gaps between reaction conditions, underlying mechanisms, and product selectivity have limited

the rational design of active, stable, and selective catalyst systems. In this work, the mechanisms of electrochemical reduction of furfural, an important biobased platform molecule and model for aldehyde reduction, are explored through a combination of voltammetry, preparative electrolysis, thiol-electrode modifications, and kinetic isotope studies. It is demonstrated that two distinct mechanisms are operable on metallic Cu electrodes in acidic electrolytes: (i) electrocatalytic hydrogenation (ECH) and (ii) direct electroreduction. The contributions of each mechanism to the observed product distribution are clarified by evaluating the requirement for direct chemical interactions with the electrode surface and the role of adsorbed hydrogen. Further analysis reveals that hydrogenation and hydrogenolysis products are generated by parallel ECH pathways. Understanding the underlying mechanisms enables the manipulation of furfural reduction by rationally tuning the electrode potential, electrolyte pH, and furfural concentration to promote selective formation of important biobased polymer precursors and fuels.

2.1 Background

Electrocatalytic hydrogenation (ECH) is emerging as an environmentally-friendly approach for the selective reduction of multifunctional chemicals. ECH is analogous to conventional thermo-catalytic hydrogenation, with the key difference that adsorbed hydrogen (H_{ads}) is electrochemically generated *in situ* on the electrode surface by proton or water reduction (Volmer reaction) rather than through the dissociation of molecular H_2.[1] In this way, the kinetic barriers for H_2 activation are avoided and hydrogenations can be performed without the need for external H_2 supply and at mild conditions.[2-4] ECH of carbonyl groups, which are prevalent in important biobased platform chemicals, may yield alcohols by hydrogenation with two H_{ads}, or alkyls through hydrogenation and

hydrogenolysis reactions with four H_{ads} (**Scheme 2.1**). However, ECH is often in competition with the hydrogen evolution reaction (HER), which consumes H_{ads} through Tafel or Heyrovsky reactions and lowers the faradaic efficiency to ECH.[5]

Scheme 2.1. Proposed pathways of electrochemical reduction of carbonyls in acidic electrolytes.
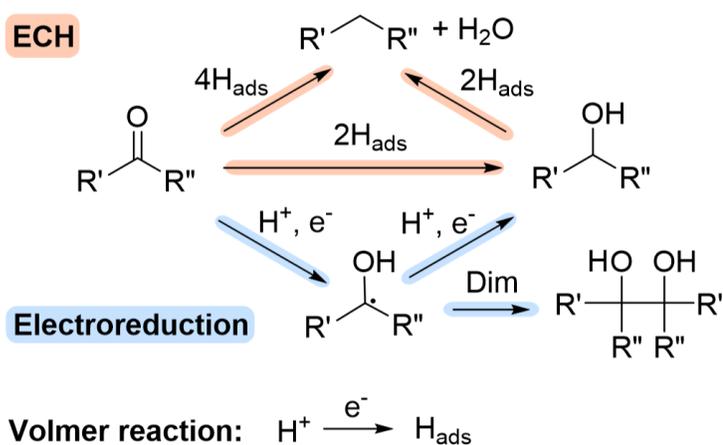
A significant challenge of performing selective electrocatalytic reductions is the coexistence of direct electroreduction routes (**Scheme 2.1**), in which carbonyls participate in electron transfer at the electrode and protonations occur in solution.[6] The reaction with one H^+/e^- pair generates a radical intermediate ($C^\bullet$–OH), which may either dimerize through C–C coupling with a second radical, or be further converted by another H^+/e^- to yield the alcohol product.[6] Alternatively, equal amounts of aldehydes and alcohols may be formed by the disproportionation of $C^\bullet$–OH. The preference for ECH or electroreduction routes is largely determined by the relative potentials required for H_{ads} and $C^\bullet$–OH formation. As a result, ECH is strongly preferred on low hydrogen overpotential electrodes (e.g. platinum-group metals), whereas electroreduction is preferred on high hydrogen overpotential electrodes such as Pb, Hg, Cd, and graphite.[1] However, the two routes may

be in competition on electrodes with intermediate hydrogen overpotentials (e.g., Ni, Co, Fe, Cu, Ag and Au), which is a complicating factor for mechanistic studies. In particular, it is not straightforward to determine the pathway of alcohol formation, which may occur through either ECH or electroreduction routes.

Biomass-derived oxygenates have the potential to replace fossil resources as feedstocks for the sustainable production of fuels and chemicals.[7-8] Currently, there is significant interest in the electrochemical conversion of furanic compounds such as furfural and 5-hydroxymethylfurfural (HMF), owing to their versatility as platform chemicals for production of polymers, fine chemicals, and biofuels, and their availability from biomass by the acid-catalyzed dehydration of pentose and hexose sugars, respectively.[9-10] In particular, the selective hydrogenation of the aldehyde groups in furfural or HMF generates furfuryl alcohol (FA) or 2,5-bis(hydroxymethyl)furan (BHMF), respectively (**Scheme 2.2**), which are precursors for production of polymers, resins, and chemicals.[11] Selective hydrogenolysis generates 2-methylfuran (MF) or 2,5-dimethylfuran (DMF), which are potential liquid transportation fuels.[12-13] It has been demonstrated that the selectivity to hydrogenation or hydrogenolysis products is influenced by the nature of the catalysts, applied potential or current density, electrolyte pH, and initial reactant concentration.[14-20] However, much of the recent literature has focused on proof-of-concepts, and there remain understanding gaps between reaction conditions, underlying mechanisms, and observed product selectivity. Notably, it remains unclear whether hydrogenations occur by H_{ads} at the electrode surface (ECH) or by H^+ in solution (electroreduction).[9, 18]

Scheme 2.2. Key hydrogenation and hydrogenolysis products of furfural and HMF.
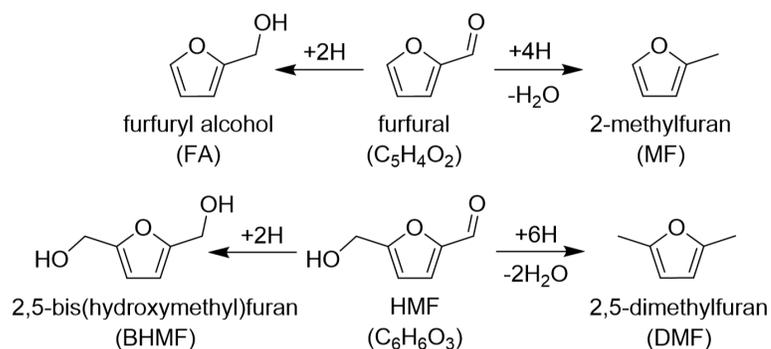
Herein, we investigate the mechanisms for electrochemical reduction of the aldehyde functionality of furfural in acidic electrolytes in order to elucidate the interplay between ECH and electroreduction routes, and their effects on observed product selectivities. Cu was selected as the electrode material because of its unique ability to generate hydrogenolysis products with high selectivity.[14] We demonstrate that both the ECH and electroreduction mechanisms are operable on Cu, leading to formation of FA, MF, and the dimer product hydrofuroin. Electrochemical measurements on electrodes modified with organothiol self-assembled monolayers (SAMs) provide strong evidence that hydrogenation and hydrogenolysis reactions require direct chemical interaction with the electrode surface, whereas hydrofuroin formation is relatively insensitive to the nature of surface. Moreover, observed H/D isotope effects, behavior under proton mass-transport-limited conditions, and a comparative study with a high hydrogen overpotential Pb electrode indicate that H_{ads} is required for hydrogenation and hydrogenolysis reactions, namely by the ECH mechanisms. A pathway study reveals that further reduction of FA to MF is not a significant contribution to the MF observed during the electrolysis of furfural, and instead those products are likely formed by parallel reactions. Finally, the reactions are

manipulated by applying knowledge of the underlying mechanisms and tuning reaction conditions to promote selective formation of important chemicals for biobased polymers and fuels synthesis. The techniques used in this work to distinguish different mechanisms are not uniquely applicable to furfural reduction, and can potentially be extended to study other important electrochemical reductions.

2.2   Experimental Details

2.2.1   Chemicals and Materials

Furfural (99%), furfuryl alcohol (98%), 2-methylfuran (99%), 3-mercaptopropionic acid (99%), 2-mercaptobenzothiazole (99%), 12-mercaptododecanoic acid (96%), sulfuric acid-d3 (95–98%, 99.5 atom% D), deuterium oxide (D_2O, 99.9 atom% D), and sodium sulfate (99%), were purchased from Sigma Aldrich. Acetonitrile (CH_3CN, 99.9% "HPLC grade"), 2-propanol (99.9%), hydrochloric acid (37%), sulfuric acid (98%), and buffer standard solutions (pH 4.00 and 7.00) were purchased from Fisher Scientific. Acetonitrile-d3 (99.8 atom% D) was obtained from Cambridge Isotope Laboratories, Inc. Water was deionized (18.2 MΩ·cm) with a Barnstead E-Pure™ purification system and used to prepare all electrolytes. Typical electrolytes were 0.5 M sulfuric acid (pH 0.5) or 0.5 M sulfate solutions (pH 1.4–3.0) with 25% v/v CH_3CN cosolvent. Electrolytes in deuterated solvents were prepared with D_2SO_4, adjusted to the desired pD according to the widely accepted formula[21]: pD = pH* + 0.40, in which pH* is the reading measured in D_2O solution with a pH meter calibrated in conventional aqueous buffers.

2.2.2 Electrochemical Measurements

Electrochemical measurements were performed with a Bio-Logic SP-300 electrochemical workstation. A double-junction Ag/AgCl (Pine Research Instrumentation) and a graphite rod (Pine Research Instrumentation) were used as the reference and counter electrodes, respectively. The reference electrode was calibrated against a reversible hydrogen electrode (RHE, eDAQ) and all potentials herein are reported on the RHE reference scale. Electrolyte pH was measured with a handheld pH meter (Hanna HI98103) calibrated in standard aqueous buffer solutions. Solution resistance between working and reference electrodes was measured by potentiostatic electrochemical impedance spectroscopy and compensated (85%) by the electrochemical workstation.

Cyclic voltammetry was performed on a Cu rotating disk electrode (RDE, 5.0 mm diameter, Pine Research Instrumentation) at 2500 rpm. The RDE was polished with an alumina suspension (0.3 µm, Allied High Tech Products, Inc.) on a microcloth polishing disk (Buehler) and cleaned with deionized water in an ultrasonic bath before each use. The electrolyte was purged with nitrogen gas before and during measurements. Cyclic voltammograms were collected using a 50 mV s^{-1} sweep rate.

Preparative electrolysis was performed in an H-cell reactor with anode and cathode chambers separated by a Nafion® 212 proton exchange membrane (PEM). Cathode electrolyte was purged with argon gas (99.999%, Airgas, Inc.) throughout the reaction to remove dissolved gases and evolved H_2, and to strip the volatile product MF into a two-chamber cold trap filled with CH_3CN and cooled to –10 °C. Cu foils (0.127 mm thick, 99.9%, Alfa Aesar) were used as electrodes for preparative electrolysis immediately after pretreatment by a cleaning sequence of 2-propanol, deionized water, dilute hydrochloric

acid, and deionized water. Pb foils (0.76 mm thick, 99.8%, Alfa Aesar) were mechanically polished with 600 grit sandpaper and cleaned with laboratory tissue. Unless noted otherwise, the exposed geometric surface area of electrodes was maintained at 5.0 cm^2, accounting for both the front and back sides. Preparative electrolysis was performed in 20 ml of aqueous electrolyte containing 0.5 M sulfuric acid (approximately pH 0.5) or 0.5 M sulfate solutions (pH 1.4–3.0) with 25% v/v CH$_3$CN cosolvent and stirred at 1000 rpm with a magnetic stir bar. For studying the effect of furfural initial concentration, a short reaction time of 30 min was used to make comparisons at low degrees of conversion and relatively constant bulk furfural concentrations. All reactions were performed at room temperature (23 ± 1 °C).

2.2.3   Product Analysis

After preparative electrolysis reactions, liquid aliquots were collected from the reactor chamber and cold trap and diluted in water or CH$_3$CN for analysis by high pressure liquid chromatography (HPLC). Hydrogen gas was quantified with a gas chromatograph connected to the outlet of the cold trap. Hydrofuroin (1,2-di(furan-2-yl)ethane-1,2-diol) was identified by ^{1}H NMR and mass spectrometry (MS), and quantified by HPLC. Two isomers of hydrofuroin are reported together for simplicity. Product analysis details and calculations of selectivity and faradaic efficiency are included in Supporting Information.

2.3   Results and Discussion

2.3.1   Distinguishing ECH and Electroreduction Mechanisms

The first challenge in bridging the understanding gaps between mechanisms, reaction conditions, and product selectivity for the electrochemical reduction of carbonyl groups is to clarify which mechanisms are responsible for hydrogenation, hydrogenolysis, and

hydrodimerization products. Electrodes modified with SAMs of organothiols were employed to experimentally determine the nature of electrode processes responsible for formation of each product. ECH involves strong interaction of reacting species with the electrode surface and requires H_{ads} as the hydrogen source. The electron transfer (ET) for H_{ads} formation is defined as an inner-sphere electrode process, and as such is highly dependent on the electrode surface properties.[5] However, for the electroreduction mechanism, protonations occur in solution, and the heterogeneous ET may proceed by either inner-sphere or outer-sphere processes. Outer-sphere reactions do not require strong interactions between reactants and the electrode surface and ET occurs by electron tunneling.[22-23] Therefore outer-sphere reactions are generally less dependent on the nature of the electrode material. Organic SAMs inhibit inner-sphere ET and ECH reactions by preventing free diffusion of electroactive species and their direct access to the electrode surface, but have only a small effect on outer-sphere ET rates if the layers are sufficiently thin for facile electron tunneling.[24-26] For the electroreduction pathway, the reduction of furfural is expected to be unaffected by such SAM-modifications if it occurs by an outer-sphere ET process.

Three organothiols that readily form compact SAMs on Cu[27-31] were selected to modify the electrodes: two carboxyl-terminated alkanethiols with different chain lengths (C3 and C12), namely 3-mercaptopropionic acid (MPA) and 12-mercaptododecanoic acid (MDA) and the heterocyclic 2-mercaptobenzothiazole (MBT). Electron tunneling resistance has an exponential dependence on tunneling distance, which is determined by the molecular length of the SAMs.[32] As a result, outer-sphere ET processes are suppressed on surfaces blocked by long-chain linear alkanethiols (e.g. MDA, C12) SAMs, whereas they are

essentially unaffected on surfaces blocked by short-chains (e.g. MPA, C3).[24] Furthermore, SAMs of conjugated molecules like MBT may be particularly effective at blocking surface sites and inner-sphere ET, while still allowing electron tunneling (outer-sphere ET).[33-36]
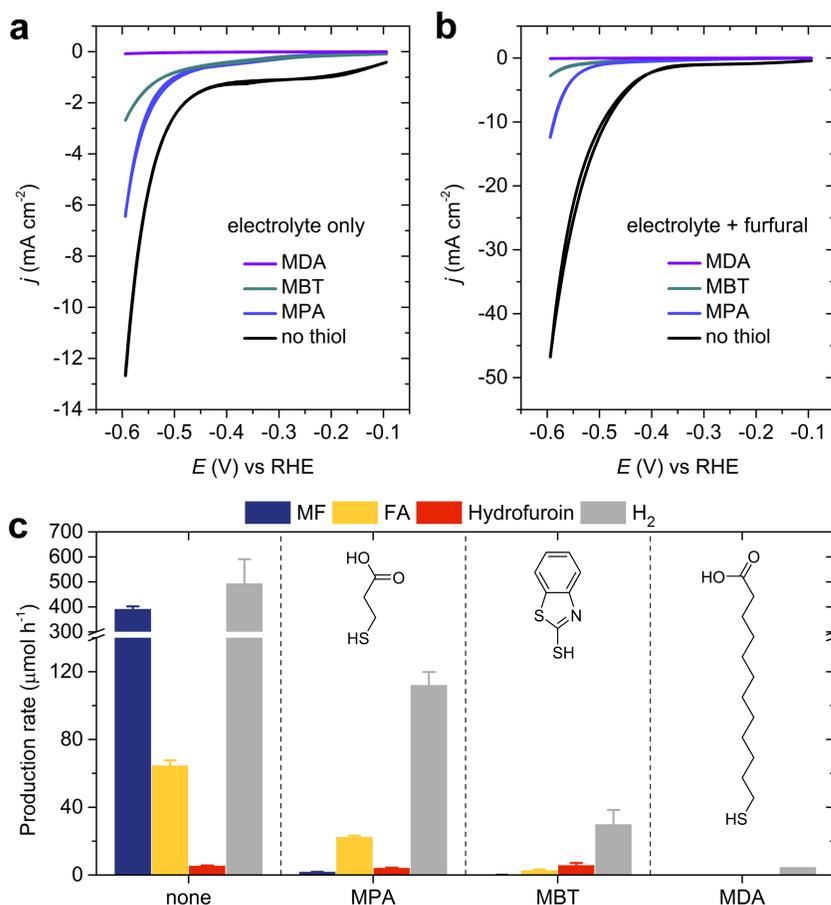
Figure 2.1. (a) Cyclic voltammograms in 0.5 M H_2SO_4 with or without the addition of 0.25 mM MPA, MBT, or MDA and (b) with 0.05 M furfural on a Cu RDE. (c) Observed production rates during preparative electrolysis of furfural on Cu, Cu-MPA, Cu-MBT, and Cu-MDA electrodes. Conditions: 0.05 M furfural and 0.25 mM of the indicated organothiol, pH 0.5 electrolyte, 1 h duration, $E = -0.55$ V.

HER can serve as a probe reaction to evaluate the quality of the SAMs and their effectiveness to inhibit ET.[37-38] Cyclic voltammetry revealed a significant decrease in HER

and double-layer charging (capacitive) currents on thiol-modified Cu electrodes (**Figure 2.1a**), indicating that the SAMs inhibited access to electrochemically-active Cu surface sites. The degree of current suppression was in the order of MPA < MBT ≪ MDA, with MDA nearly completely blocking both faradaic and non-faradaic processes. Longer-chain thiols, such as MDA, assemble into complete and impenetrable SAMs owing to their stronger van der Waals intermolecular attractions,[39] and as noted above their SAMs are of sufficient thickness to inhibit electron tunneling. Layers of MPA and MBT would be expected to completely suppress inner-sphere reactions, so the fact that HER current was observed suggests that those films are incomplete or contain pinhole defects which allow access to some active metal sites. MBT was more effective at inhibiting HER than MPA, likely owing to the stronger intermolecular attractions of its aromatic structure.[40] The same trend of current suppression was observed in the presence of furfural (**Figure 2.1b**), demonstrating that the thiol-modified electrodes also reduced the overall rate of furfural reduction.

Constant-potential preparative electrolysis of furfural conducted in 0.5 M H_2SO_4 electrolyte confirmed that both furfural reduction and HER were inhibited by the SAMs. Moreover, the distribution of furfural reduction products was very sensitive to surface modifications, as shown in **Figure 2.1c**. FA and MF production rates were severely suppressed on thiol-modified electrodes; for example, FA decreased from 64.5 to 2.7 μmol h^{-1} and MF decreased from 391.0 to <0.1 μmol h^{-1} on Cu-MBT compared to unmodified Cu. Similar results were obtained in a pH 3.0 electrolyte, in which FA and MF were both suppressed on SAM-modified electrodes (**Figure S2.4**). Only trace amounts of furfural reduction products or H_2 were detected on the MDA-Cu electrode, confirming that C12

thiol SAMs block nearly all the electrode reactions. These results indicate that hydrogenation and hydrogenolysis pathways to FA and MF require direct interaction of reactants with the Cu surface. In contrast, hydrofuroin formation rate was remarkably unchanged on MPA-Cu (decreased 24%) and MBT-Cu (increased 6.1%) compared to the unmodified Cu, strongly suggesting that the first e$^-$ transfer of the electroreduction pathway may occur through outer-sphere ET, which does not require specific adsorption of furfural or H.

Electrochemical experiments performed with H/D isotopically substituted solvents and electrolytes were performed to further elucidate the mechanisms of furfural hydrogenation and hydrogenolysis. Kinetic isotopic effects (KIE) have been observed for HER on many electrode materials, including Cu, where the kinetics (i.e. exchange current density) of HER are greater than deuterium evolution reaction (DER).[41] This is exemplified by the cathodic shift between the HER/DER waves (e.g. 87 mV at 10 mA cm^{-2}) in deuterated electrolytes, shown in **Figure 2.2a**. A normal KIE is also expected for the ECH mechanism, which shares a common step with HER (Volmer reaction) and also involves reactions with H$_{ads}$. The voltammograms in **Figure 2.2b** show that furfural reduction experiences a KIE, and that its magnitude is similar to HER (e.g. 98 mV shift at 10 mA cm^{-2}). Production rates for MF and FA determined by preparative electrolysis at –0.55 V decreased by 95.6% and 21.5% in pD 0.5 electrolyte, respectively, compared to pH 0.5 (**Figure 2.2c**). We rationalize that the relatively minor decrease in FA rate compared to MF is attributed to a selectivity change from MF to FA under deuterated conditions. Analogous experiments performed at pH 3.0, a condition at which FA is the major product, showed that the production rates for both MF and FA were significantly decreased (47.1% and 76.6%,

respectively) in D-electrolyte compared to H-electrolyte. In contrast, the rate of hydrofuroin production actually increased in D-electrolyte compared to H-electrolyte at both pH (or pD) conditions, which may be a result of an equilibrium-shift for a preceding homogeneous reaction (e.g. protonation) due to thermodynamic isotope effects.[42] These results are consistent with the behavior expected if MF and FA are from ECH reactions and hydrofuroin is from electroreduction, and therefore are in agreement with the study on thiol-modified electrodes.
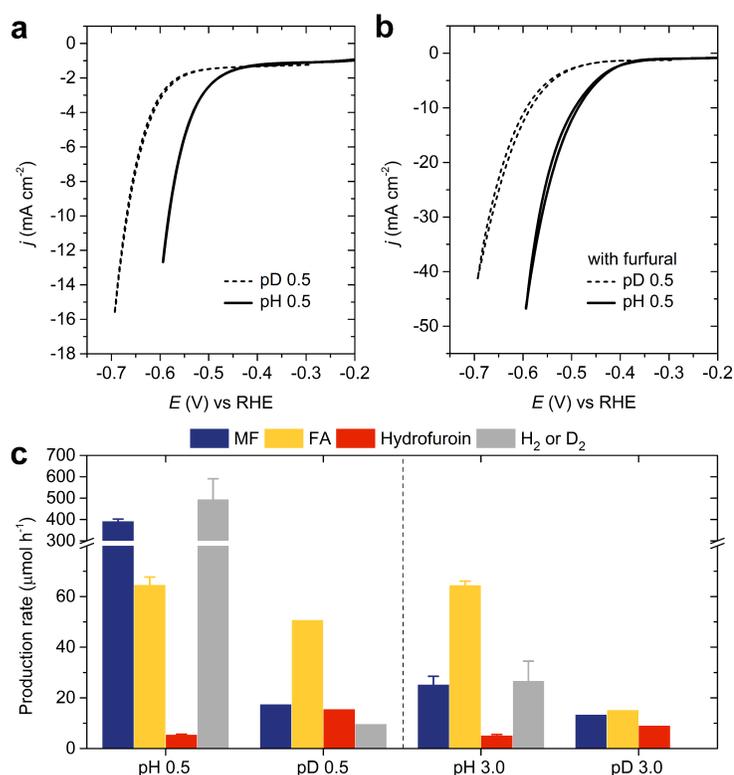
Figure 2.2. (a) Cyclic voltammograms in 0.5 M H_2SO_4/H_2O (pH 0.5) or D_2SO_4/D_2O (pD 0.5) and (b) with 0.05 M furfural on a Cu RDE. (c) Observed production rates during preparative electrolysis of furfural on Cu electrodes in H- or D- electrolytes. Conditions: 0.05 M furfural, 1 h duration, $E = -0.55$ V.

ECH and electroreduction mechanisms can be further distinguished by studying furfural reduction under a special case of mass-transport-limited conditions. The rates of reactions which consume protons at the electrode/electrolyte interface (e.g. HER and ECH) can become completely mass-transport-limited in mildly acidic conditions at moderate current densities, owing to the low bulk proton concentrations. This is shown by the rotating-disk voltammogram in **Figure 2.3a**, in which the rate of HER plateaus to a mass-transport-limited current density ($j_{l,HER}$) of –20.9 mA cm^{-2} in a pH 3.0 electrolyte. Similarly, ECH reactions consume interfacial protons through the Volmer reaction ($H^+ + e^- \rightarrow H_{ads}$). Consequently, if furfural reduction proceeds solely by ECH, it would also be subject to proton transport limitations and its rate would be limited accordingly. In contrast, if furfural reduction proceeds only by electroreduction, in which protonations occur in the bulk solution, its rate would not be limited by proton transport to the electrode surface. This has been demonstrated for the similar case of benzaldehyde electroreduction, for which the mass-transport-limited current was proportional to substrate concentration, even in very mild acidic conditions (i.e. pH 5.2).[43] Preparative electrolysis results (**Figure 2.3b**) show that H$_2$, FA, MF, and hydrofuroin formation accounted for 11.6%, 44.8%, 26.9%, and 4.9% of the total current at –0.75 V, a potential within the transport-limited region under electrolysis conditions (**Figure S2.6**). Assuming that FA and MF are from ECH reactions and hydrofuroin is from electroreduction, this would indicate that the vast majority of the total current should be subject to proton transport limitations (i.e. 83.3% to H$_2$, FA, and MF), while a minor fraction would not (i.e. 4.9% to hydrofuroin). **Figure 2.3a** shows that mass-transport-limited furfural reduction currents were remarkably similar to $j_{l,HER}$, and increased only slightly as furfural concentration was increased (e.g. +5.2% difference with

0.04 M furfural). Therefore, the comparison between mass-transport-limited currents for HER and furfural reduction is very consistent with the proposal that FA and MF are products of ECH and hydrofuroin is from electroreduction. Moreover, **Figure 2.3b** shows that the product distribution was nearly identical at lower potentials (e.g. –0.55 V), which is evidence that these mechanisms are applicable within the potential range of interest.
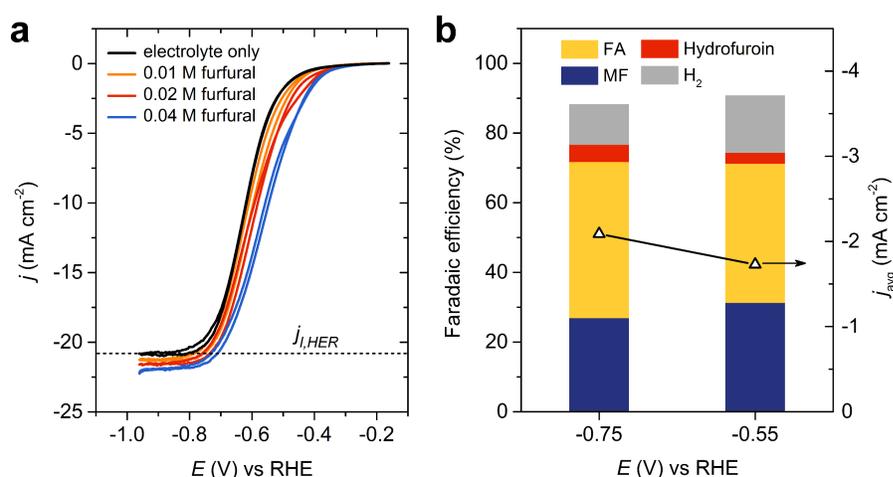
Figure 2.3. (a) Cyclic voltammograms at pH 3.0 with various furfural concentrations recorded on a Cu RDE. Baseline correction was performed to remove the contribution of double-layer charging currents. (b) Faradaic efficiency to furfural reduction products and H_2 measured from preparative electrolysis. Conditions: pH 3.0 electrolyte, 0.05 M furfural, 1 h duration.

Additional mechanistic insight may be gained by comparing Cu to a different electrode material on which direct electroreduction mechanisms are known to dominate. Pb electrodes are commonly used to perform electroreductions without competition from interfering reactions (e.g. HER or electrocatalytic reactions), owing to their weak hydrogen adsorption properties.[44] In fact, the onset potential for furfural reduction on Pb is more than

400 mV more positive than HER (**Figure S2.7**), indicating that H_{ads} does not participate in furfural reduction mechanisms. Hydrofuroin was the major detected product from preparative electrolysis at –0.55 V on Pb, corresponding to faradaic efficiencies of 34% and 38% at pH 0.5 and pH 3.0, respectively (**Figure 2.4**). On the other hand, no H_2 or MF, and very little FA (<2% faradaic efficiency), were detected under these conditions. A resinous precipitate in the reactor and unidentified peaks in the product chromatographs were observed which were not identified or quantified in this work, but likely contributed to the low total faradaic efficiencies to detected products. Such products have been previously observed during electrochemical furfural reduction,[16, 45] and may be other dimer or oligomer byproducts of electroreduction reactions.[46] **Figure 2.4** also shows that the products observed on Pb were distinctly different than Cu, on which FA and MF were the main products. This result is further evidence that FA and MF formation requires H_{ads} and occurs through ECH mechanisms on Cu.
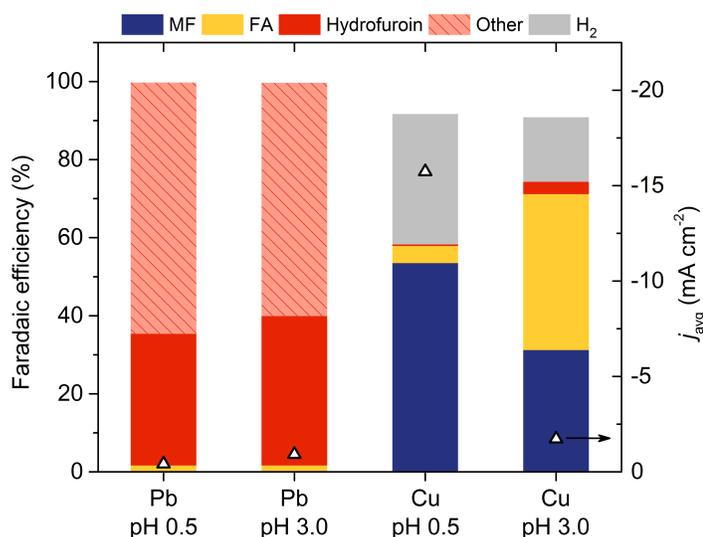
Figure 2.4. Comparison of furfural preparative electrolysis in pH 0.5 or pH 3.0 electrolytes on Pb or Cu electrodes. Conditions: 0.05 M furfural, 1 h duration; E = –0.55 V.

2.3.2 Reaction Pathways

It has been previously implied that MF is a secondary product of furfural reduction on Cu, with FA formed as an intermediate under electrochemical conditions.[14, 16, 19] This would suggest that ECH product selectivity can be tuned by varying the extent of reaction, with MF preferred at high conversion after subsequent hydrogenolysis of FA. In clear contradiction, we found that FA and MF selectivities were remarkably constant with respect to reaction duration and degree of furfural conversion (**Figure 2.5a**), which suggests that the two products are mainly generated from parallel, not consecutive reactions, on Cu electrodes.

The cyclic voltammogram of FA was nearly identical to that of the blank electrolyte, which suggests that HER was the dominant electrode reaction in the presence of FA (**Figure 2.5b**). Preparative electrolysis of FA resulted in *ca.* 100% efficiency to HER at – 0.55 V at both pH 0.5 and 3.0 on the Cu electrode, whereas only a negligible amount of MF was detected corresponding to <1% efficiency (**Figure 2.5c**). An initial FA concentration of 0.01 M was chosen to represent typical bulk concentrations present during furfural reduction. These results indicate that hydrogenolysis of FA is very slow under these conditions; therefore, the large amount of MF produced during furfural reduction is generated in parallel with FA, rather than from the decoupled sequential reduction of FA product.
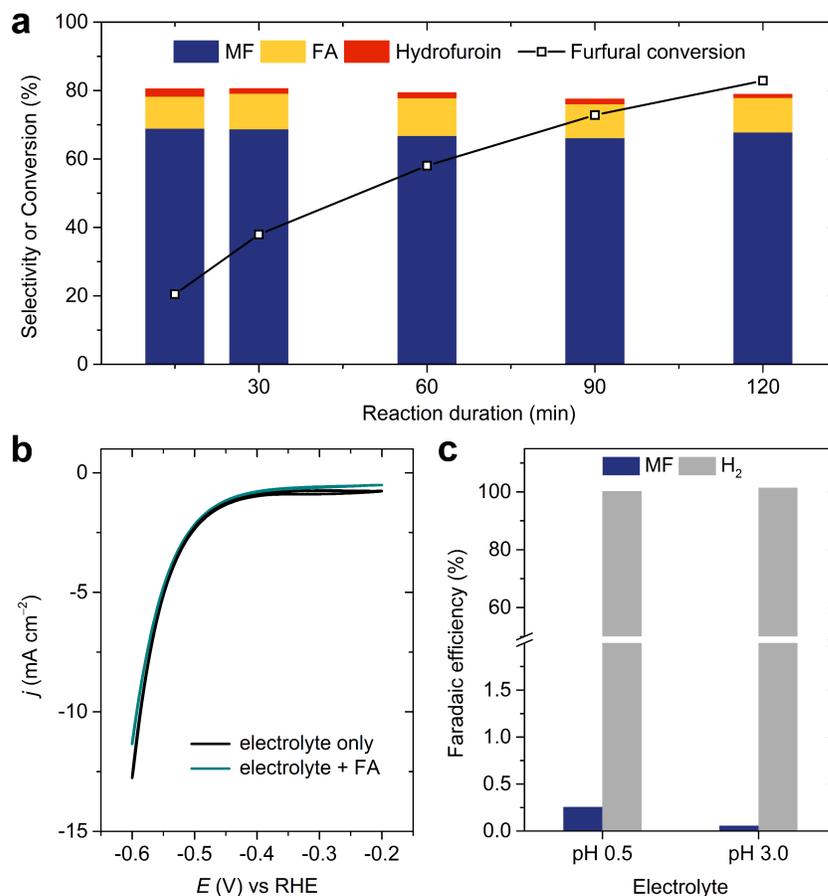
Figure 2.5. (a) Conversion and selectivity over time during the preparative electrolysis on Cu. Conditions: 0.05 M furfural, pH 0.5 electrolyte, $E = -0.55$ V. Each bar represents an independent experiment. (b) Cyclic voltammograms in 0.5 M H_2SO_4 with or without 0.01 M FA recorded on a Cu RDE. (c) Faradaic efficiency to MF and H_2 during the preparative electrolysis of 0.01 M FA performed on Cu. Conditions: pH 0.5 or 3.0 electrolyte, 1 h duration, $E = -0.55$ V.

Insight into feasible pathways for MF formation which bypass the FA intermediate was obtained by Shi et al. who explored the catalytic conversion of furfural to FA and MF on Cu(111) surfaces on the basis of density functional theory (DFT) calculations.[47] They found that H addition or decomposition pathways of the preferred monohydrogenated

alkoxyl intermediate (C_4H_3O–CH_2O) had similar energy barriers (1.17 and 1.18 eV, respectively) and thermodynamic free energy changes (0.24 and 0.33 eV, respectively), and therefore parallel routes to FA or MF through this intermediate should be competitive. Comprehensive DFT modeling of furfural conversion under electrochemical conditions and *in situ* spectroscopy should be focuses of future work to confirm the pathway.

2.3.3 Impact of Reaction Conditions

The efficiency and selectivity of furfural reduction can be manipulated by applying knowledge of the underlying mechanisms to rationally choose experimental conditions such as electrode potential, reactant concentration, and electrolyte pH. The faradaic efficiency for furfural reduction is determined by its kinetic competition with HER. It is generally accepted that HER on Cu occurs by the Volmer-Heyrovsky mechanism,[5] shown in Equations 1–2 for acidic electrolytes.

$$H^+ + e^- \rightarrow H_{ads} \tag{1}$$

$$H_{ads} + H^+ + e^- \rightarrow H_2 \tag{2}$$

The present work provides strong evidence that FA and MF are produced by ECH reactions through parallel hydrogenation and hydrogenolysis pathways. Accordingly, their formation rates will be dependent on the surface coverages of both H_{ads} and furfural adsorbates.[3] The surface coverage of H_{ads} is determined by the relative kinetics of its adsorption and desorption (Equations 1–2), which are potential-dependent electrochemical reactions, as well as the non-electrochemical reaction between furfural adsorbates and H_{ads}. Therefore, the rate of ECH will depend on potential and other factors which influence H_{ads} and furfural adsorbate coverage, including furfural concentration and electrolyte pH.

Hydrofuroin formation *via* the electroreduction mechanism does not involve H$_{ads}$, however its formation is also dependent on potential, substrate concentration, and electrolyte pH.[48] Furthermore, it was shown in this work that the ET preceding dimerization can occur by an outer-sphere process, and is not sensitive to the presence of surface adsorbates.
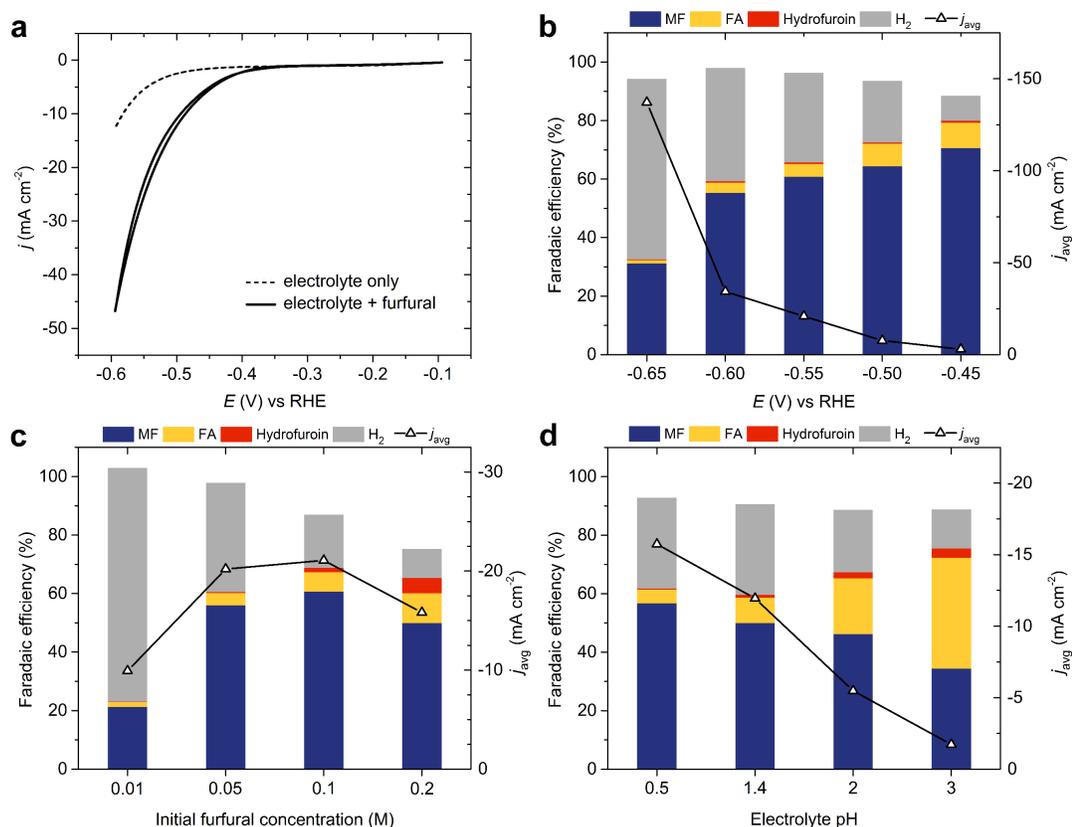
Figure 2.6. (a) Cyclic voltammograms in 0.5 M H$_2$SO$_4$ with or without 0.05 M furfural on a Cu RDE. (b) Preparative electrolysis of furfural at varying cathode potentials. Conditions: 0.05 M furfural, pH 0.5 electrolyte, 144 C charge transferred, electrode area was 2.5 cm^2 for –0.6 and –0.65 V. (c) Preparative electrolysis of furfural with various initial furfural concentration. Conditions: pH 0.5 electrolyte, 30 min duration, $E = -0.55$ V (d) Preparative electrolysis of furfural with electrolyte pH 0.5–3.0. Conditions: 0.05 M furfural, 1 h duration, $E = -0.55$ V.

The onset potential of furfural reduction on Cu is about –0.35 V, as shown by the increased cathodic current in the presence of furfural compared to HER (**Figure 2.6a**). Preparative electrolysis was performed at constant potentials ranging from –0.45 V to –0.65 V. **Figure 2.6b** shows that FA and MF were the dominant furfural reduction products over the evaluated potential range, indicating that there was sufficient H_{ads} on the electrode surface for the ECH mechanism to dominate under these conditions (i.e. pH 0.5, initial furfural concentration 0.05 M). Accordingly, hydrofuroin formation *via* the electroreduction mechanism was minor, with typically less than 2% faradaic efficiency. The total current density increased at more negative potentials, however, faradaic efficiency to furfural reduction decreased significantly, corresponding to an increase in H_2 production. The rate of the Volmer reaction (Equation 1) is enhanced at more negative potentials, resulting in a greater total availability of H_{ads} for HER or ECH. However, HER will outpace ECH at more negative potentials because the rate constant of the Heyrovsky reaction (Equation 2) increases exponentially with potential, whereas the reaction between furfural adsorbates and H_{ads} is non-electrochemical and the rate constant is potential-independent. Cathode potential also influenced the ECH selectivity, with the preference for MF more pronounced at increasingly negative potentials, as seen qualitatively by the relative faradaic efficiencies of MF and FA in **Figure 2.6b**. Electrode potential regulates the charge transfer kinetics, surface states, and stability of adsorbed species, and therefore can have significant influence on the selectivity of complex multistep reactions.[49]

The influence of initial furfural concentration was evaluated over the range of 0.01 to 0.2 M in a pH 0.5 electrolyte. **Figure 2.6c** shows that the competition between furfural reduction and HER was highly dependent on furfural concentration, evidenced by the

decrease in FE_{HER} from 80.0% to 9.9% over the evaluated concentration range. Increasing

bulk furfural concentrations generally facilitated higher surface coverage of furfural

adsorbates, and consequently enhanced rates of ECH reactions forming FA and MF.

Conversely, the rate of HER was decreased owing to the increased competition for

available H_{ads}. Interestingly, the ECH rate actually decreased when furfural concentration

was further increased from 0.1 M to 0.2 M, indicating that the electrode surface became

oversaturated with furfural-related adsorbates. In contrast, the rate of hydrofuroin

formation, which does not require H_{ads}, increased steadily over the range of furfural

concentrations. Additionally, the selectivity of ECH reactions was sensitive to furfural

concentration, as the molar ratio of MF to FA products decreased from *ca.* 6.2 at 0.01 M

to 2.4 at 0.2 M furfural concentration. Unidentified products were also observed after tests

in which greater hydrofuroin formation occurred (e.g. 0.1 and 0.2 M furfural), and likely

contributed to the lower total faradaic efficiencies at those conditions, similarly to the

previously mentioned results of furfural reduction on Pb electrodes.

Varying electrolyte pH had a significant effect on the selectivity and efficiency of

furfural reduction, as shown by the preparative electrolysis results at –0.55 V in **Figure

2.6d**. The different pH conditions were compared at a constant potential versus the pH-

corrected RHE reference scale in order to account for the change in equilibrium reduction

potentials with electrolyte pH. Even so, the rates of HER and ECH decreased notably with

increasing electrolyte pH, which can be rationalized by considering mass transport effects.

HER and ECH consume protons at the electrode/electrolyte interface and can become

mass-transport-limited if proton transport from the bulk solution is insufficient, as is the

case in mildly acidic electrolytes (e.g. pH 3.0, see **Figure S2.6**). In contrast, the rate of

hydrofuroin formation, which does not require surface hydrogen, was not significantly affected by pH. The increased faradaic efficiency to hydrofuroin at higher pH can be attributed to the lower relative contributions from ECH and HER. The preference to FA or MF was very sensitive to changes in electrolyte pH, which suggests that the electrocatalytic hydrogenation and hydrogenolysis pathways may have different pH dependences. MF was preferred at low pH, whereas FA was the major product at pH 3.0 (FA/MF molar ratio = 2.6). It has been previously suggested that the ratio of hydrogenation and hydrogenolysis products of ECH reactions is sensitive to the presence of metal ions, such as Na^+, in electrolytes.[50] However, this effect is unlikely to explain the present results because the same selectivity trends were observed when H_2SO_4/Na_2SO_4 electrolytes were replaced with dilute H_2SO_4 electrolytes (**Figure S2.5**). The increased selectivity to FA at higher pH may be a result of the lower relative availability of H_{ads} compared to furfural adsorbates. As previously discussed, the rates of HER and ECH reactions decreased at higher pH owing to limited availability of protons at the electrode/electrolyte interface. It is plausible that the hydrogenation pathway to FA, which requires two H_{ads}, and the hydrogenolysis pathway to MF in which four H_{ads} participate could be sensitive to the relative availability of H_{ads} and furfural adsorbates. This explanation would also be consistent with the initial concentration study (**Figure 2.6c**), in which MF was more favorable at lower furfural concentrations, which facilitate higher coverage of H_{ads} relative to furfural adsorbates. However, without direct analysis of surface species the exact nature of this selectivity change remains a focus for future investigations.

2.4   Conclusions

The electrochemical reduction of furfural in acidic electrolytes was explored with the goals of distinguishing mechanisms of product formation and bridging understanding gaps between mechanisms, reaction conditions, and product selectivity. Electrodes modified with organothiol SAMs were utilized to determine the requirement for direct reactant-electrode interactions, and the nature of heterogeneous ET responsible for formation of hydrogenation, hydrogenolysis, and hydrodimerization products. FA and MF formation were inhibited on electrodes modified with MPA and MBT, which indicates those processes require direct interaction with the electrode surface. In comparison, hydrofuroin formation was unaffected, which suggests that the first electron transferred in the electroreduction mechanism, prior to dimerization, is an outer-sphere process and is therefore insensitive to the electrode surface properties or catalytic activity. Production rates of FA and MF exhibited a strong H/D isotope effect, which strongly suggests they are formed through the ECH mechanism by a reaction with electrochemically adsorbed H (or D). An investigation of furfural reduction under proton mass-transport-limited conditions by RDE voltammetry confirmed that MF and FA formation consume protons at the electrode/electrolyte interface, consistent with the ECH mechanism. A comparison of the products formed on a Cu electrode to those formed on a high hydrogen overpotential Pb electrode provided additional evidence that MF and FA formation requires H_{ads}, through the ECH mechanisms. A pathway study revealed that hydrogenation and hydrogenolysis products, FA and MF, are formed mainly through parallel reactions, in which FA is not a major intermediate for MF formation. Finally, understanding of the underlying mechanisms enabled the manipulation of electrochemical furfural reduction by rationally

tuning the electrode potential, electrolyte pH, and furfural concentration to promote selective formation of important chemicals for bio-based polymers and fuels production. Collectively, these studies highlight the decisive role that reaction conditions play in determining the selectivity of ECH reactions of bioderived oxygenates to hydrogenation or hydrogenolysis products, and the competition between ECH, electroreduction, and HER pathways.

2.5   Acknowledgements

2.6   References

[1] Lessard, J., Electrocatalytic Hydrogenation. In *Organic Electrochemistry*, 5th ed.; Hammerich, O.; Speiser, B., Eds. CRC Press: Boca Raton, FL, 2015; pp 1658-1664.

[2] Coche, L.; Moutet, J.-C., Electrocatalytic Hydrogenation of Organic Compounds on Carbon Electrodes Modified by Precious Metal Microparticles in Redox Active Polymer Films. *J. Am. Chem. Soc.* **1987,** *109*, 6887–6889.

[3]   Chapuzet, J. M.; Lasia, A.; Lessard, J., Electrocatalytic Hydrogenation of Organic Compounds. In *Electrocatalysis*, Lipkowski, J.; Ross, P. N., Eds. Wiley-VCH: New York, 1998; pp 155–159.

[4]   Suastegui, M.; Matthiesen, J. E.; Carraher, J. M.; Nacu Hernandez; Quiroz, N. R.; Okerlund, A.; Cochran, E. W.; Shao, Z.; Tessonnier, J.-P., Combining Metabolic Engineering and Electrocatalysis: Application to the Production of Polyamides from Sugar. *Angew. Chem. Int. Ed.* **2016,** *55*, 2368–2373.

[5]   Schmickler, W.; Santos, E., Hydrogen reaction and electrocatalysis. In *Interfacial Electrochemistry*, 2nd ed.; Schmickler, W.; Santos, E., Eds. Springer-Verlag: Berlin Heidelberg, 2010; pp 163–164.

[6]   Ludvík, J., Reduction of Aldehydes Ketones and Azomethines. In *Organic Electrochemistry*, 5th ed.; Hammerich, O.; Speiser, B., Eds. CRC Press: Boca Raton, FL, 2015; pp 1202–1205.

[7]   Jiang, Y.; Wang, X.; Cao, Q.; Dong, L.; Guan, J.; Mu, X., Chemical Conversion of Biomass to Green Chemicals. In *Sustainable Production of Bulk Chemicals*, 1st ed.; Xian, M., Ed. Springer: Dordrecht, 2016; p 19.

[8]   Chheda, J. N.; Huber, G. W.; Dumesic, J. A., Liquid-Phase Catalytic Processing of Biomass-Derived Oxygenated Hydrocarbons to Fuels and Chemicals. *Angew. Chem. Int. Ed.* **2007,** *46*, 7164–7183.

[9]   Kwon, Y.; Schouten, K. J. P.; van der Waal, J. C.; de Jong, E.; Koper, M. T. M., Electrocatalytic Conversion of Furanic Compounds. *ACS Catal.* **2016,** *6*, 6704−6717.

[10]   Binder, J. B.; Raines, R. T., Simple chemical transformation of lignocellulosic biomass into furans for fuels and chemicals. *J. Am. Chem. Soc.* **2009,** *131*, 1979–1985.

[11]   Jiang, Y.; Woortman, A. J.; Alberda van Ekenstein, G. O.; Petrović, D. M.; Loos, K., Enzymatic synthesis of biobased polyesters using 2,5-bis(hydroxymethyl)furan as the building block. *Biomacromolecules* **2014,** *15*, 2482–2493.

[12]   Thananatthanachon, T.; Rauchfuss, T. B., Efficient production of the liquid fuel 2,5-dimethylfuran from fructose using formic acid as a reagent. *Angew. Chem. Int. Ed.* **2010,** *49*, 6616–6618.

[13]   Bohre, A.; Dutta, S.; Saha, B.; Abu-Omar, M. M., Upgrading Furfurals to Drop-in Biofuels: An Overview. *ACS Sustainable Chem. Eng.* **2015,** *3*, 1263-1277.

[14]   Nilges, P.; Schröder, U., Electrochemistry for biofuel generation: production of furans by electrocatalytic hydrogenation of furfurals. *Energy Environ. Sci.* **2013,** *6*, 2925–2931.

[15]   Roylance, J. J.; Kim, T. W.; Choi, K.-S., Efficient and Selective Electrochemical and Photoelectrochemical Reduction of 5-Hydroxymethylfurfural to 2,5-

Bis(hydroxymethyl)furan using Water as the Hydrogen Source. *ACS Catal.* **2016,** *6*, 1840-1847.

[16] Jung, S.; Biddinger, E. J., Electrocatalytic Hydrogenation and Hydrogenolysis of Furfural and the Impact of Homogeneous Side Reactions of Furanic Compounds in Acidic Electrolytes. *ACS Sustainable Chem. Eng.* **2016,** *4*, 6500–6508.

[17] Kwon, Y.; de Jong, E.; Raoufmoghaddam, S.; Koper, M. T. M., Electrocatalytic hydrogenation of 5-hydroxymethylfurfural in the absence and presence of glucose. *ChemSusChem* **2013,** *6*, 1659–1667.

[18] Kwon, Y.; Birdja, Y. Y.; Raoufmoghaddam, S.; Koper, M. T. M., Electrocatalytic Hydrogenation of 5-Hydroxymethylfurfural in Acidic Solution. *ChemSusChem* **2015,** *8*, 1745–1751.

[19] Li, Z.; Kelkar, S.; Lam, C. H.; Luczek, K.; Jackson, J. E.; Miller, D. J.; Saffron, C. M., Aqueous electrocatalytic hydrogenation of furfural using a sacrificial anode. *Electrochim. Acta* **2012,** *64*, 87–93.

[20] Parpot, P.; Bettencourt, A. P.; Chamoulaud, G.; Kokoh, K. B.; Belgsir, E. M., Electrochemical investigations of the oxidation–reduction of furfural in aqueous medium. *Electrochim. Acta* **2004,** *49*, 397-403.

[21] Glasoe, P. K.; Long, F. A., Use of glass electrodes to measure acidities in deuterium oxide. *J. Phys. Chem.* **1960,** *64*, 188–190.

[22] Bard, A. J.; Faulkner, L. R., *Electrochemical Methods: Fundamentals and Applications*. 2nd ed.; John Wiley & Sons, Inc.: New York, 2001; p 116.

[23] Schmickler, W.; Santos, E., Theoretical considerations of electron-transfer reactions. In *Interfacial Electrochemistry*, 2nd ed.; Schmickler, W.; Santos, E., Eds. Springer-Verlag: Berlin Heidelberg, 2010; p 99.

[24] Xiao, X.; Pan, S.; Jang, J. S.; Fan, F.-R. F.; Bard, A. J., Single Nanoparticle Electrocatalysis: Effect of Monolayers on Particle and Electrode on Electron Transfer. *J. Phys. Chem. C* **2009,** *113*, 14978–14982.

[25] Bard, A. J., Inner-sphere heterogeneous electrode reactions. electrocatalysis and photocatalysis: the challenge. *J. Am. Chem. Soc.* **2010,** *132*, 7559–7567.

[26] Love, J. C.; Estroff, L. A.; Kriebel, J. K.; Nuzzo, R. G.; Whitesides, G. M., Self-assembled monolayers of thiolates on metals as a form of nanotechnology. *Chem. Rev.* **2005,** *105*, 1103−1169.

[27] Tan, Y. S.; Srinivasan, M. P.; Pehkonen, S. O.; Chooi, S. Y. M., Self-assembled organic thin films on electroplated copper for prevention of corrosion. *J. Vac. Sci. Technol. A* **2004,** *22*, 1917-1925.

[28] Arkhipushkin, I. A.; Pronin, Y. E.; Vesely, S. S.; Kazansky, L. P., Electrochemical and XPS study of 2-mercaptobenzothiazole nanolayers on zinc and copper surface. *Int. J. Corros. Scale Inhib.* **2014,** *3*, 78-88.

[29] Woods, R.; Hope, G. A.; Watling, K., A SERS spectroelectrochemical investigation of the interaction of 2-mercaptobenzothiazole with copper, silver and gold surfaces. *J. Appl. Electrochem.* **2000,** *30*, 1209–1222.

[30] Marconato, J. C.; Bulhões, L. O.; Temperini, M. L., A spectroelectrochemical study of the inhibition of the electrode process on copper by 2-mercaptobenzothiazole in ethanolic solutions. *Electrochim. Acta* **1998,** *43*, 771–780.

[31] Täubert, C. E.; Kolb, D. M.; Memmert, U.; Meyer, H., Adsorption of the Additives MPA, MPSA, and SPS onto Cu(111) from Sulfuric Acid Solutions. *J. Electrochem. Soc.* **2007,** *154*, D293–D299.

[32] Wang, W.; Lee, T.; Reed, M. A., Mechanism of electron conduction in self-assembled alkanethiol monolayer devices. *Phys. Rev. B.* **2003,** *68*, 035416-1–035416-7.

[33] Sachs, S. B.; Dudek, S. P.; Hsung, R. P.; Sita, L. R.; Smalley, J. F.; Newton, M. D.; Feldberg, S. W.; Chidsey, C. E. D., Rates of Interfacial Electron Transfer through π-Conjugated Spacers. *J. Am. Chem. Soc.* **1997,** *119*, 10563–10564.

[34] Wold, D. J.; Haag, R.; Rampi, M. A.; Frisbie, C. D., Distance Dependence of Electron Tunneling through Self-Assembled Monolayers Measured by Conducting Probe Atomic Force Microscopy: Unsaturated versus Saturated Molecular Junctions. *J. Phys. Chem. B* **2002,** *106*, 2813–2816.

[35] Cohen, R.; Stokbro, K.; Martin, J. M. L.; Ratner, M. A., Charge Transport in Conjugated Aromatic Molecular Junctions: Molecular Conjugation and Molecule−Electrode Coupling. *J. Phys. Chem. C.* **2007,** *111*, 14893−14902.

[36] Berchmans, S.; Yegnaraman, V.; Rao, G. P., Self-assembled monolayers on electrode surfaces: a probe for redox kinetics. *J. Solid. State. Electrochem.* **1998,** *3*, 52–54.

[37] Malkhandi, S.; Yang, B.; Manohar, A. K.; Prakash, G. K.; Narayanan, S. R., Self-assembled monolayers of n-alkanethiols suppress hydrogen evolution and increase the efficiency of rechargeable iron battery electrodes. *J. Am. Chem. Soc.* **2013,** *135*, 347–353.

[38] Yang, B.; Malkhandi, S.; Manohar, A. K.; Surya Prakash, G. K.; Narayanan, S. R., Organo-sulfur molecules enable iron-based battery electrodes to meet the challenges of large-scale electrical energy storage. *Energy Environ. Sci.* **2014,** *7*, 2753–2763.

[39] Dai, Z.; Ju, H., Effect of chain length on the surface properties of ω-carboxy alkanethiol self-assembled monolayers. *Phys. Chem. Chem. Phys.* **2001,** *3*, 3769-3773.

[40] Zharnikov, M.; Grunze, M., Spectroscopic characterization of thiol-derived self-assembling monolayers. *J. Phys. Condens. Matter* **2001,** *13*, 11333–11365.

[41] Conway, B. E., Kinetics of electrolytic hydrogen and deuterium evolution. *Proc. Royal Soc. A* **1960,** *256*, 128–144.

[42] Ozaki, A., *Isotopic Studies of Heterogeneous Catalysis*. Kodansha Ltd.: Tokyo, 1977; p 183.

[43] Guena, T.; Pletcher, D., Electrosyntheses from Aromatic Aldehydes in a Flow Cell. Part I. The Reduction of Benzaldehyde. *Acta Chim. Scand.* **1998,** *52*, 23–31.

[44] Birkett, M. D.; Kuhn, A. T., The Catalytic Hydrogenation of Organic Compounds - A Comparison Between the Gas-phase, Liquid-phase, and Electrochemical Routes. In *Catalysis*, Bond, G. C.; Webb, G., Eds. The Royal Society of Chemistry: London, 1983; Vol. 6, pp 61–89.

[45] Albert, W. C.; Lowy, A., The Electrochemical Reduction of Furfural. *Trans. Electrochem. Soc.* **1939,** *75*, 367–375.

[46] Zhou, F.; Bard, A. J., Detection of the Electrohydrodimerization Intermediate Acrylonitrile Radical Anion by Scanning Electrochemical Microscopy. *J. Am. Chem. Soc.* **1994,** *116*, 393–394.

[47] Shi, Y.; Zhu, Y.; Yang, Y.; Li, Y.-W.; Jiao, H., Exploring Furfural Catalytic Conversion on Cu(111) from Computation. *ACS Catal.* **2015,** *5*, 4020-4032.

[48] Stradins, J. P., Studies on the electrochemical mechanism of reduction of carbonyl compounds. *Electrochim. Acta.* **1964,** *9*, 711−720.

[49] Horányi, G., Heterogeneous catalysis and electrocatalysis. *Catal. Today* **1994,** *19*, 285–312

[50] Pletcher, D.; Razaq, M., The reduction of acetophenone to ethylbenzene at a platinised platinum electrode. *Electrochim. Acta* **1981,** *26*, 819−824.

2.7 Supporting Information

2.7.1   Nafion® 212 Membrane Pretreatment

Nafion® 212 membranes were placed in a bath of 3% H_2O_2 solution heated to 80 °C for 1 h under magnetic stirring to remove organic impurities. Then, the membranes were rinsed in deionized water and placed in a deionized water bath at 100 °C for 2 h under magnetic stirring. Next, the membranes were placed in bath of 0.5 M H_2SO_4 at 80 °C for 1 h under

magnetic stirring. Finally, the membranes were rinsed in deionized water at 80 °C and stored in deionized water.

2.7.2 Product Separation, Identification, and Quantification

Liquid aliquots were taken from the reactor chamber and gas trap and diluted in water or CH_3CN for product analysis with an HPLC (Agilent Technologies 1260) equipped with a variable wavelength detector (VWD, G1314B) at 210 nm. Additionally, the reactor and components were rinsed in deionized water after completion of the reaction to collect residual species. The column (Phenomenex Inc., Gemini C18, 3 μm 110 Å) was operated at 45 °C with a binary gradient method containing water and CH_3CN at 0.6 ml min^{-1} flow rate. The CH_3CN fraction was increased from an initial 15% (v/v) to 60% during 5–15 min, and then was decreased to 15% from 17–24 min. Peaks for FA, furfural and MF eluded at 10.8, 12.7, and 22.7 min, respectively. Hydrofuroin (1,2-di(furan-2-yl)ethane-1,2-diol) eluded at two different times (14.0 and 16.3 min). Products were identified by comparison with authentic samples prepared in 25% or 100% CH_3CN solutions, except for hydrofuroin which was identified by fraction collection combined with ^{1}H NMR (**Figure S2.2** and **Figure S2.3**) and MS analysis (details in **Section 2.7.4**).

A gas chromatograph (SRI Instrument 8610C MG#3) equipped with HaySep D column and MolSieve 5 Å columns was used for analyzing H_2 gas. A schematic of the gas flow path for preparative electrolysis experiments is shown in **Figure S2.1**. A thermal conductivity detector (TCD) was used to detect H_2 with Ar (Airgas, 99.999%) as the carrier gas. H_2 was calibrated with a commercial gas mixture (Matheson Tri Gas MicroMAT 14) under operating conditions. Gas aliquots were sampled every 12 minutes with the first injection starting approximately four minutes after the reaction initialized. The amount of

gas evolved from D-electrolytes was approximated assuming 100% D_2 product, and quantified using a calibration constant derived from the H_2 calibration after being adjusted for the different thermal conductivities of H_2 (1828 W cm^{-1} K^{-1}) and D_2 (1372 W cm^{-1} K^{-1}) at 298 K.[1]
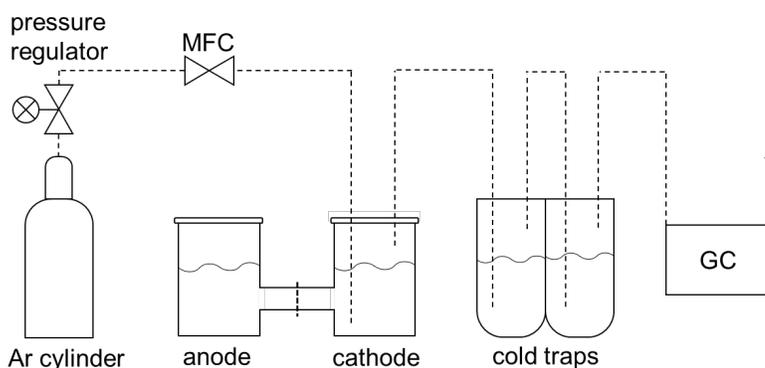
Figure S2.1. Schematic of gas flow path for preparative electrolysis experiments. MFC = mass flow controller, GC = gas chromatograph.

Reference:

[1] Dean, J. A., *Lange's Handbook of Chemistry*. Fifthteenth ed.; McGraw-Hill, Inc.: New York, 1999.

2.7.3   Calculations of Selectivity and Faradaic Efficiency

Faradaic efficiency (FE) to liquid product i (i = MF, FA, hydrofuroin) was calculated by:

$$FE_i = \frac{N_i z_i F}{Q} \cdot 100\% \tag{S1}$$

where N_i is the number of moles of product i, z_i is the number of electrons transferred per molecule of product ($z = 4$ for MF and 2 for FA and hydrofuroin), F is the Faraday constant (96,485.3 C mol^{-1}), and Q is the total charge in coulombs transferred in the external circuit

as measured by the electrochemical workstation. Product selectivity (S_i) was calculated using Equations S2–S4:

$$S_{FA} = \frac{N_{FA}}{N_{f,0}-N_{f,t}} \cdot 100\% \tag{S2}$$

$$S_{MF} = \frac{N_{MF}}{N_{f,0}-N_{f,t}} \cdot 100\% \tag{S3}$$

$$S_{hydrofuroin} = \frac{2N_{hydrofuroin}}{N_{f,0}-N_{f,t}} \cdot 100\% \tag{S4}$$

where $n_{f,0}$ and $n_{f,t}$ are the initial and final amounts of furfural (moles).

The incremental amount of evolved H_2 (n_{H_2}, moles) was calculated by Equation S5:

$$n_{H_2} = C_{H_2} \cdot 10^{-6} \cdot \frac{PV}{RT} \tag{S5}$$

where C_{H_2} is the concentration (ppm) of H_2 measured by GC, P is atmospheric pressure ($P = 1.013 \times 10^5$ Pa), V is the volume of GC sampling loop ($V = 1$ cm^3), R is the gas constant ($R = 8.314$ J mol^{-1} K^{-1}), T is absolute temperature ($T = 293$ K). The instantaneous faradaic efficiency of H_2 (fe_{H_2}) was calculated by Equation S6:

$$fe_{H_2} = \frac{n_{H_2}z_{H_2}F}{\Delta Q} \cdot 100\% \tag{S6}$$

where z_{H_2} is the number of electrons transferred per molecule of H_2 ($z_{H_2} = 2$), ΔQ is the incremental charge transferred during the time (t) required to fill the sampling loop. The time to fill the sample loop (t) was determined as: $t = \frac{V}{flow\ rate} = \frac{1\ cm^3}{208\ cm^3/min} \cdot \frac{60\ s}{1\ min} = 0.288\ s$. Overall faradaic efficiency to H_2 (FE_{H_2}) was determined as the average of fe_{H_2} values measured throughout the reaction.

The total amount of H_2 evolved (N_{H2}) during a reaction was estimated according to Equation S7:

$$N_{H2} = \frac{FE_{H_2}Q}{z_{H_2}F} \tag{S7}$$

2.7.4 Identification and Quantification of Hydrofuroin

A fraction of hydrofuroin was collected using an HPLC (Waters Alliance) equipped with an automatic fraction collector (Waters Fraction Collector III). The same column conditions and pumping method were used as described in **Section 2.7.2**, except that 0.1% formic acid (Optima^{TM} LC/MS grade, Fisher) was added to the mobile phases. The collected fractions were dried in a vacuum oven and dissolved in water and CH_3CN and analyzed with a Waters Acquity H-Class ultra-performance liquid chromatography (UPLC) instrument equipped with a mass detector (Waters ACQUITY QDa) operated in positive ion mode. Both fractions were also dried in a vacuum oven and reconstituted in acetonitrile-d3 (99.8 atom%, Cambridge Isotope Laboratories, Inc.) for ^{1}H NMR analysis with a Bruker 600 MHz NMR spectrometer (AVIII600). DMSO (99.9%, Fisher Scientific) was added as an internal standard to determine the concentration of hydrofuroin. The same samples were analyzed by HPLC (as described in **Section 2.7.2**) to acquire quantitative calibration curves based on the concentrations determined by ^{1}H NMR. Those calibrations curves were used for quantitation of hydrofuroin used throughout the main text.

1,2-di(furan-2-yl)ethane-1,2-diol (hydrofuroin 1)

^{1}H NMR (600 MHz, CD$_3$CN) δ 7.48 (dd, J = 1.9, 0.8 Hz, 2H), 6.41 (dd, J = 3.2, 1.8 Hz, 2H), 6.34 (dd, J = 3.2, 0.8 Hz, 2H), 4.87 (d, J = 3.2 Hz, 2H), 3.56 (s, 2H).

ESI-MS: $[M + H – H_2O]^+$ calculated m/z 177, found m/z 177.

1,2-di(furan-2-yl)ethane-1,2-diol (hydrofuroin 2)

^{1}H NMR (600 MHz, CD$_3$CN) δ 7.41 (dd, J = 1.8, 0.9 Hz, 2H), 6.33 (dd, J = 3.2, 1.8 Hz, 2H), 6.25 (dd, J = 3.2, 0.9 Hz, 2H), 4.88 (d, J = 2.5 Hz, 2H), 3.81 (s, 2H)

ESI-MS: $[M + H – H_2O]^+$ calculated m/z 177, found m/z 177.
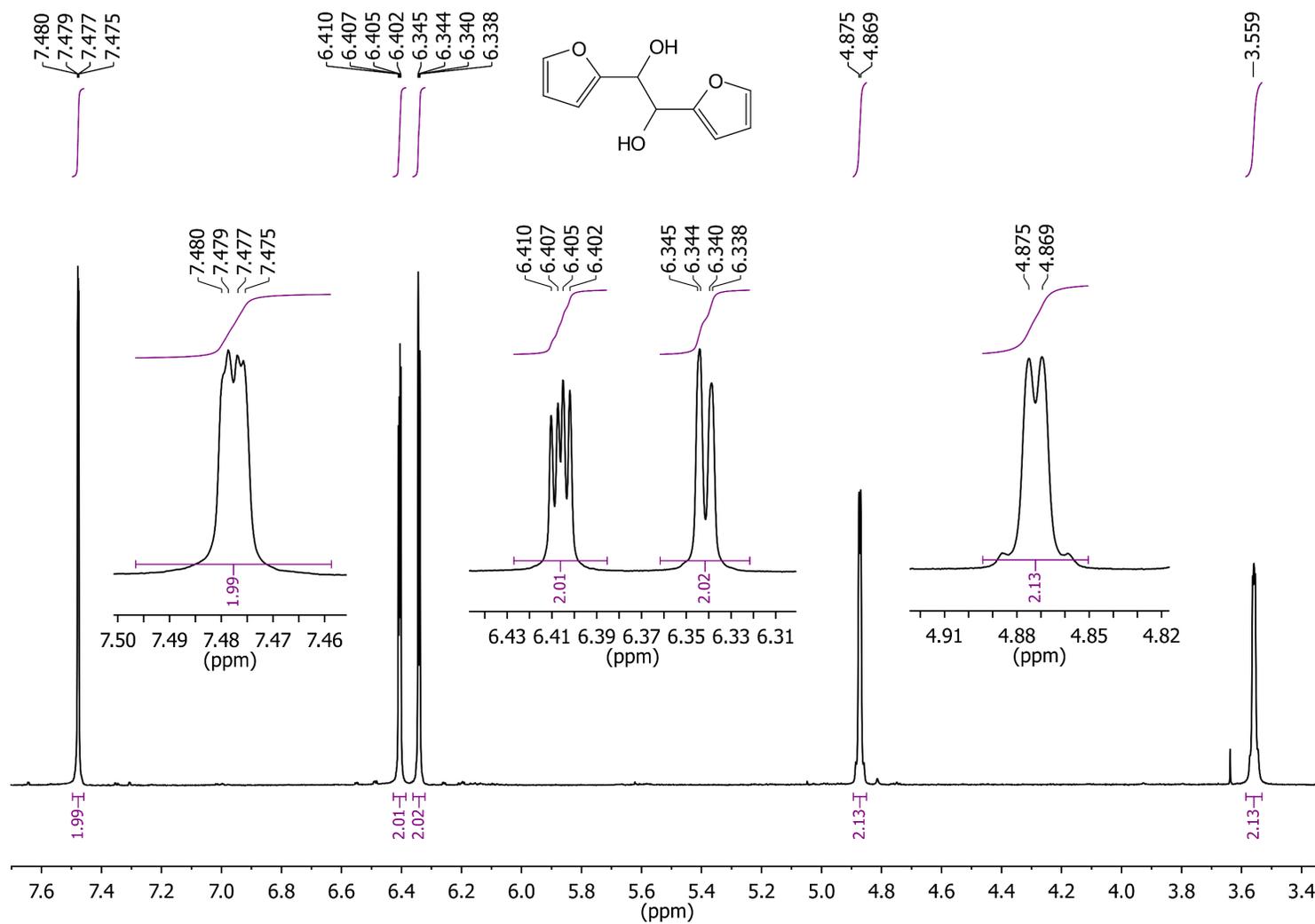
Figure S2.2. ^{1}H-NMR spectra of hydrofuroin-1
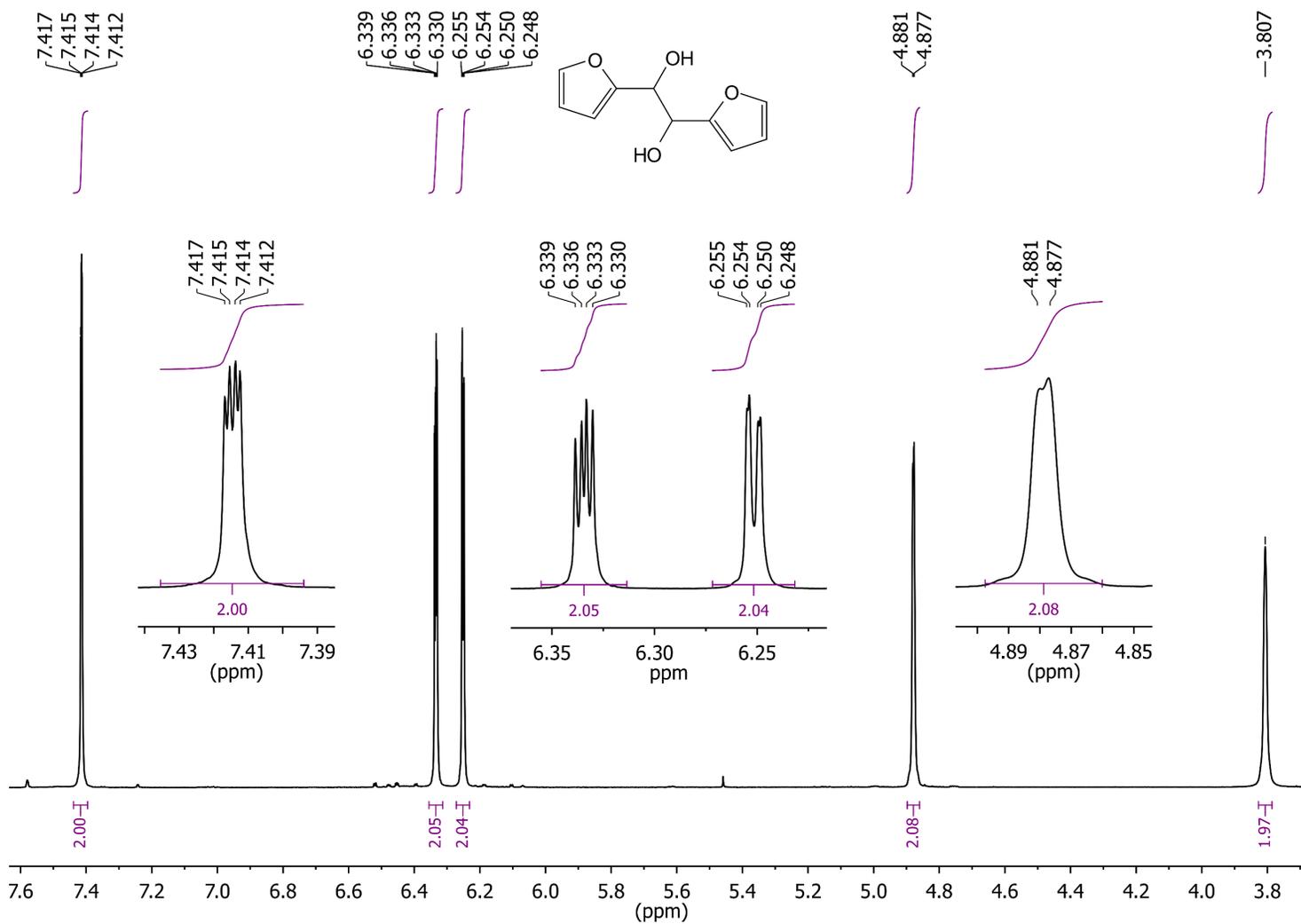
Figure S2.3. ^{1}H-NMR spectra of hydrofuroin-2

2.7.5   Additional Preparative Electrolysis Data

Table S2.1. Preparative electrolysis of 0.01 M furfuryl alcohol.[a]

entry	electrode	E (V)	pH	j_{avg} (mA cm^{-2})	FA loss (mol%)	MF detected (μmol h^{-1})	FE_{H2} (%)	FE_{MF} (%)
1	Cu	–0.55	0.5	–6.7	9.6	1.28	100.2	0.26
2	Cu[b]	OCP	0.5	0	10.5	0.02	-	-
3	none[c]	n/a	0.5	0	11.7	0.03	-	-
4	Cu	–0.55	3.0	–1.7	1.8	0.09	101.4	0.06

[a] Conditions: reaction time: 1 h. [b] control test with identical conditions to entry 1 except at open circuit potential conditions (OCP). [c] control test with no working electrode present.

Table S2.2. Preparative electrolysis of 0.05 M furfural at various applied potentials at pH 0.5.[a]

E (V vs RHE)	electrode area (cm^2)	time (min)	S_{MF} (%)	S_{FA} (%)	$S_{hydrofuroin}$ (%)	conversion (%)
–0.45	5	164	52.8	13.0	2.2	49.6
–0.50	5	63	67.8	16.3	1.6	34.8
–0.55	5	23	66.4	9.6	2.4	33.9
–0.60	2.5	28	71.2	9.0	2.5	28.6
–0.65	2.5	7	70.1	5.0	1.9	16.6

[a] Charge transferred 144 C.

Table S2.3. Preparative electrolysis of furfural at various initial furfural concentrations at pH 0.5.[a]

initial concentration (M)	Q (C)	S_{MF} (%)	S_{FA} (%)	$S_{hydrofuroin}$ (%)	conversion (%)
0.01	89.2	70.1	11.3	0.8	36.9
0.05	181.8	68.6	10.4	1.6	37.9
0.1	189.7	55.2	12.1	5.3	27.4
0.2	142.3	32.7	13.4	13.6	14.6

[a] Conditions: E = –0.55 V, reaction time: 30 min.

Table S2.4. Preparative Electrolysis of 0.05 M furfural with various electrolyte pH.[a]

pH	Q (C)	S_{MF} (%)	S_{FA} (%)	$S_{hydrofuroin}$ (%)	conversion (%)
0.5[b]	283.2	66.8	11.0	1.8	57.9
1.4	215.0	53.2	18.6	3.9	52.1
2	98.6	31.4	26.0	5.5	36.9
3[b]	31.1	15.4	39.6	6.2	16.4

[a] Conditions: E = –0.55 V, reaction time: 1 h. [b] values for pH 0.5 and 3.0 are averages of three experiments (see **Table S2.6**).

Table S2.5. Preparative electrolysis of 0.05 M furfural on Cu-MPA, Cu-MBT, and Cu-MDA electrodes.[a]

pH	thiol	Exp.	Q (C)	N_{MF} (µmol)	N_{FA} (µmol)	$N_{hydrofuroin}$ (µmol)	N_{H2} (µmol)
		1	30.4	1.82	22.7	4.24	119
		2	29.6	1.77	23.1	4.16	114
0.5	MPA	3	26.4	1.68	21.4	3.85	104
		average	28.8	1.76	22.4	4.08	112
		σ	2.1	0.07	0.9	0.21	7.7
		1	10.1	0.088	2.81	6.35	33.5
		2	6.7	0.028	2.02	4.13	20.1
0.5	MBT	3	11.0	0.086	3.17	6.61	35.9
		average	9.3	0.067	2.66	5.70	29.9
		σ	2.3	0.034	0.59	1.36	8.5
0.5	MDA	1	1.57	0.21	0.26	0.12	4.56
		1	22.2	4.80	12.4	3.75	86.4
		2	22.0	5.28	11.3	4.05	85.7
3.0	MPA	3	28.2	9.98	16.7	5.96	96.1
		average	24.2	6.69	13.5	4.59	89.4
		σ	3.5	2.86	2.9	1.20	5.8
		1	4.1	0.033	2.05	3.30	9.96
		2	6.0	0.035	2.22	2.91	19.5
3.0	MBT	3	5.1	0.029	2.19	3.49	14.5
		average	5.1	0.032	2.15	3.24	14.7
		σ	0.9	0.003	0.09	0.30	4.8
3.0	MDA	1	0.97	0.106	0.292	1.250	0.080

[a] Conditions: E = –0.55 V, thiol concentration: 0.25 mM, reaction time: 1 h.

Table S2.6. Preparative electrolysis of 0.05 M furfural on Cu.[a]

pH	Exp.	Q (C)	N_{MF} (μmol)	N_{FA} (μmol)	$N_{hydrofuroin}$ (μmol)	N_{H2} (μmol)	FE_{MF} (%)	FE_{FA} (%)	$FE_{hydrofuroin}$ (%)	FE_{H2} (%)
	1	271.5	399	65.9	5.05	436	56.7	4.7	0.4	31.0
	2	310.0	395	66.8	5.59	606	49.2	4.2	0.3	37.7
0.5	3	268.1	379	60.9	5.46	438	54.6	4.4	0.4	31.5
	average	283.2	391	64.5	5.37	493	53.5	4.4	0.4	33.4
	σ	23.3	11	3.2	0.29	97.4	3.9	0.3	0.0	3.7
	1	32.0	28.5	62.9	5.18	22.1	34.4	37.9	3.1	13.3
	2	29.6	25.1	64.1	5.45	22.1	32.7	41.7	3.5	14.4
3.0	3	31.7	21.8	66.2	4.61	35.7	26.5	40.3	2.8	21.7
	average	31.1	25.2	64.4	5.08	26.6	31.2	40.0	3.2	16.5
	σ	1.3	3.4	1.7	0.42	7.9	4.1	1.9	0.4	4.6

[a] Conditions: $E = -0.55$ V, thiol concentration: 0.25 mM, reaction time: 1 h.
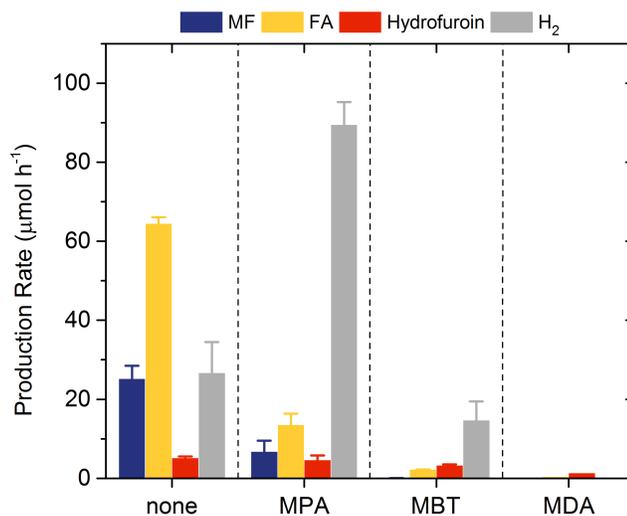
Figure S2.4. Observed production rates during preparative electrolysis of furfural on Cu, Cu-MPA, Cu-MBT, and Cu-MDA electrodes. Conditions: 0.05 M furfural and 0.25 mM of the indicated organothiol, pH 3.0 electrolyte, 1 h; $E = -0.55$ V.
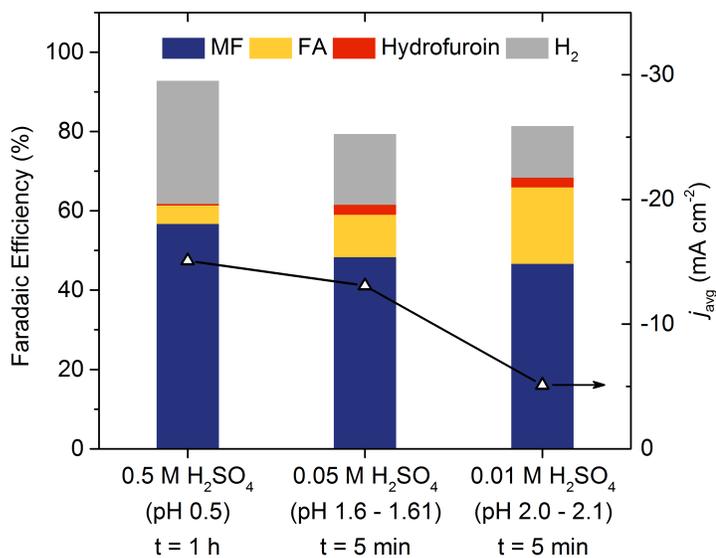
Figure S2.5. Preparative electrolysis of furfural with electrolyte of various H_2SO_4 concentrations. Conditions: 0.05 M furfural, $E = -0.55$ V.

2.7.6 Additional RDE Voltammetry
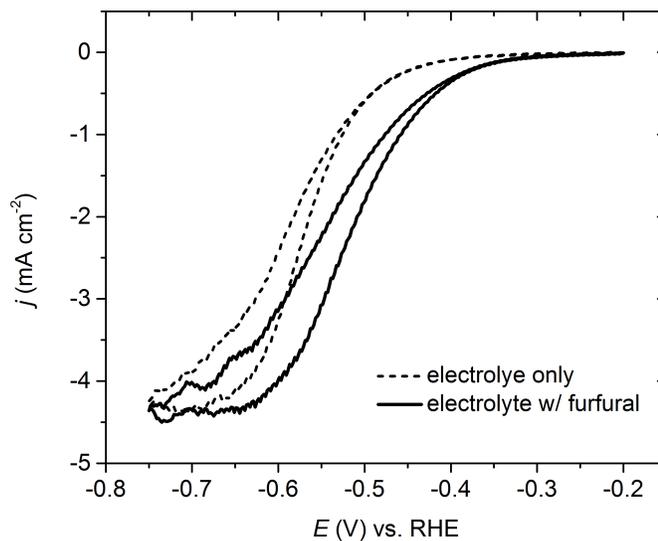
Figure S2.6. Cyclic voltammograms recorded on a 5.0 cm^2 Cu foil electrode under actual electrolysis conditions: sweep rate 50 mV s^{-1}; magnetic stirring at 1000 rpm setting; pH 3.0 electrolyte with or without 0.05 M furfural.
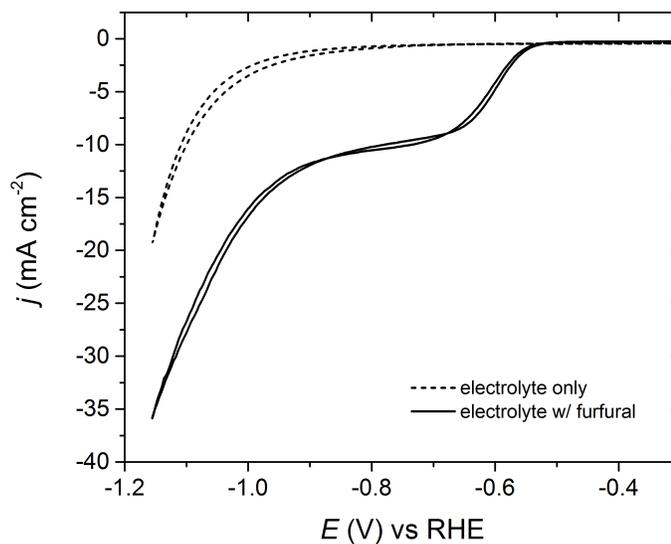
Figure S2.7. Cyclic voltammograms in 0.5 M H$_2$SO$_4$ with or without 0.05 M furfural on a Pb RDE (5.0 mm diameter, Pine Research Instrumentation) at 2500 rpm.

CHAPTER 3

PAIRED ELECTROCATALYTIC HYDROGENATION AND OXIDATION OF 5-(HYDROXYMETHYL)FURFURAL FOR EFFICIENT PRODUCTION OF BIOMASS-DERIVED MONOMERS

This manuscript is currently in preparation for a future submission

Xiaotong H. Chadderdon,[a] David J. Chadderdon,[a] Toni Pfennig,[a,b] Brent H. Shanks,[a,b] Wenzhen Li[a,c,*]

[a]Department of Chemical and Biological Engineering, Iowa State University, 618 Bissell Road, Ames, Iowa 50011, United States

[b]NSF Engineering Research Center for Biorenewable Chemicals (CBiRC), 617 Bissell Road, Ames, Iowa 50011, United States

[c]US Department of Energy Ames Laboratory, 2408 Pammel Drive, Ames, Iowa 50011, United States

[*]Corresponding Author

ABSTRACT

Electrochemical conversion of biomass-derived compounds is a promising route for sustainable chemical production. Herein, we report unprecedentedly high efficiency for conversion of 5-(hydroxymethyl)furfural (HMF) to biobased monomers by pairing HMF reduction and oxidation half-reactions in a single electrochemical cell. Electrocatalytic hydrogenation of HMF to 2,5-bis(hydroxymethyl)furan (BHMF) was achieved under mild

conditions using carbon-supported Ag nanoparticles (Ag/C) as the cathode catalyst. The competition between Ag-catalyzed HMF hydrogenation to BHMF and undesired HMF hydrodimerization and hydrogen evolution reactions was sensitive to cathode potential. Also, the carbon support material in Ag/C was active for HMF reduction at strongly cathodic potentials, leading to additional hydrodimerization and low BHMF selectivity. Accordingly, precise control of the cathode potential was critical for achieving high BHMF selectivity and efficiency. In contrast, the selectivity of HMF oxidation facilitated by a homogeneous electrocatalyst, 4-acetamido-TEMPO (ACT, TEMPO = 2,2,6,6-tetramethylpiperidine-1-oxyl), together with an inexpensive carbon felt electrode, was intrinsically insensitive to anode potential. Thus, it was feasible to conduct HMF hydrogenation to BHMF and oxidation to 2,5-furandicarboxylic acid (FDCA) in a single cathode-potential-controlled cell. Electrocatalytic HMF conversion in the paired cell achieved high yields of BHMF and FDCA (85% and 98%, respectively) and a combined electron efficiency of 187%, corresponding to a nearly two-fold enhancement compared to the unpaired cells.

3.1 Background

Organic electrosynthesis has emerged as a promising methodology for environmentally-friendly chemical production.[1] In electroorganic reactions, electrons serve as an inherently clean reagent to replace stoichiometric oxidants or reductants, and thereby eliminate toxic waste and byproducts.[2] The driving force of electrode reactions can be directly manipulated by controlling the potential, which can enable very high selectivity for desired molecular transformations. Moreover, the electrochemical cells can potentially be powered by electricity from renewable sources,[3-4] thereby reducing the overall carbon footprint.

Despite these advantages, the industrial electrosynthesis of organic molecules is very limited in terms of number of processes and production volumes.[5] Factors limiting its widespread application are poor catalyst activity and reaction rates, as well as high energy demands.[6]

Electrocatalytic hydrogenation (ECH) of biomass-derived molecules has received great attention in recent years.[7-12] ECH is analogous to thermal catalytic hydrogenation, with the key difference that surface-adsorbed hydrogen atoms are generated electrochemically from water or proton reduction, rather than from hydrogen gas.[13] In this way, the large kinetic barriers for H_2 dissociation are avoided, therefore allowing ECH to proceed at mild temperatures and pressures and without the need for conventional hydrogenation catalysts (e.g., Pt, Pd, Ni). However, it can be challenging to obtain high selectivity and efficiency for the desired transformation because multiple reaction pathways and competing reactions may exist.[11] Electrocatalytic hydrogen evolution reaction (HER) is operable on metal electrodes at cathodic potentials, and consumes adsorbed hydrogen atoms in competition with ECH. Additionally, carbonyl-containing substrates may undergo direct electroreduction and hydrodimerization reactions.[14]

Electrochemical half-reactions always occur in pairs, but most commercialized electrochemical processes only utilize one of the two electrodes for generation of desired products.[15] For example, electrochemical reductions are typically paired with water oxidation as a benign counter reaction. However, water oxidation has sluggish kinetics and the oxygen gas produced is not valuable. Therefore, substantial gains in terms of economic feasibility and energy efficiency can be made by pairing two half-reactions that generate desired products in single electrochemical cell.[16] In this way, the theoretical maximum

electron efficiency is 200%, two times greater than in conventional unpaired cells.[17] Moreover, the paired electrolysis approach can lower capital and operation costs by reducing the number of reactors or processing steps required. Nevertheless, there are challenges arising from mismatched optimal current densities for the two half-reactions, chemical incompatibilities, and crossover issues.[18]

Utilizing renewable feedstocks is a pillar of green chemistry.[19] One promising renewable molecule is 5-(hydroxymethyl)furfural (HMF). HMF is accessible from biomass through the dehydration of fructose or glucose, and is an important platform chemical that can be diversified into a variety of value-added chemicals and fuels.[20-22] Electrocatalytic conversion has recently received great attention as a promising method for HMF hydrogenation or oxidation to biobased monomers (**Scheme 3.1**).[23] Specifically, the selective hydrogenation of HMF generates 2,5-bis(hydroxymethyl)furan (BHMF), which is an important precursor for production of polyesters and polyurethane foams.[24] Selective oxidation of HMF generates 2,5-furandicarboxylic acid (FDCA). FDCA is a feedstock for production of polyethylene 2,5-furandicarboxylate (PEF), a promising biobased alternative to petroleum-derived polyethylene terephthalate.[25]

Scheme 3.1. Conversion of HMF by hydrogenation to BHMF or oxidation to FDCA.

2,5-bis(hydroxymethyl)furan
BHMF

5-(hydroxymethyl)furfural
HMF

2,5-furandicarboxylic acid
FDCA
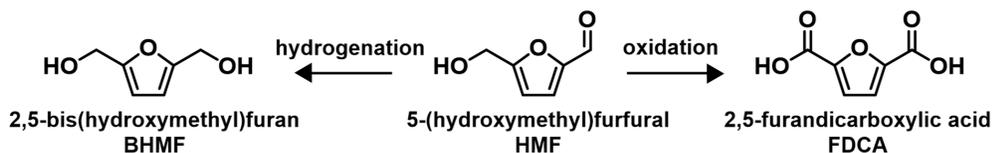
It was recently shown in two separate reports that electrocatalytic hydrogenation of HMF to BHMF and redox-mediated oxidation of HMF to FDCA can both be conducted in mildly basic electrolytes (i.e. pH 9.2) and with good selectivity.[10, 26] Such conditions are

well suited for electrochemical conversion of biomass-derived chemicals including HMF, which are typically unstable in extremely acidic or basic environments. Moreover, there is an untapped opportunity to integrate the two HMF half-reactions in a paired electrochemical cell, without additional issues related to electrolyte or HMF crossover. The overall reaction would consume only HMF, water, and electricity, and generate no waste products. Despite the attractiveness, the paired electrocatalytic conversion of HMF has yet to be accomplished.[27]

Herein, we demonstrate the paired electrocatalytic conversion of HMF to BHMF and FDCA for the first time. A self-synthesized Ag/C catalyst facilitated HMF hydrogenation to BHMF with enhanced faradaic efficiency compared to a polycrystalline Ag electrode. We elucidated the contribution of the carbon black (CB) support material in Ag/C to the observed product selectivity. Operating at cathode potentials more positive than –1.4 V alleviated the impact of HMF reduction on CB, and the optimal BHMF selectivity and efficiency for Ag/C was obtained at –1.3 V. For the anode reaction, a homogeneous electrocatalyst, 4-acetamido-TEMPO (ACT, TEMPO = 2,2,6,6-tetramethylpiperidine-1-oxyl), enabled indirect electrochemical HMF oxidation to FDCA with nearly 100% efficiency. The ACT-mediated HMF oxidation was conducted using an inexpensive carbon felt anode, mild electrolyte conditions (pH 9.2), and ambient temperature. Electrocatalytic HMF conversion in a paired electrochemical cell achieved a combined electron efficiency to BMHF and FDCA of 187%, which corresponds to a nearly two-fold enhancement compared to the unpaired cells. The individual molar yields for BHMF and FDCA (85% and 98%, respectively) were very close to those in unpaired cells, indicating that the two half-reactions were compatible and proceeded without severe complications or adverse

effects. This approach satisfies many principles of green chemistry and demonstrates the feasibility of paired electrosynthesis for biomass conversion.

3.2 Results and Discussion

3.2.1 Ag/C Synthesis and Characterizations

Silver nanoparticles (Ag NPs) were synthesized by the reduction of silver nitrate in oleylamine and oleic acid according to literature.[28] Ag/C was prepared by depositing Ag NPs onto Vulcan XC-72R carbon black (CB). A transmission electron microscopy (TEM) image of the Ag/C catalyst is shown in **Figure 3.1.** The particle sizes for Ag NPs ranged from approximately 2.0 to 6.0 nm. More detailed analysis revealed that the mean particle diameter was 3.9 nm (**Figure S3.5**). X-ray diffraction (XRD) showed that the Ag NPs were crystalline with a face-centered cubic structure, and average crystallite size of approximately 2.3 nm (**Figure S3.6**). The Ag loading on the CB support was estimated by thermal gravimetric analysis (TGA) to be approximately 9.1%.
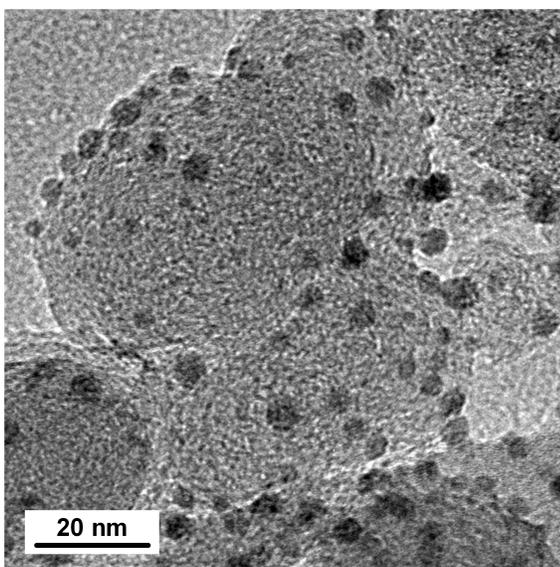

Figure 3.1. TEM image of the as-prepared Ag/C catalyst.

3.2.2 Ag/C Catalysts for Electrochemical HMF Reduction

The Ag/C catalyst was initially evaluated for HMF reduction in a borate buffer (pH 9.2) electrolyte by cyclic voltammetry. Electrodes were prepared by drop-casting an ink dispersion of Ag/C onto a glassy carbon disk electrode. Additionally, CB-modified glassy carbon and polycrystalline silver (Ag-pc) disk electrodes were tested for comparison. The electrochemically-active surface area (ECSA) for Ag was determined by oxidative stripping voltammetry of under-potential deposited lead (Pb_{UPD}). The amount of Ag/C drop-cast onto the glassy carbon electrode was chosen in order to give similar Ag ECSA as the Ag-pc disk electrode (details in **Section 3.4.9**).

Cyclic voltammetry revealed that Ag-pc, Ag/C and CB electrodes were active for HMF reduction (**Figure 3.2**). The onset potentials for HMF reduction were –1.03 V, –1.05 V, and –1.21 V for Ag/C, Ag-pc, and CB, respectively, as defined herein as the potential at which background-corrected current density reached –0.1 mA cm^{-2}. This suggests that the CB support material present in Ag/C may participate in HMF reduction at potentials more negative than –1.21 V. The peak currents densities for Ag/C and Ag-pc (–6.8 and –7.0 mA cm^{-2}, respectively) were approximately two-fold higher than for CB (–3.3 mA cm^{-2}). Koutecký-Levich analysis of the reduction waves indicated that the electron transfer number (*n*) with respect to HMF was approximately two for Ag-pc and Ag/C and one for CB (see **Figure S3.7**). This suggests that different HMF reduction mechanisms may be operable for Ag-based electrodes than for CB electrodes. **Figure 3.3** also shows voltammograms measured in electrolytes without HMF, for which the reduction waves can be assigned to the hydrogen evolution reaction (HER). The HER current was negligible at potentials close to the onset of HMF reduction, but increased substantially at potentials

more negative than about –1.4 V. This corresponds to the potential range at which a second reduction wave initiated for electrolytes containing HMF, suggesting that HMF reduction and HER can proceed concurrently at very negative potentials. The second reduction wave was less notable for CB, reflecting the lower HER activity for CB compared to Ag-based electrodes.
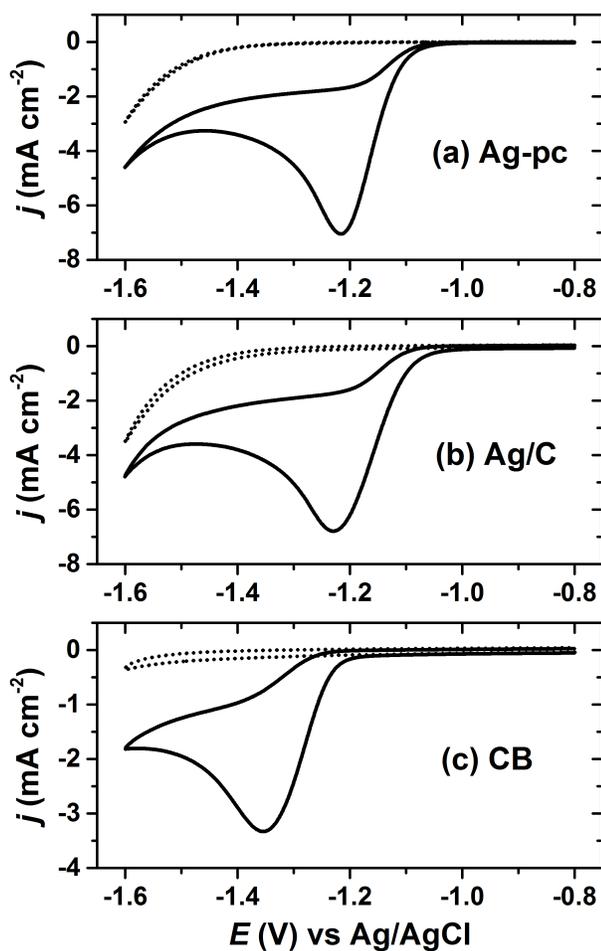

Figure 3.2. Cyclic voltammograms for (a) polycrystalline Ag (Ag-pc), (b) carbon-supported Ag nanoparticles (Ag/C), and (c) Vulcan XC-72R carbon black (CB). Solid lines with HMF (20.0 mM), broken lines without HMF.

HMF reduction was studied using potential-controlled electrolysis over the range of –1.15 V to –1.5 V. Electrodes were prepared by drop-casting an ink dispersion of Ag/C onto a carbon paper substrate. The amount of Ag/C loaded onto the carbon paper was chosen to give similar Ag ECSA as the Ag-pc electrode, as determined by Pb$_{UPD}$ stripping voltammetry (see **Section 3.4.9**). HMF reduction products for Ag/C and Ag-pc were evaluated in terms of selectivity and faradaic efficiency. The main HMF reduction products were BHMF from hydrogenation and BHH (5,5'-bis(hydroxymethyl)hydrofuroin) from hydrodimerization (**Scheme 3.2**). The product distribution was highly dependent on the cathode potential (**Figure 3.3**). BHMF selectivity increased and BHH decreased with more negative potentials over the range of –1.15 V to –1.3 V. BHMF selectivity was notably higher for Ag/C than Ag-pc over this potential range; however, it decreased at more negative potentials for Ag/C, corresponding to increased formation of BHH and unidentified products. In contrast, BHMF selectivity continued to rise with more negative potentials for Ag-pc. However, HER was active at those potentials and the faradaic efficiency for BHMF was reduced (e.g. 73.7% at –1.5 V for Ag-pc). As a result, the optimal BHMF generation in terms of efficiency was obtained using Ag/C at –1.3 V, for which BHMF efficiency reached 96.2%.

**Scheme 3.2.** HMF reduction to BHMF and BHH.
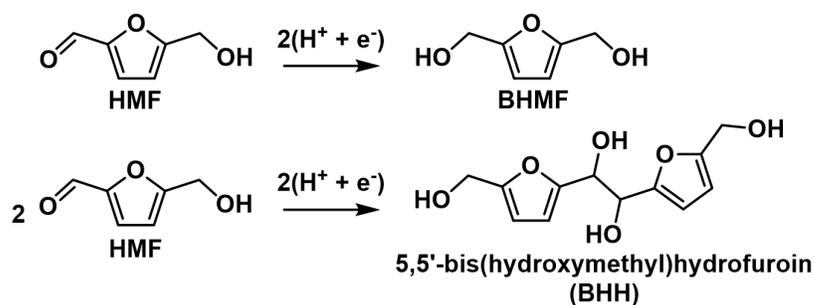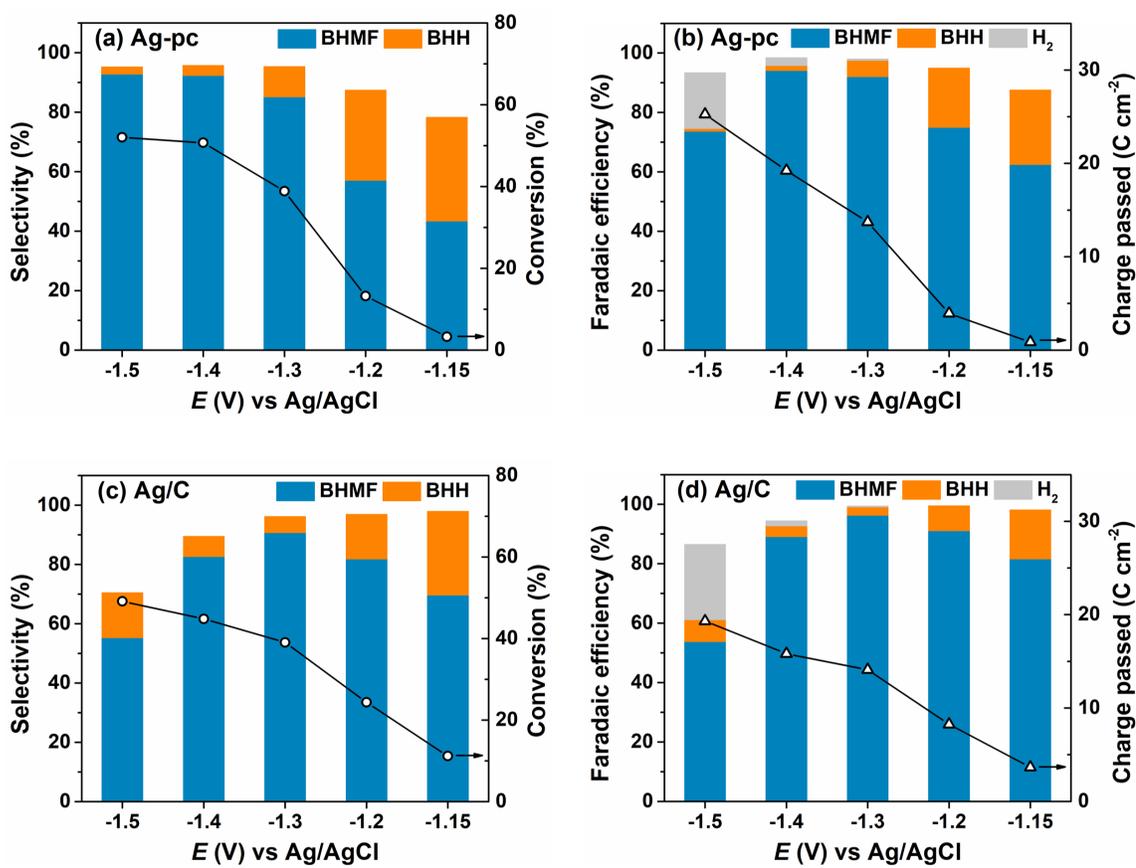
Figure 3.3. Electrochemical reduction of HMF at various potentials. (a) HMF conversion and product selectivity and (b) faradaic efficiency and total charge transferred in external circuit for Ag-pc. Corresponding results for Ag/C are shown in (c) and (d). Conditions: pH 9.2 electrolyte, 20.0 mM HMF, 30 minute reaction.

HMF reduction was conducted using CB-modified carbon paper electrodes to decouple the contributions of Ag NPs and the CB support material to the observed product selectivities for Ag/C. HMF reduction products were detected at –1.2 V for CB electrodes, however HMF conversion was too low (i.e. <1%) to allow quantitative product analysis. **Figure 3.4** shows that HMF conversion rates were enhanced at more negative potentials and reached 50% at –1.5 V, which is comparable to the values for Ag/C and Ag-pc (i.e.,

49% and 52%, respectively). In sharp contrast to Ag-based electrodes, BHH was the major detected product for CB electrodes, and very little BHMF was generated (i.e. <3% selectivity). Also, HER was a minor contribution to the total charge passed (i.e. ~2% faradaic efficiency at –1.5 V), reflecting the poor HER activity of CB.
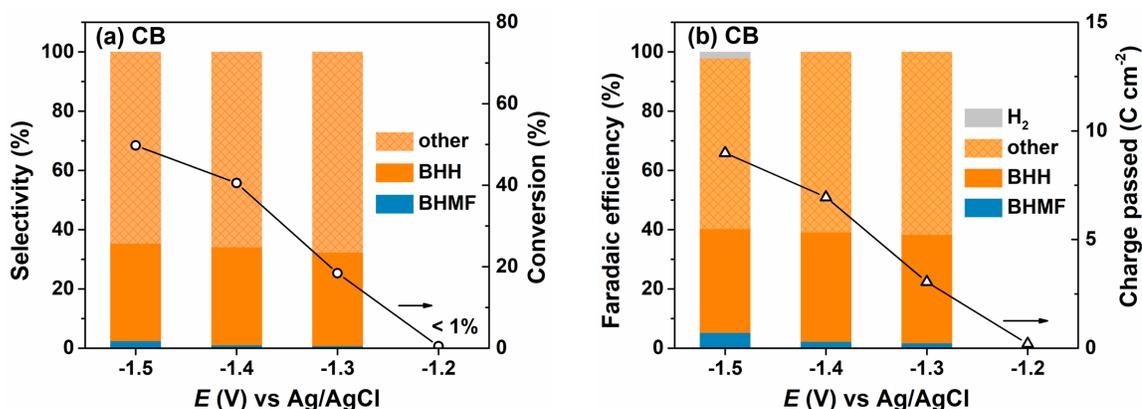

Figure 3.4. Electrochemical reduction of HMF at various potentials with CB electrode including (a) HMF conversion and product selectivity and (b) faradaic efficiency and total charge transferred in external circuit. Conditions: pH 9.2 electrolyte, 20.0 mM HMF, 30 minute reaction.

The combined selectivities for BHH and BHMF were low (i.e. 32–35%), indicating that other products were generated from HMF reduction with CB electrodes. We detected several unknown products in the HPLC chromatographs and ^{1}H NMR spectra, which were not identified or quantified in this work. As previously discussed, the Koutecký-Levich analysis indicated that HMF reduction on CB electrodes proceeds mainly by a one-electron transfer process. Therefore, we hypothesize that the unidentified species are dimer or oligomer byproducts of HMF hydrodimerization reactions, which consume one electron per HMF (cf. **Scheme 3.2**), rather than products of hydrogenation or hydrogenolysis

reactions as suggested in an earlier report.[7] These results show that CB electrodes were active for HMF reduction and generated substantial amounts of BHH and unidentified products starting around –1.3 V. On this basis, we attribute the lower BHMF and total selectivities for Ag/C compared to Ag-pc at –1.4 V and –1.5 V (cf. **Figure 3.3**) to the activity of the CB support material in Ag/C.

Regarding the mechanism of HMF hydrogenation to BHMF in basic or neutral media, there is uncertainty whether the hydrogen source is water or surface adsorbed hydrogen (H[*]),[7-8, 10, 27] as depicted in Equations 1 and 2, respectively.

$$HMF + 2H_2O + 2e^- \rightarrow BHMF + 2OH^- \tag{1}$$

$$HMF + 2H^* \rightarrow BHMF \tag{2}$$
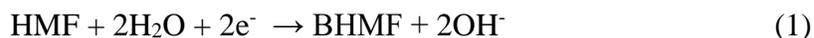
The latter pathway is known as electrocatalytic hydrogenation (ECH).[13] The electrochemical formation of H[*] (i.e. Volmer step) occurs by water reduction in basic or neutral media (Equation 3),[29] in which * designates a surface site.

$$H_2O + * + e^- \rightarrow H^* + OH^- \tag{3}$$

ECH reactions involve strong interactions between the electrode surface and reactants, and are therefore highly dependent on the nature of the electrode material.[30] Kwon et al. hypothesized that HMF hydrogenation to BHMF in neutral media occurs directly by water molecules (Equation 1) on the basis of the nearly identical onset potentials observed for a wide range of metallic electrodes.[7] On the other hand, Roylance et al. studied HMF reduction on Ag-based electrodes in basic media (i.e. pH 9.2) and reported that H[*] was likely involved in BHMF formation within the potential region where HER, and therefore H[*] formation, were possible.[10] Our viewpoint is that ECH was the major BHMF generation pathway for Ag-based electrodes under the conditions reported herein. This is self-

consistent with the low BHMF selectivity we report for CB electrodes (cf. **Figure 3.4**), as carbon is known to have very weak H^* adsorption,[31] and is therefore not expected to facilitate ECH reactions. However, it should be noted that BHMF was a major product for Ag/C and Ag-pc electrodes even within the potential region where HER current was negligible (i.e. -1.15 V $\geq E \geq -1.3$ V). A recent density functional theory (DFT) study of Ag cathodes indicated that the lowest energy pathway for HER via water reduction is the Volmer-Heyrovsky sequence, and the Heyrovsky step is rate-limiting.[32] Therefore, it is plausible that HMF hydrogenation by H^* (i.e. ECH) can proceed within a potential region where the Volmer step is facile but HER is kinetically-limited by the Heyrovsky step.

We found that the selectivity of HMF reduction to BHMF or BHH was dependent on the cathode potential for Ag-based electrodes; BHMF selectivity increased at more negative potentials down to -1.3 V for Ag/C and -1.5 V for Ag-pc (cf. **Figure 3.3**). The Volmer step (**eq. 3**) is accelerated at more negative potentials, so one explanation for the selectivity trend is that BHMF formation was promoted by higher H^* availability. Additional experiments were performed with different initial HMF concentrations to gain more insight regarding BHMF and BHH selectivity. Ag-pc electrodes were used instead of Ag/C to avoid contributions of the CB support material to the observed product selectivities. **Figure 3.5** shows that BHMF selectivity at -1.2 V decreased from 81% to 41% when the HMF concentration was increased from 5.0 mM to 50 mM. It is likely that higher concentrations led to increased surface coverage of HMF, and that BHMF formation via ECH was less favorable due to insufficient availability of H^* relative to adsorbed HMF. Accordingly, another reasonable explanation for the higher BHMF selectivities observed at more negative potentials (cf. **Figure 3.3)** would be that higher degrees of HMF

conversion were achieved at those potentials, and therefore lower bulk HMF concentrations were present. However, we conducted an extended electrolysis at –1.2 V and found that BHMF selectivity (56%) was still notably lower than at –1.3 V (i.e. 85%), even though similar HMF conversion was reached (**Table S3.1**).
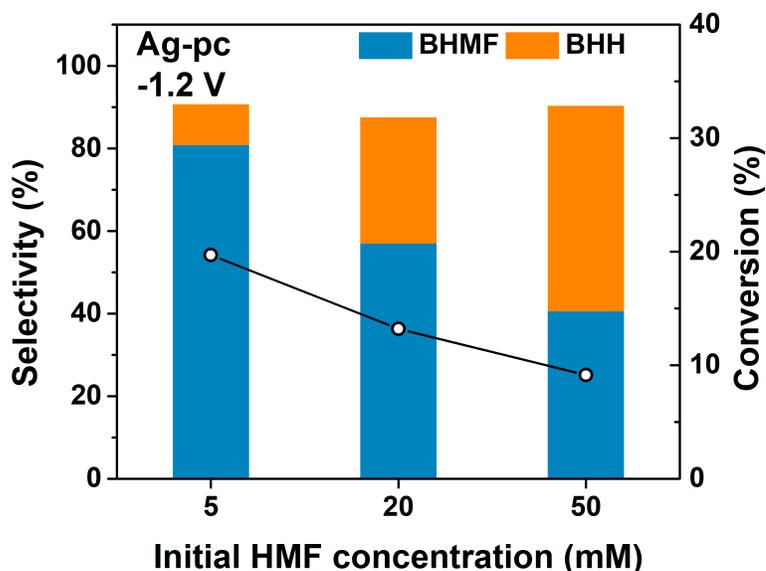
Figure 3.5. HMF conversion and product selectivity for the electrochemical reduction of HMF with Ag/C electrodes for various initial HMF concentrations. Conditions: pH 9.2 electrolyte, $E = –1.2$ V, 30 minute reaction.

As a heterogeneous process, electrochemical HMF reduction may be subject to external mass-transport limitations. In this way, the HMF concentration at the electrode surface may be significantly lower than in the bulk electrolyte, which may impact the selectivity of HMF reduction. Quasi-steady-state current densities were measured over a wide potential range using conditions (i.e., reactor geometry, electrode size, stirring rate) identical to electrolysis experiments. **Figure 3.6** shows the logarithm of current density $\log(j)$ versus potential (E) for Ag/C and Ag-pc. For both electrodes, Tafel-like behavior (i.e. linear $\log(j)$

versus *E* relationship) was observed within the potential range of approximately –1.05 to –1.15 V, indicating that HMF reduction rate was limited by charge-transfer kinetics.[33] Within this potential region, HMF reduction currents were 2–3 times higher on Ag/C than Ag-pc, even though the Ag ECSA values were very similar (i.e., 2.52 cm^2 and 2.51 cm^2 for Ag/C and Ag-pc, respectively). This suggests that Ag/C may have intrinsically higher catalytic activity for HMF reduction than bulk, polycrystalline Ag; however, definitive elucidation of nanoscale or particle size effects is beyond of the scope of this work. At potentials more negative than about –1.15 V, the plots of log(*j*) versus *E* (**Figure 3.6**) for both electrodes deviated from Tafel-like behavior, indicative of mass-transport control. Almost completely mass-transport-limited behavior was observed from about –1.30 V to –1.50 V, which corresponds to the optimal potential range for BHMF formation (cf. **Figure 3.3**). We previously showed that BHMF was favored at low HMF concentrations (cf. **Figure 3.5**), so we hypothesize that the higher BHMF selectivities observed at more negative potentials was at least partially derived from lower local HMF concentrations at the electrode surface resulting from mass-transport limitations.
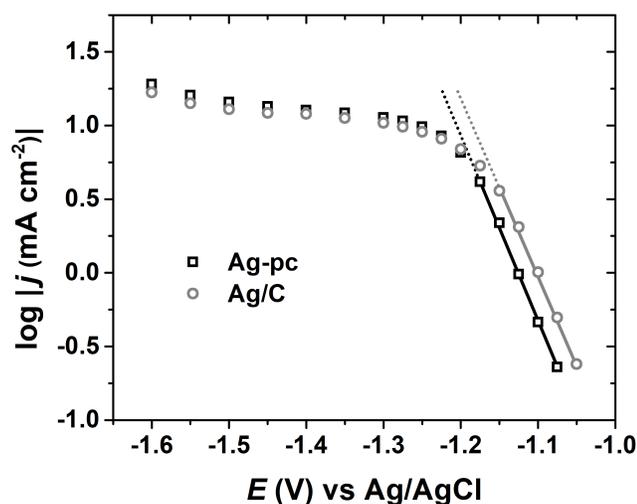

Figure 3.6. Logarithm of current density versus potential for Ag/C and Ag-pc electrodes.

3.2.3 ACT-mediated HMF Oxidation

In electrochemical cells, the two electrodes are constrained to have equal, but opposite, current flow. As a result, a major challenge of paired electrolysis is that the operating potentials for the two half-reactions cannot be independently controlled via the external circuit. We found that the selectivity and efficiency of Ag-catalyzed HMF hydrogenation were very sensitive to the cathode potential (cf. **Figure 3.3**). Therefore, in order to successfully pair HMF oxidation to FDCA and hydrogenation to BHMF in a single cell, it is necessary to find a method to facilitate selective oxidation of HMF that is insensitive to anode potential. Unfortunately, it has been shown that the selectivity of electrocatalytic HMF oxidation on carbon-supported metal catalysts is very dependent on anode potential.[34]

An alternative approach is to use a homogeneous electrocatalyst to facilitate indirect electrochemical HMF oxidation.[26] Organic nitroxyl radical catalysts, such as TEMPO and its derivatives, are widely used for selective oxidation of alcohols.[35] In particular, 4-acetamido-TEMPO (ACT) has been identified as a very promising homogeneous electrocatalyst for alcohol oxidation, owing to its superior activity and lower cost.[36] **Figure 3.7a** shows the cyclic voltammogram for ACT with a glassy carbon electrode in borate buffer electrolyte (pH 9.2). ACT exhibited reversible one-electron oxidation/reduction waves; ACT was oxidized to an oxoammonium cation (ACT$^+$) on the anodic sweep and subsequently reduced back to a nitroxyl radical on the cathodic sweep. After addition of HMF to the ACT-containing electrolyte, the anodic current was increased. This is attributed to the regeneration of ACT following the reaction between HMF and ACT$^+$ (**Figure 3.7b**). The regeneration of ACT may occur either by the reoxidation of the ACT

hydroxylamine (ACTH) or by the comproportionation of ACT^+ and ACTH.[37] The cathodic wave disappeared in the presence of HMF because ACT^+ was consumed during the HMF oxidation reaction, and therefore not present to be electrochemically reduced. No HMF oxidation current was observed in electrolyte without ACT, demonstrating that non-mediated HMF oxidation was not operable under these conditions.
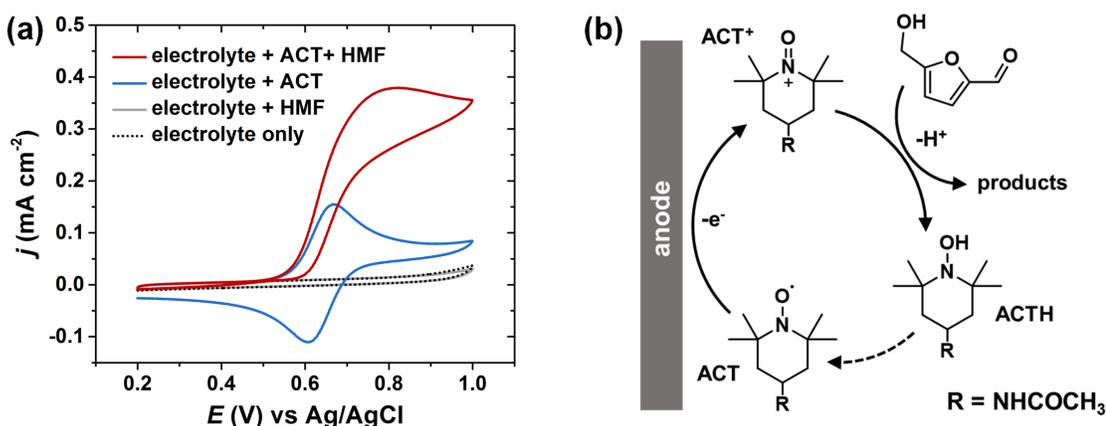
Figure 3.7. (a) Cyclic voltammograms measured with a glassy-carbon electrode for different electrolyte mixtures. ACT and HMF concentrations were 1.0 mM each. (b) Schematic of ACT-mediated electrochemical oxidation of HMF.

ACT-mediated HMF oxidation was conducted in an H-type cell using a carbon felt anode. In this system, HMF is oxidized through the non-electrochemical reaction with ACT^+ in solution; therefore, HMF product selectivity is not directly dependent on the anode potential. **Figure 3.8a** shows that HMF oxidation can proceed by two pathways, both leading to FDCA. Accordingly, the selectivity of ACT-mediated HMF oxidation to FDCA is mainly determined by the overall extent of reaction. This was demonstrated by performing the reaction at three different anode potentials while controlling the total amount of charge passed for each experiment to obtain the same extent of reaction (i.e.

~50%). In this way, HMF product distribution was largely unaffected as anode potential was varied between 0.7 V and 0.9 V (**Figure 3.8b**). **Figure 3.8c** shows that high HMF conversion was achieved after ACT-mediated HMF oxidation was run to completion (i.e. 72.2 C of charge passed). The reaction sequence appeared to be: HMF → 2,5-diformylfuran (DFF) → 5-formyl-2-furoic acid (FFCA) → FDCA. The final yield and faradaic efficiency for FDCA were about 97% and 98%, respectively.
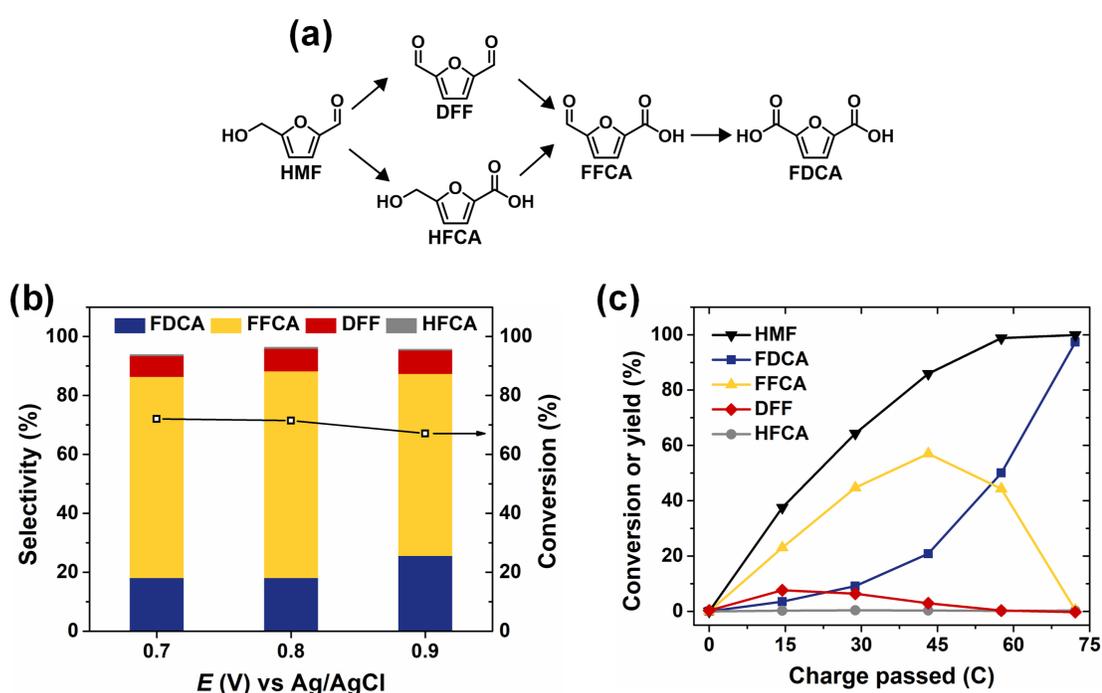

Figure 3.8. (a) Possible reaction pathways for HMF oxidation to FDCA. (b) Conversion of HMF and selectivity of oxidation products for ACT-mediated HMF oxidation at various potentials. Conditions: carbon felt electrode, pH 9.2 electrolyte with 1.0 mM ACT and 10.0 mM HMF. Reaction time was varied to obtain the 36.1 C charge transferred for each experiment. (c) Conversion of HMF and yield of oxidation products during the electrochemical oxidation of HMF at 0.7 V versus Ag/AgCl for electrolyte containing 1.0 mM ACT and 10 mM HMF.

3.2.4 Paired HMF Hydrogenation and Oxidation

Simultaneous conversion of HMF to BHMF and FDCA was achieved in a paired electrochemical cell. The cathode potential was controlled at –1.3 V to minimize undesired hydrodimerization and hydrogen evolution reactions at the Ag/C electrode. ACT-mediated HMF oxidation at the anode effectively served as the counter reaction, as its potential was not controlled. The cathode and anode electrolytes were separated by an anion-exchange membrane. The initial amount of HMF in the cathode electrolyte was three times greater than for the anode, accounting for the stoichiometry shown in Equations 4–6.

$$\text{Cathode: HMF} + 2H_2O + 2e^- \rightarrow \text{BHMF} + 2OH^- \tag{4}$$

$$\text{Anode: HMF} + 6OH^- \rightarrow \text{FDCA} + 6e^- + 4H_2O \tag{5}$$

$$\text{Overall: } 4\text{HMF} + 2H_2O \rightarrow 3\text{BHMF} + \text{FDCA} \tag{6}$$
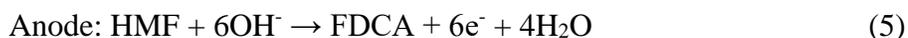
Figure 3.9a shows that the individual yields for BHMF and FDCA reached 85% and 98%, respectively, after 72.2 C of charge was passed in the paired cell. The yields were very similar to those in separate (unpaired) cells, indicating that the two half-reactions were compatible and proceeded without severe complications or adverse effects. A key feature of the paired electrolysis is that each transferred electron participates in the generation of two desired products (i.e. BHMF and FDCA). Accordingly, the combined electron efficiency to BHMF and FDCA was 187% for the paired cell, a nearly two-fold enhancement compared to the unpaired cells (**Figure 3.9b**). To the best of our knowledge, this is the first demonstration of paired HMF electrolysis, and the highest reported electron efficiency for HMF conversion.
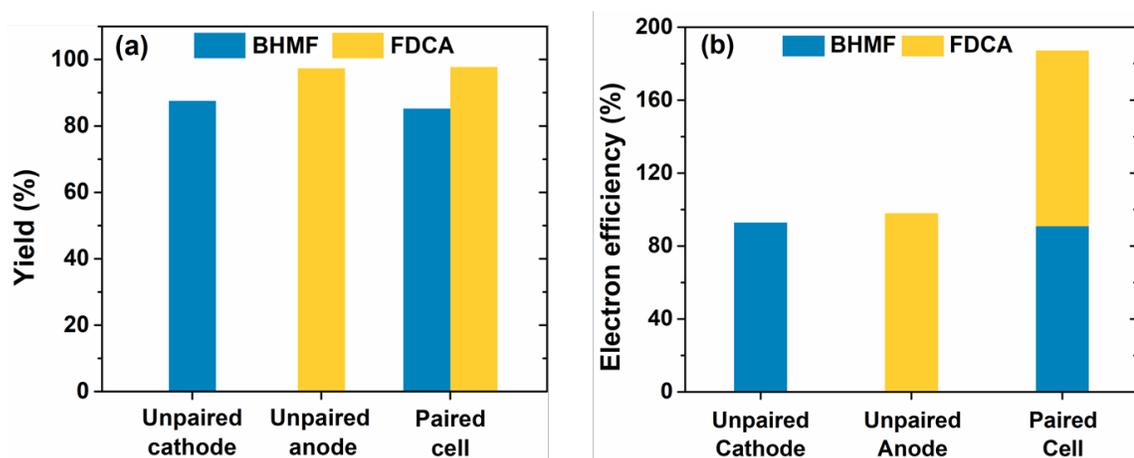
Figure 3.9. (a) Yield and (b) electron efficiency of HMF conversion to BHMF and FDCA for unpaired and paired electrochemical cells. Charge passed was 72.2 C. Yields for each product in the paired cell were calculated individually with respect to the corresponding half-reactions.

3.3   Conclusions

This work demonstrated that HMF can be efficiently converted to two important biobased polymer precursors, BHMF and FDCA, in a paired electrochemical cell. Electrocatalytic hydrogenation of HMF to BHMF was achieved using self-prepared Ag/C as the cathode catalyst. The selectivity and efficiency for BHMF formation were dependent on cathode potential and bulk HMF concentration. We also showed that the carbon support material in Ag/C was active for HMF reduction at cathodic potentials more negative than about –1.2 V, leading to hydrodimerization to BHH and low BHMF selectivity. A key feature of this work was the application of ACT as a homogeneous electrocatalyst to facilitate indirect HMF oxidation at the anode. The selectivity of ACT-mediated HMF oxidation was not dependent on anode potential, which enabled us to successfully pair HMF hydrogenation and oxidation half-reactions in a single cathode-potential-controlled

cell. Electrocatalytic HMF conversion in the paired cell achieved high yields for BHMF and FDCA (85% and 98%, respectively) and a combined electron efficiency of 187%, corresponding to a nearly two-fold enhancement compared to the unpaired cells. This approach shows the potential of using paired electrochemical cells for the sustainable production of chemicals.

3.4 Experimental Details

3.4.1 Chemicals and Materials

Sodium hydroxide (97%), 4-acetamido-TEMPO (ACT, 98%), oleylamine (70%), oleic acid (90%), 5-(hydroxymethyl)furfural (HMF, 99%), 2,5-furandicarboxylic acid (FDCA, 97%), 5-hydroxymethyl-2-furancarboxylic acid (HFCA), and 2,5-diformylfuran (DFF, 97%) were purchased from Sigma Aldrich. Acetone (99.8%), hexanes (99.9%), 2-propanol (99.9%), boric acid (100%) and buffer standard solutions (pH 7.0 and 10.0) were purchased from Fisher Scientific. Silver(I) nitrate (99.5%) and lead(II) nitrate (99%) were purchased from Acros Organics. 2,5-Bis(hydroxymethyl)furan (98%) was purchased from Ark Pharm, Inc. 5-Formyl-2-furoic acid (FFCA, 99%) was purchased from TCI. Silver foil (99.998%) and carbon felt (99.0%) were obtained from Alfa Aesar. Deionized water (18.2 MΩ•cm) obtained from a Barnstead E-Pure™ purification system was used to prepare all electrolytes.

3.4.2 Catalyst Synthesis

Ag nanoparticles (Ag NPs) were synthesized using a procedure adapted from literature.[28] Briefly, silver nitrate (1.5 mmol) was dissolved in oleylamine (30 mL) and oleic acid (1.0 mL). The solution was stirred at 350 rpm with a magnetic stir bar and kept under nitrogen atmosphere. The solution was heated to 60 °C and held for 5 minutes to

ensure the silver precursor was completely dissolved. The solution temperature was then ramped to 120 °C and held for 2 hours. The solution was cooled to approximately 25 °C and 30 mL of acetone was added. Then, the solution was divided into six tubes and additional acetone (25 mL) was added to each tube. The mixtures were centrifuged for 8 minutes at 8500 rpm and then the liquid was decanted. The Ag NPs were washed two more times with acetone by centrifugation (8 minutes at 8500 rpm). Ag/C was prepared by depositing Ag NPs onto carbon black (Vulcan XC-72R, Cabot). Separately, Ag NPs were redispersed in hexane (8.0 mg mL^{-1}) and carbon black was dispersed in a 1:1 hexane/acetone solution (1.0 mg mL^{-1}). For a typical synthesis, 2.0 mL of the Ag NPs dispersion was added drop-wise into 64.0 mL of carbon black dispersion under ultrasonication. The mixture was kept under ultrasonication for 1 hour. Finally, the Ag/C catalyst was recovered by vacuum filtration and dried overnight in a vacuum oven at 30 °C.

3.4.3 Physical Characterizations

X-ray diffraction (XRD) patterns were collected with a Rigaku Ultima IV system operated with a Cu K$_\alpha$ source (λ = 1.5406 Å) at 40 kV and 44 mA and equipped with a diffracted beam monochromator (carbon). The average crystal size was estimated from the Ag (220) diffraction peak according to Scherrer equation (Equation 7):

$$\tau = \frac{K\lambda}{\beta cos\theta} \tag{7}$$

in which τ is the mean size of the ordered crystalline domains, K is a dimensionless shape factor (0.9), λ is the wavelength, β is the line broadening at half the maximum intensity (FWHM) in radians, and θ is the Bragg angle. The particle size distribution and morphology of Ag/C were characterized using a FEI Tecnai G2-F20 200 kV instrument. Thermal gravimetric analysis (TGA) was performed with a TA Instruments Discovery

Thermal Gravimetric Analyzer using a temperature ramp of 10 °C min^{-1} and an air flow of 100 mL min^{-1}.

3.4.4   Electrochemical Measurements

Electrochemical tests were performed with a BioLogic SP-300 electrochemical workstation. The reference electrode was a single-junction Ag/AgCl (Pine Research Instrumentation) for all experiments. Solution resistance was determined by potentiostatic electrochemical impedance spectroscopy and compensated (90%) by the electrochemical workstation. All current density values are reported with respect to geometric surface area. The electrolyte was a sodium borate buffer (0.5 M) prepared from boric acid and sodium hydroxide, adjusted to pH 9.2, as measured by a pH probe (Hanna HI98103).

3.4.5   Cyclic Voltammetry and Koutecký-Levich Analysis

Cyclic voltammetry (CV) for HMF reduction was performed for a polycrystalline silver (Ag-pc) disk electrode (5.0 mm diameter, Pine Research Instrumentation) and for glassy carbon disk electrodes (GCE, 5.0 mm diameter, Pine Research Instrumentation) modified with Ag/C or carbon black (CB). CVs for ACT-mediated HMF oxidation were performed on a bare GCE. Before use, the disk electrodes were polished with an alumina suspension (0.3 µm, Allied High Tech Products, Inc.) on a microcloth polishing disk (Buehler) and cleaned with deionized water in an ultrasonic bath. Ink was prepared by dispersing Ag/C or CB in a solution of isopropanol and deionized water (1:1 v/v) at a concentration of 1.0 mg mL^{-1}. Nafion solution (5% w/w, Ion Power) was added to the ink to achieve a Nafion loading of 10% w/w in the dry catalyst film. The ink dispersion was mixed ultrasonically and then drop-cast on the GCE. The amount of CB ink drop-cast onto GCE was 6.4 µL. The amount of Ag/C drop-cast onto GCE was 8.0 µL, which was chosen to give similar

Ag ECSA as the Ag-pc disk electrode (see **Section 3.4.9**) The counter electrode was a platinum coil, separated from the main electrolyte with a fritted glass tube. The electrochemical cell was purged with nitrogen gas before and during measurements. Cyclic voltammograms were collected with a 50 mV s^{-1} sweep rate.

Linear sweep voltammograms for HMF reduction were collected at various electrode rotation rates using a MSR Rotator (Pine Research Instrumentation) for Koutecký-Levich analysis. The electron transfer number for HMF reduction, n, was extracted from the slope of the Koutecký-Levich plot, defined by Equation 8:

$$\text{slope} = \left(0.201 nFD^{\frac{2}{3}} v^{-\frac{1}{6}} C\right)^{-1}$$

(8)

in which F is the Faraday constant (96485.3 C mol^{-1}), D is the diffusion coefficient of HMF in water (9.169×10^{-6} cm^2 s^{-1}),[38] v is the kinematic viscosity of water (0.01 cm^2 s^{-1}), and C is the HMF concentration (20.0 mM).

3.4.6 Electrolysis of HMF

Electrocatalytic hydrogenation was performed in an H-type cell. Anode and cathode chambers were separated with an anion-exchange membrane (Tokuyama Corp., A201). The cathode electrolyte was purged with argon gas (99.999%, Airgas, Inc.) throughout the reaction to remove dissolved O_2 and evolved H_2. Electrolysis was conducted using 20 mL electrolyte containing HMF (typically 20.0 mM) in the cathode. The cathode electrolyte was stirred with a PTFE-coated magnetic bar (size: 7/8" × 3/16") at 500 rpm. A graphite rod was used as the counter anode.

ACT-mediated HMF oxidation was performed in an H-type cell with a similar configuration. The anode electrode was replaced with a carbon felt electrode (exposed geometric area: ~3 cm^2). Ag-pc served as the counter cathode. The anode electrolyte

volume was 12.5 mL and contained 10.0 mM HMF and 1.0 mM ACT. Carbon felt electrodes were washed with acetonitrile to remove organic residues and then rinsed with deionized water before each use. The anode electrolyte was purged with argon gas (99.999%, Airgas, Inc.) throughout the reaction and was stirred with a small PTFE-coated stir bar at 500 rpm.

3.4.7 Quasi-steady-state Current Measurements

Quasi-steady-state current densities were measured by staircase voltammetry in an H-type cell (pH 9.2, 20 mM HMF). Each potential step was held for 15 seconds and the average current measured over the last 10 seconds of each step was reported.

3.4.8 Electrode Preparation for Electrolysis

Electrodes were prepared by drop-casting an ink dispersion of Ag/C or CB onto carbon paper (exposed geometric area: 2 cm^2) for electrolysis. The ink was prepared by dispersing Ag/C or CB in a solution of isopropanol and deionized water (9:1 v/v) at a concentration of 1.0 mg mL^{-1}. Nafion (5% w/w Liquion® solution, Ion Power) was added to the ink with a target loading with a catalyst/Nafion ratio of 9/1. The ink dispersion was sonicated for 3 minutes immediately before being drop-cast. The amount of Ag/C drop-cast was chosen in order to give similar Ag ECSA as the Ag-pc disk electrode.

3.4.9 Determination of Ag ECSA

Stripping voltammetry of Pb$_{UPD}$ was performed for Ag-pc and Ag/C electrodes to estimate the Ag ECSA. The electrolyte was 0.5 M borate buffer solution containing 125 μM lead nitrate. The electrolyte was purged with nitrogen before and during experiments. For Ag/C, Pb UPD was conducted by holding –0.55 V for 2 min. The Pb$_{UPD}$ stripping voltammogram was collected immediately after deposition by sweeping from the

deposition potential to 0.0 V at 20 mV s^{-1}. The same procedure was used for Ag-pc, except the deposition potential was changed to –0.5 V to avoid bulk Pb deposition. The Ag ECSA was determined using Equation 9:

$$ECSA = \frac{Q_{strip}}{q} \qquad (9)$$

in which Q_{strip} is the charge integrated from the anodic stripping peak, and q is the charge density (0.26 mC cm^{-2}) for Pb$_{UPD}$ on Ag from literature.[39] **Table S3.2** shows a summary of Pb$_{UPD}$ stripping charges and calculated ECSA values for electrodes used for voltammetry and electrolysis experiments.

3.4.10 Product Analysis

After electrolysis, the cathode and anode electrolytes were sampled and analyzed by high-performance liquid chromatography (HPLC). Evolved H$_2$ gas was quantified with a gas chromatography connected to the outlet of the cathode chamber. BHH was identified by ^{1}H NMR and HSQC and quantified by HPLC. Two isomers of BHH are reported together for simplicity. Details of product analysis and calculations for selectivity, faradaic efficiency, and combined electron efficiency are provided in **Section 3.7**.

3.5 Acknowledgements

3.6 References

[1] Frontana-Uribe, B. A.; Little, R. D.; Ibanez, J. G.; Palma, A.; Vasquez-Medrano, R., Organic electrosynthesis: a promising green methodology in organic chemistry. *Green Chem.* **2010,** *12*, 2099–2119.

[2] Horn, E. J.; Rosen, B. R.; Baran, P. S., Synthetic Organic Electrochemistry: An Enabling and Innately Sustainable Method. *ACS Cent. Sci.* **2016,** *2*, 302-308.

[3] Nguyen, B. H.; Perkins, R. J.; Smith, J. A.; Moeller, K. D., Photovoltaic-driven organic electrosynthesis and efforts toward more sustainable oxidation reactions. *Beilstein J. Org. Chem.* **2015,** *11*, 280-287.

[4] Nguyen, B. H.; Redden, A.; Moeller, K. D., Sunlight, electrochemistry, and sustainable oxidation reactions. *Green Chem.* **2014,** *16*, 69-72.

[5] Harnisch, F.; Urban, C., Electrobiorefineries: Unlocking the Synergy of Electrochemical and Microbial Conversions. *Angewandte Chemie* **2018**.

[6] Cardoso, D. S. P.; Šljukić, B.; Santos, D. M. F.; Sequeira, C. A. C., Organic Electrosynthesis: From Laboratorial Practice to Industrial Applications. *Organic Process Research & Development* **2017**.

[7] Kwon, Y.; de Jong, E.; Raoufmoghaddam, S.; Koper, M. T. M., Electrocatalytic hydrogenation of 5-hydroxymethylfurfural in the absence and presence of glucose. *ChemSusChem* **2013,** *6*, 1659–1667.

[8] Kwon, Y.; Birdja, Y. Y.; Raoufmoghaddam, S.; Koper, M. T. M., Electrocatalytic Hydrogenation of 5-Hydroxymethylfurfural in Acidic Solution. *ChemSusChem* **2015,** *8*, 1745–1751.

[9] Holzhäuser, F. J.; Artz, J.; Palkovits, S.; Kreyenschulte, D.; Büchs, J.; Palkovits, R., Electrocatalytic upgrading of itaconic acid to methylsuccinic acid using fermentation broth as a substrate solution. *Green Chem.* **2017**, 10.1039/c6gc03153f.

[10] Roylance, J. J.; Kim, T. W.; Choi, K.-S., Efficient and Selective Electrochemical and Photoelectrochemical Reduction of 5-Hydroxymethylfurfural to 2,5-Bis(hydroxymethyl)furan using Water as the Hydrogen Source. *ACS Catal.* **2016,** *6*, 1840-1847.

[11] Chadderdon, X. H.; Chadderdon, D. J.; Matthiesen, J. E.; Qiu, Y.; Carraher, J. M.; Tessonnier, J. P.; Li, W., Mechanisms of furfural reduction on metal electrodes: distinguishing pathways for selective hydrogenation of bioderived oxygenates. *J. Am. Chem. Soc.* **2017,** *139*, 14120-14128.

[12] Suastegui, M.; Matthiesen, J. E.; Carraher, J. M.; Nacu Hernandez; Quiroz, N. R.; Okerlund, A.; Cochran, E. W.; Shao, Z.; Tessonnier, J.-P., Combining Metabolic

Engineering and Electrocatalysis: Application to the Production of Polyamides from Sugar. *Angew. Chem. Int. Ed.* **2016,** *55*, 2368–2373.

[13] Lessard, J., Electrocatalytic Hydrogenation. In *Organic Electrochemistry*, 5th ed.; Hammerich, O.; Speiser, B., Eds. CRC Press: Boca Raton, FL, 2015; pp 1658-1664.

[14] Nilges, P.; Schröder, U., Electrochemistry for biofuel generation: production of furans by electrocatalytic hydrogenation of furfurals. *Energy Environ. Sci.* **2013,** *6*, 2925–2931.

[15] Ibanez, J. G.; Frontana-Uribe, B. A.; Vasquez-Medrano, R., Paired Electrochemical Processes: Overview, Systematization, Selection Criteria, Design Strategies, and Projection. *J. Mex. Chem. Soc.* **2016,** *60*, 247–260.

[16] Llorente, M. J.; Nguyen, B. H.; Kubiak, C. P.; Moeller, K. D., Paired Electrolysis in the Simultaneous Production of Synthetic Intermediates and Substrates. *Journal of the American Chemical Society* **2016,** *138*, 15110-15113.

[17] Ibanez, J. G.; Frontana-Uribe, B. A.; Vasquez-Medrano, R., Paired electrochemical processes: overview, systematization, selection criteria, design strategies, and projection. *J. Mex. Chem. Soc.* **2016,** *60*, 247-260.

[18] Chamoulaud, G.; Floner, D.; Moinet, C.; Lamy, C.; Belgsir, E. M., Biomass conversion II: simultaneous electrosyntheses of furoic acid and furfuryl alcohol on modified graphite felt electrodes. *Electrochim. Acta* **2001,** *46*, 2757–2760.

[19] Sheldon, R. A., Green and sustainable manufacture of chemicals from biomass: state of the art. *Green Chem.* **2014,** *16*, 950−963.

[20] Chheda, J. N.; Roman-Leshkov, Y.; Dumesic, J. A., Production of 5-hydroxymethylfurfural and furfural by dehydration of biomass-derived mono- and poly-saccharides. *Green Chem.* **2007,** *9*, 342-350.

[21] Gallo, J. M. R.; Alonso, D. M.; Mellmer, M. A.; Dumesic, J. A., Production and upgrading of 5-hydroxymethylfurfural using heterogeneous catalysts and biomass-derived solvents. *Green Chem.* **2013,** *15*, 85-90.

[22] Jiang, Y.; Wang, X.; Cao, Q.; Dong, L.; Guan, J.; Mu, X., Chemical Conversion of Biomass to Green Chemicals. In *Sustainable Production of Bulk Chemicals*, Xian, M., Ed. Springer: 2016.

[23] Kwon, Y.; Schouten, K. J. P.; van der Waal, J. C.; de Jong, E.; Koper, M. T. M., Electrocatalytic Conversion of Furanic Compounds. *ACS Catal.* **2016,** *6*, 6704–6717.

[24] Moreaua, C.; Belgacemb, M. N.; Gandini, A., Recent Catalytic Advances in the Chemistry of Substituted Furans from Carbohydrates and in the Ensuing Polymers. *Top. in Catal.* **2004,** *27*, 11-30.

[25] Gandini, A.; Silvestre, A. J. D.; Neto, C. P.; Sousa, A. F.; Gomes, M., The furan counterpart of poly(ethylene terephthalate): An alternative material based on renewable resources. *J. Polym. Sci. A Polym. Chem.* **2009,** *47*, 295–298.

[26] Cha, H. G.; Choi, K.-S., Combined biomass valorization and hydrogen production in a photoelectrochemical cell. *Nat. Chem.* **2015,** *7*, 328–333.

[27] Kwon, Y.; Schouten, K. J. P.; van der Waal, J. C.; de Jong, E.; Koper, M. T. M., Electrocatalytic Conversion of Furanic Compounds. *ACS Catal.* **2016,** *6*, 6704−6717.

[28] Peng, S.; McMahon, J. M.; Schatz, G. C.; Gray, S. K.; Sun, Y., Reversing the size-dependence of surface plasmon resonances. *Proc. Natl. Acad. Sci.* **2010,** *107*, 14530-14534.

[29] Conway, B. E.; Tilak, B. V., Interfacial processes involving electrocatalytic evolution and oxidation of H2, and the role of chemisorbed H. *Electrochim. Acta* **2002**.

[30] Bard, A. J., Inner-sphere heterogeneous electrode reactions. electrocatalysis and photocatalysis: the challenge. *J. Am. Chem. Soc.* **2010,** *132*, 7559–7567.

[31] Zheng, Y.; Jiao, Y.; Li, L. H.; Xing, T.; Chen, Y.; Jaroniec, M.; Qiao, S. Z., Toward Design of Synergistically Active Carbon-Based Catalysts for Electrocatalytic Hydrogen Evolution. *ACS Nano* **2014,** *5*, 5290–5296.

[32] Singh, M. R.; Goodpaster, J. D.; Weber, A. Z.; Head-Gordon, M.; Bell, A. T., Mechanistic insights into electrochemical reduction of CO2 over Ag using density functional theory and transport models. *Proceedings of the National Academy of Sciences of the United States of America* **2017**.

[33]   Bard, A. J.; Faulkner, L. R., *Electrochemical Methods: Fundamentals and Applications*. 2nd ed.; John Wiley & Sons, Inc.: New York, 2001; p 116.

[34] Chadderdon, D. J.; Xin, L.; Qi, J.; Qiu, Y.; Krishna, P.; More, K. L.; Li, W., Electrocatalytic oxidation of 5-hydroxymethylfurfural to 2,5-furandicarboxylic acid on supported Au and Pd bimetallic nanoparticles. *Green Chem.* **2014,** *16*, 3778–3786.

[35] Nooy, A. E. J. d.; Besemer, A. C.; Bekkum, H. v., On the Use of Stable Organic Nitroxyl Radicals for the Oxidation of Primary and Secondary Alcohols. *Synthesis* **1996,** *10*, 1153-1176.

[36] Rafiee, M.; Miles, K. C.; Stahl, S. S., Electrocatalytic alcohol oxidation with TEMPO and bicyclic nitroxyl derivatives: driving force trumps steric effects. *J. Am. Chem. Soc.* **2015,** *137*, 14751-14757.

[37] Ciriminna, R.; Ghahremani, M.; Karimi, B.; Pagliaro, M., Electrochemical alcohol oxidation mediated by TEMPO-like nitroxyl radicals. *ChemistryOpen* **2017,** *6*, 5-10.

[38]   Yui, K.; Yamazaki, N.; Funazukuri, T., Infinite Dilution Binary Diffusion Coefficients for Compounds Derived from Biomass in Water at 0.1 MPa and Temperatures from (298.2 to 353.2) K. *J. Chem. Eng. Data* **2012,** *58*, 183-186.

[39] Kirowa-Eisner, E.; Bonfil, Y.; Tzur, D.; Gileadi, E., Thermodynamics and kinetics of upd of lead on polycrystalline silver and gold. *J. Electroanal. Chem.* **2003,** *552*, 171-183.

3.7 Supporting Information

3.7.1   Product Separation, Identification, and Quantification

Liquid samples were collected and diluted with deionized water for analysis with HPLC (Agilent Technologies 1260) equipped with a variable wavelength detector (VWD, G1314B) at 225 nm and 260 nm for cathode and anode samples, respectively. Additionally, the reactor and components were rinsed in deionized water after completion of the reaction to collect residual species. The column (Phenomenex Inc., Gemini C18, 3µm 110 Å) for analysis of cathode samples was operated at 45 °C with a binary gradient pumping method of water and CH_3CN at 0.6 mL min^{-1} flow rate. The CH_3CN fraction was increased from the initial 15% (v/v) to 30% over the 5 to 8.33 minute period, then was increased from 30% to 50% over the 8.33 to 10 minute period, and then was decreased to 15% from the 10 to 13 minute period. BHMF and HMF eluted around 6.7 and 7.9 minutes, respectively. Two isomers of the HMF dimer, 5,5'-bis(hydroxymethyl)hydrofuroin (BHH), eluded at different retention times (6.2 and 7.0 minutes), and are reported together for simplicity. The column for analyzing anode samples (Bio-Rad Aminex HPX-87H) was operated at 50 °C with a 0.01 M aqueous H_2SO_4 mobile phase at 0.5 mL min^{-1}. FDCA, HFCA, FFCA, HMF, and DFF eluted around 22.3, 27.0, 31.0, 39.7, 49.2 minutes, respectively. HMF and electrochemical reaction products were identified and quantified by comparison to genuine samples, except for BHH which was identified by fraction collection combined with [1]H

NMR, as described in more detail in **Section 3.7.3**. The reaction profiles shown in **Figure 3.8c** for ACT-mediated HMF oxidation were analyzed by sampling the reaction mixtures after 14.4, 28.8, 43.2, and 57.6 C of charge were passed. The data point for 72.2 C was taken from independent experiments conducted without intermediate sampling, identical to the experiment depicted in **Figure 3.9.** Evolved H_2 was quantified with a gas chromatography (SRI Instrument 8610C MG#3), using the similar methods explained in Chapter 2, and thus omitted here.

3.7.2 Calculation of Selectivity and Faradaic Efficiency

The faradaic efficiency (*FE*) of each HMF product i (i = BHMF, BHH, FDCA, DFF, HFCA, or FFCA) was calculated by Equation S1:

$$FE_i = \frac{n_i z_i F}{Q} \times 100\% \tag{S1}$$

in which n_i is the amount of product i (moles), z_i is the number of moles of electrons transferred per mole of product (z = 2 for BHMF, BHH, HFCA and DFF, 4 for FFCA, and 6 for FDCA), F is the Faraday constant (96485.3 C mol^{-1}), and Q is the total charge in coulombs transferred through the external circuit. The combined electron efficiency (*EE*) to desired products (i.e. BHMF and FDCA) was defined by Equation S2:

$$EE = \frac{[2n_{BHMF} + 6n_{FDCA}]F}{Q} \times 100\% \tag{S2}$$

Product selectivity (S_i) was calculated using Equation S3:

$$S_i = \frac{n_i}{n^*_{HMF}} \times 100\% \tag{S3}$$

in which n^*_{HMF} is the amount of HMF reacted (moles). Product yield was calculated using Equation S4:

$$Y_i = \frac{n_i}{N_{HMF}} \times 100\% \tag{S4}$$

in which N_{HMF} is the initial amount of HMF (moles). For paired electrolysis, the individual yields for BHMF and FDCA were calculated based on separate values of N_{HMF} for the cathode and anode. Faradaic efficiency for hydrogen gas was calculated using the same methods explained in Chapter 2, and thus omitted here.

3.7.3   Evaluation of 5,5'-Bis(hydroxymethyl)hydrofuroin

Samples of the HMF dimers (i.e. BHH) were collected using an HPLC (Water Alliance) equipped with an automatic fraction collector (Waters Fraction Collector III). The same column conditions and pumping method were used as described above. The collected fractions were dried in a vacuum oven and reconstituted in acetonitrile-d3 (99.8 atom%, Cambridge Isotope Laboratories, Inc.) for ^{1}H NMR and HSQC analysis with a Bruker 600 MHz NMR spectrometer (AVIII-600) (see **Figures S3.1–S3.4**). N,N-Dimethyl-formamide (DMF, 99%, Fisher Scientific) was added as an internal standard to allow determination of the BHH concentration. The same samples were analyzed by HPLC (as described in **Section 3.7.1**) to acquire quantitative calibration curves based on the concentrations determined by ^{1}H NMR. Those calibration curves were used for quantification of BHH.

BHH-1

^{1}H NMR (600 MHz, Acetonitrile-d3) δ 6.28 (d, J = 3.1 Hz, 2H), 6.25 (d, J = 3.1 Hz, 2H), 4.84 (dd, J = 3.9, 1.8 Hz, 2H), 4.48 (d, J = 5.9 Hz, 4H), 3.62 (dd, J = 3.9, 1.8 Hz, 2H), 3.34 (t, J = 5.9 Hz, 2H).

BHH-2

^{1}H NMR (600 MHz, Acetonitrile-d3) δ 6.19 (d, J = 3.2 Hz, 2H), 6.17 (d, J = 3.3 Hz, 2H), 4.84 (dd, J = 3.0 Hz, 2H), 4.43 (d, J = 5.9 Hz, 4H), 3.87 (dd, J = 2.4 Hz, 2H), 3.28 (t, J = 5.9 Hz, 2H).
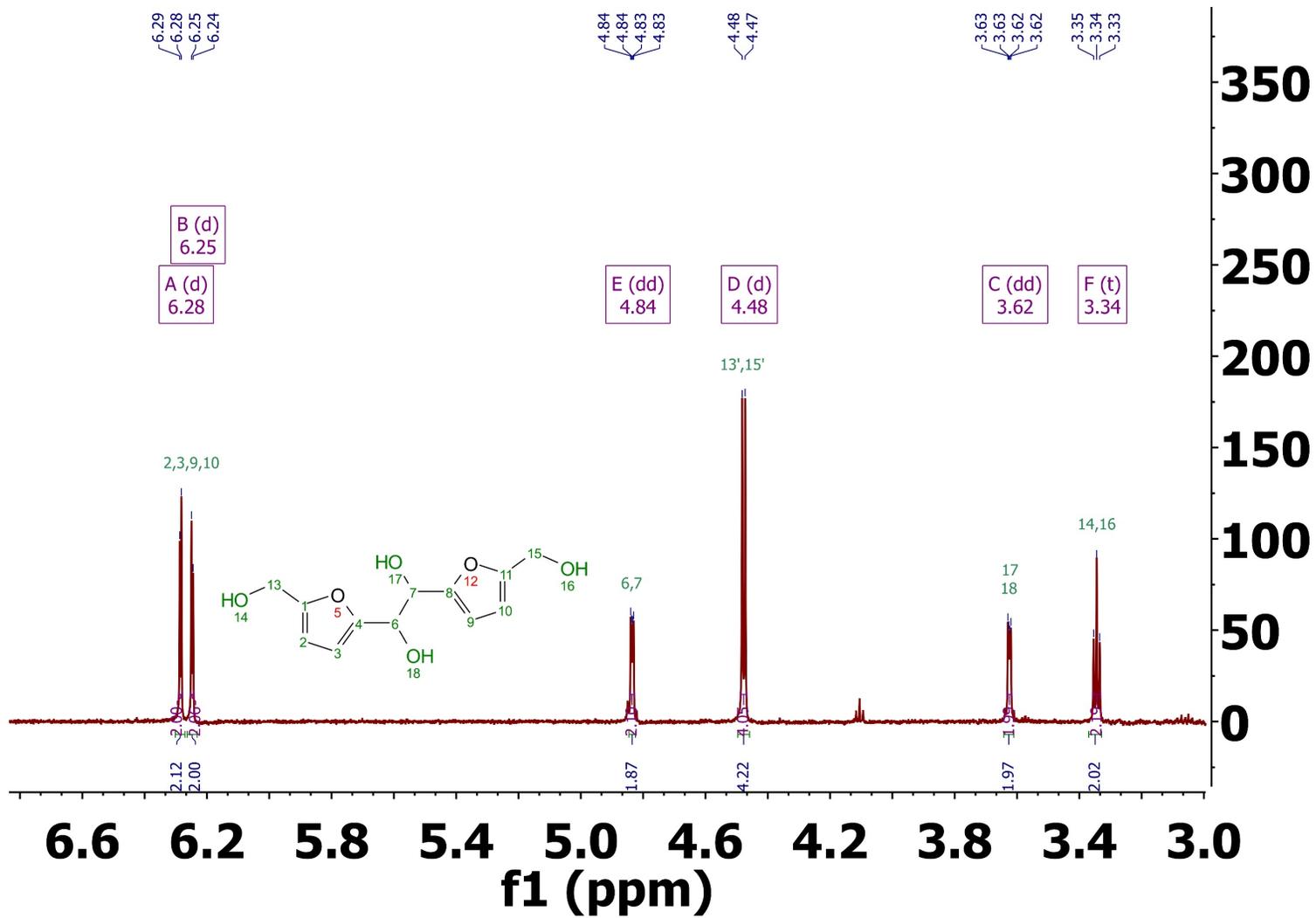
Figure S3.1. ^{1}H-NMR spectra of BHH-1
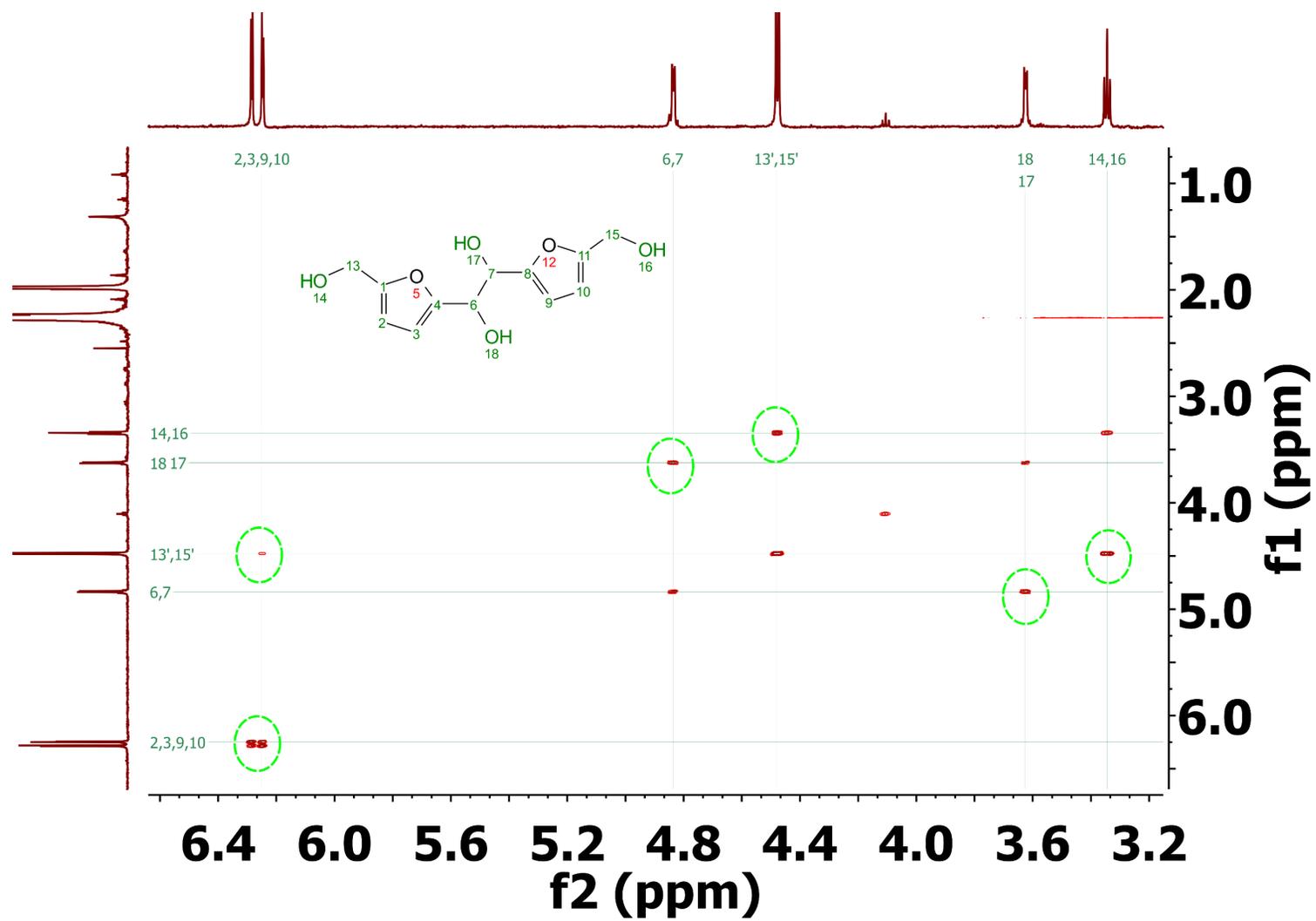
Figure S3.2. HSQC spectra of BHH-1
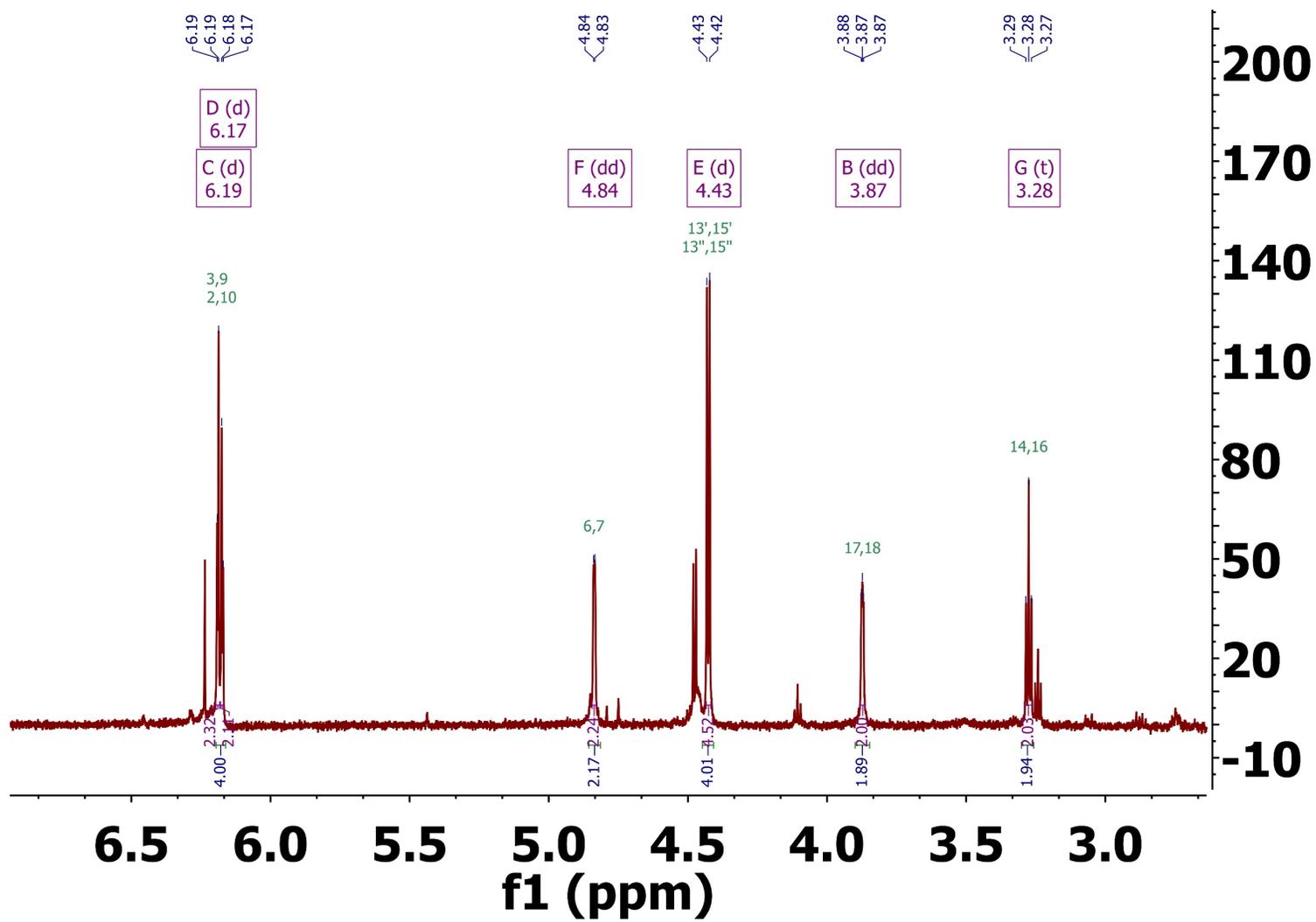
**Figure S3.3.** ^{1}H-NMR spectra of BHH-2
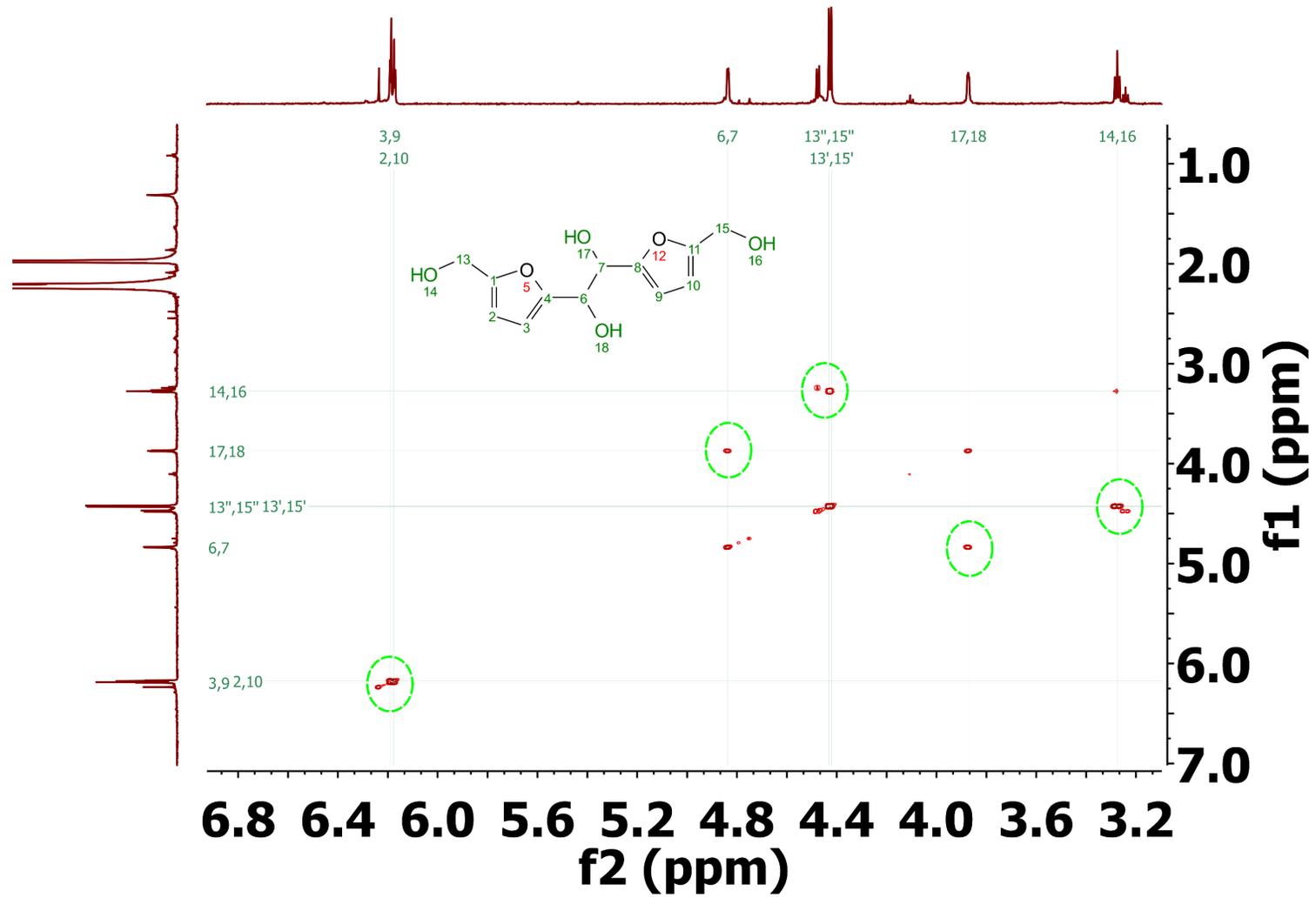
**Figure S3.4.** HSQC spectra of BHH-2

3.7.4   Additional Results
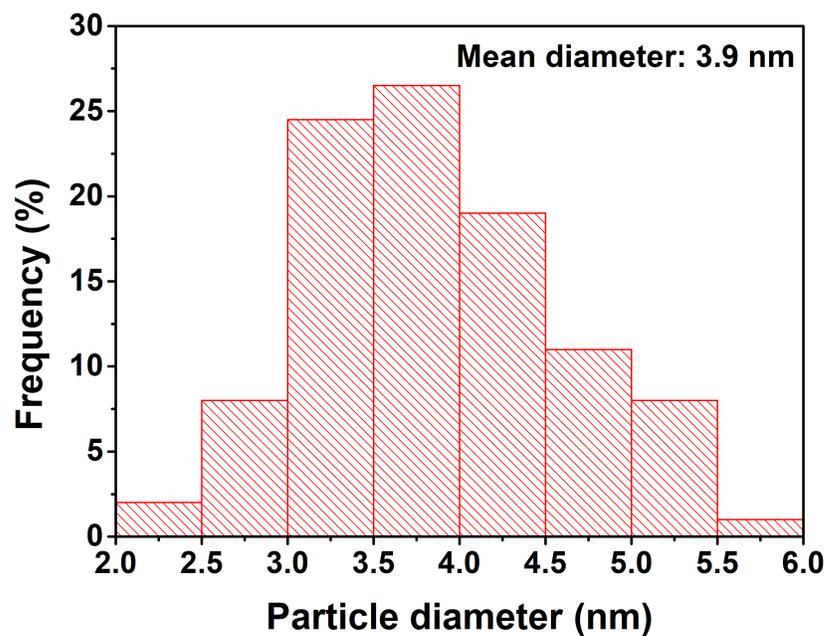
**Figure S3.5.** Ag particle size histogram for Ag/C from TEM measurements.
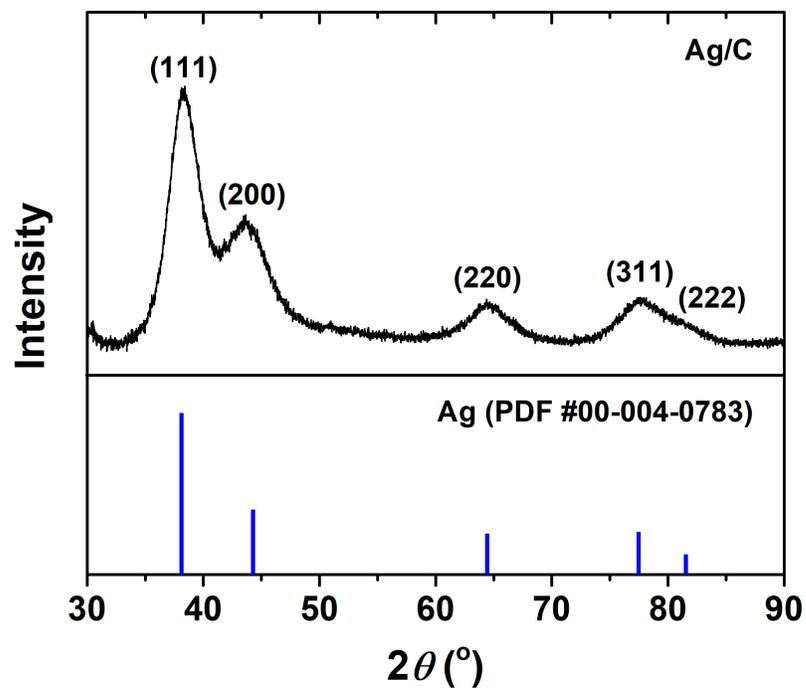
Figure S3.6. XRD pattern for the Ag/C catalyst.
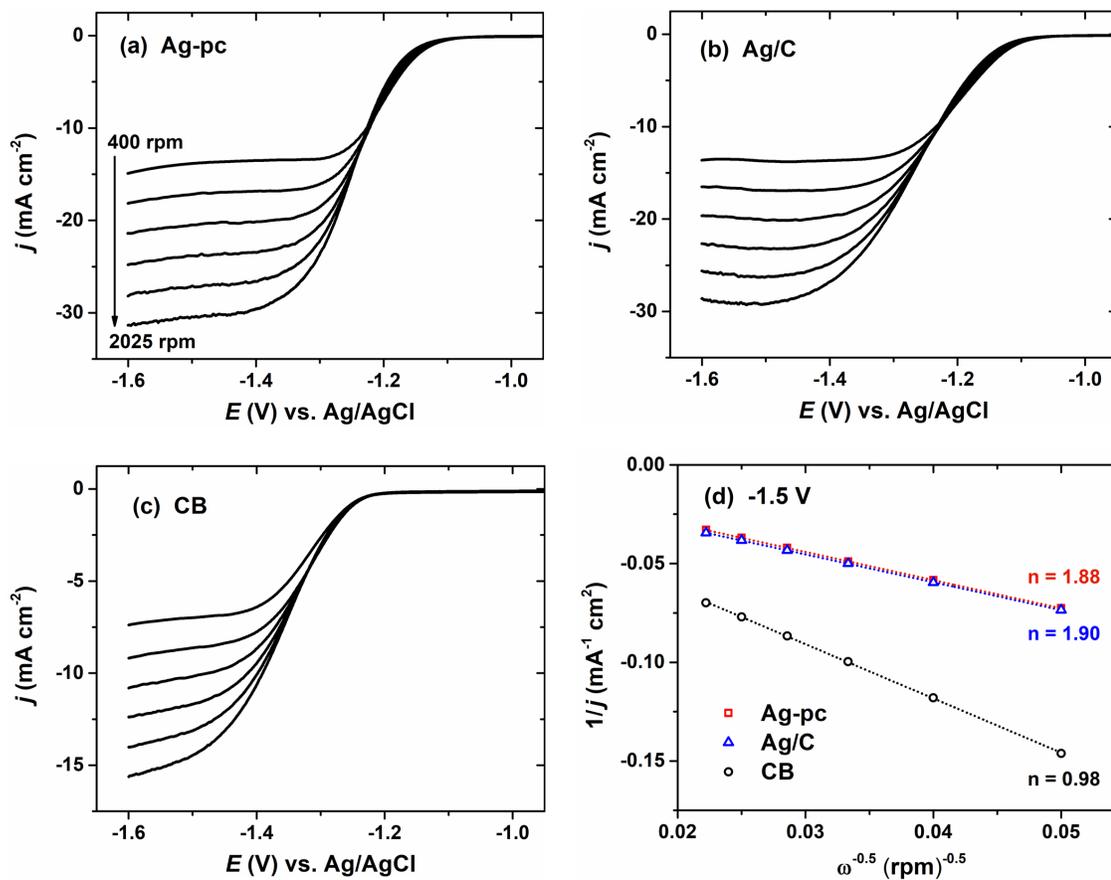
Figure S3.7. Cathodic linear sweep voltammograms for (a) Ag-pc, (b) Ag/C, and (c) CB collected at 50 mV s^{-1} and rotation rates of 400, 625, 900, 1225, 1600, and 2025 rpm, and (d) corresponding Koutecký-Levich plots. The number of electrons transferred (*n*) was calculated from the value of the slope. Electrolytes contained 20.0 mM HMF.
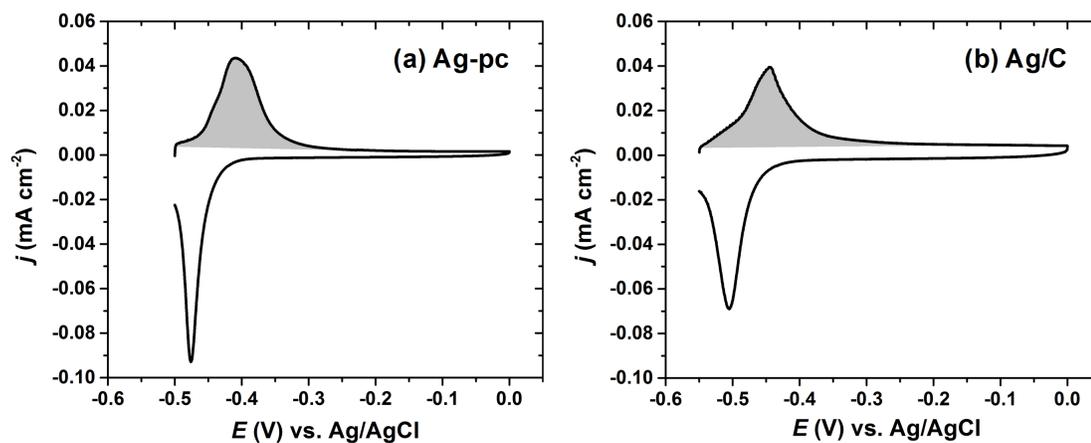
Figure S3.8. Stripping voltammograms of Pb$_{UPD}$ for (a) Ag-pc and (b) Ag/C. Shaded areas indicate the corresponding Pb$_{UPD}$ charges used for calculation of Ag ECSA.
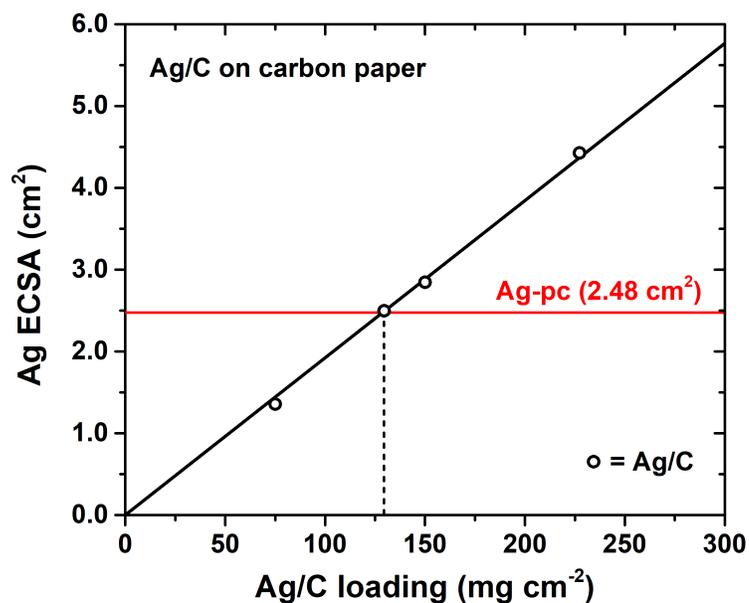
Figure S3.9. Electrochemically-active surface area (ECSA) of Ag/C determined by Pb$_{UPD}$ stripping as a function of catalyst loading, compared to ECSA for Ag-pc.

Table S3.1. Electrocatalytic HMF reduction with Ag-pc electrodes.[a]

[HMF] (mM)	Duration (min)	Q (C)	Conversion (%)	S_{BHMF} (%)	S_{BHH} (%)	FE_{BHMF} (%)	FE_{BHH} (%)	FE_{H2} (%)
5	30	3.42	19.7	80.9	9.6	89.3	5.3	2.0
20	30	7.85	13.2	57.1	30.2	75.0	19.9	0.0
50	30	12.1	9.1	40.7	49.5	57.8	35.3	0.0
20	300	26.5	44.6	55.8	31.3	72.7	20.4	0.0

[a] Conditions: 0.5 M pH 9.2 borate buffer solution. $E = -1.2$ V vs Ag/AgCl.

Table S3.2. Summary of electrodes used for HMF reduction.

electrode	geometric area (cm^2)	Pb$_{UPD}$ stripping charge (mC)	Ag ECSA (cm^2)
Ag-pc foil	2.0	0.652	2.51
Ag/C on carbon paper	2.0	0.654	2.52
CB on carbon paper	2.0	-	-
Ag-pc disk	0.196	0.102	0.391
Ag/C on GCE	0.196	0.092	0.354
CB on GCE	0.196	-	-

CHAPTER 4

CONCLUDING REMARKS AND FUTURE DIRECTION

The focus of this research was to explore the fundamental and practical aspects of electrochemical conversion routes of biobased furanic compounds for production of chemicals and fuels. I demonstrated that electrochemical conversion is a promising approach for upgrading furanics, including furfural and HMF, at mild conditions (i.e. aqueous electrolytes, ambient temperature and pressure). These studies highlighted that understanding the reaction mechanisms and pathways of ECH, as well as competing reactions such as electroreduction and HER, is pivotal to guide the selection of electrocatalysts and reaction conditions and to obtain high selectivity, efficiency and activity. Supported nanoparticle catalysts benefited from high surface area to mass ratios, however the activity of the support material must be considered. The insights gained will aid the development of efficient and selective electrochemical processes, with the goal of broadening our ability to utilize renewable carbon and renewable electricity sources.

Chapter 2 investigated the electrochemical reduction of furfural in acidic electrolytes using Cu electrodes, and provided insights into distinguishing ECH and ER mechanisms and rationally tuning the selectivity to MF (biofuel additive), FA (important precursor for polymers and resins) and dimerization product. A combination of electrochemical studies including SAM-modified electrodes, H/D kinetic isotope effects, cyclic voltammetry and preparative electrolysis were conducted to elucidate the mechanisms and pathways of product formation. Results suggested that hydrogenation and hydrogenolysis products were formed through inner-sphere electron transfer processes by parallel reaction pathways. Electrolysis studies demonstrated that reaction conditions have a key role in

controlling the selectivity and efficiency of electrochemical furfural reduction. The relative availability of H_{ads} and furfural adsorbates on the electrode surface was a major factor in determining the competition between reduction pathways. Therefore, achieving desired chemisorption properties is critical for the development of new, highly selective, and effective catalyst materials. Future breakthroughs in catalyst design may employ bimetallic or nanostructured electrodes to tune those properties to optimize the yield of desired products.

Chapter 3 demonstrated the feasibility of pairing HMF hydrogenation and oxidation for production of important biobased monomers, BHMF and FDCA, with high yield and efficiency in a single electrochemical cell. The selectivity and efficiency for Ag-catalyzed BHMF formation were sensitive to cathode potential, due to competition from water reduction and HMF hydrodimerization reactions. The carbon support material was also active for HMF reduction and contributed to undesired dimer formation at strongly cathodic potentials. The competing reactions limited the usable potential range for Ag/C, and the optimal potential was –1.3 V versus Ag/AgCl for high selectivity and efficiency to BHMF. Fortunately, HMF oxidation was facilitated under the same electrolyte conditions by a homogeneous electrocatalyst, ACT, for which the selectivity was insensitive to anode potential. This allowed HMF hydrogenation and oxidation half-reactions to be performed together in a single cathode-potential-controlled reactor. In the future, Ag nanoparticle size effects should be studied to further enhance BHMF yield. Reactor design should be optimized to reduce internal resistance, cell potential, and energy demands. Additionally, performing the paired electrolysis in continuous-flow reactors should be explored, to facilitate future process scale-up efforts.